CRETACEOUS TO CENOZOIC TECTONICS OF NORTH AMERICA: FROM INTRAPLATE MAGMATISM TO INTRACONTINENTAL RIFTING

A Dissertation Presented to

the Faculty of the Department of Earth and Atmospheric Sciences

University of Houston

In Partial Fulfillment

of the Requirements for the Degree

Doctor of Philosophy

By

Yiduo Andy Liu

December 2016

CRETACEOUS TO CENOZOIC TECTONICS OF NORTH AMERICA: FROM INTRAPLATE MAGMATISM TO INTRACONTINENTAL RIFTING

Yiduo Andy Liu

APPROVED:

Dr. Michael A. Murphy, Chairman

Dr. Jonathan E. Snow

Dr. Alexander C. Robinson

Dr. Jolante van Wijk

Dean, College of Natural Sciences and Mathematics

ACKNOWLEDGEMENTS

First and foremost, I am extremely grateful to my advisor Prof. Michael A. Murphy. He trained me in field mapping and critical thinking as a structural geologist, which is my primary goal for the PhD pursuit. He instructed me in detail how to write research proposals, which is an invaluable experience that not every student is trained on. He demonstrated to me what great leadership should look like. His persistence, after the brain surgery, deeply motivated me every time I thought about giving up. He taught me how to drive a van, lent me his pick-up truck for months, free, and he even showed up as the sole guest/photographer/witness at my "shotgun-style" wedding! Murphy is truly a role model.

For the Gulf of Mexico magmatism chapter, I want to acknowledge Profs. Michael Murphy for initiating the project and providing free atmosphere for me to conduct research; Jonathan E. Snow for his patient guidance on how to understand geochemical data; Jolante van Wijk for significantly deepening my understanding and love of continental rift and subduction zone dynamics; Dale Bird, Stuart Hall, and Alexander C. Robinson for critical comments and help on data interpretations; John Casey and Alan Brandon for leading me into mantle geochemistry in graduate courses; Chase Parsons for providing a figure; and Yipeng Li, John Matthew Cannon, Zhicheng Jing, Lijun Liu, Quan Zhou, and Jiachao Liu for insightful discussions. I am very grateful to Dr. Kevin Burke because he showed me the importance of integrating multi-disciplinary knowledge, and his noble scientific spirit of admitting past mistakes during

the pursuit of the truth. Anadarko and Chesapeake provided financial support to the iGoM consortium. The GCAGS Student Grant also funded me for this study.

On the Rio Grande rift study, I received tremendous support from Ross Andrea who sets up a professional-level standard for any field assistant. Discussions with Drs. Jolante van Wijk, Alexander C. Robinson, Joel Saylor, Gary Axen, and Randolph Williams were very helpful for me to better understand the structure, kinematics, and basin evolution of the Rio Grande rift. Also, Kevin O'Keeffe, Jason Kegel, John Matthew Cannon, Tyson Smith, Anna Khadeeva, and Michael Sullivan assisted me in the field and brought smart discussions, logistics, and a lot of fun to New Mexico. I also deeply appreciate the hospitality of the local people in Abiquiu, NM. This study would have been impossible without the financial support from the AAPG Foundation Grants-in-Aid in 2015 and the GSA Graduate Research Grant in 2016.

I am very grateful to Drs. Wenrong Cao and Jeni McDermott for the magnificent fieldwork opportunities they offered me in the Sierra Nevada, California and the Himalaya in Nepal, respectively.

I dedicate this dissertation to the most important women in my life, my mom, Wenli Li, and my wife, Xiaohua Wei. Both are extraordinarily patient and unconditionally supportive to me in my life.

CRETACEOUS TO CENOZOIC TECTONICS OF NORTH AMERICA: FROM INTRAPLATE MAGMATISM TO INTRACONTINENTAL RIFTING

An Abstract of a Dissertation

Presented to

the Faculty of the Department of Earth and Atmospheric Sciences

University of Houston

In Partial Fulfillment

of the Requirements for the Degree

Doctor of Philosophy

By

Yiduo Andy Liu

December 2016

ABSTRACT

The tectonic mechanism driving Cretaceous magmatism in the Gulf of Mexico (GoM) region is debated. This magmatism postdates GoM seafloor spreading by 40 Myr, initiated at 108 Ma and lasted through the Cretaceous. Spanning Texas to Mississippi it consists of igneous rocks with geochemical signatures pointing to a sub-lithospheric mantle origin. Hypotheses for this magmatism include: (1) the Bermuda hotspot; (2) edge-driven convection; (3) lithospheric reactivation; and (4) deep, low-angle subduction. My research shows none are fully satisfactory and that GoM magmatism should be correlated to other Cretaceous – Eocene kimberlites and lamproites from Arkansas to the Northwest Territories. They are located 1000+ km inboard from, and aligned sub-parallel to, the western margin of North America (NA). I propose that the Farallon slabs stagnated in the mantle transition zone in the Early Cretaceous, and generated sporadic, dense, low-degree partial melts by dehydration and decarbonation. As the slabs penetrated the lower mantle, instabilities at slab edges caused upwelling that brought alkali-rich carbonatitic melts to the base of the lithosphere. Subsequently, the NA lithosphere with varying thickness, discontinuities, and compositions interacted with the rising melt, producing a variety of magmatic rocks. This model connects intraplate magmatism with slab stagnation, and provides a critical constraint on the Cretaceous NA history.

Following the Laramide orogeny, Cenozoic extension dominated the western US, forming the Rio Grande rift (RGR). Kinematics of the extension is critical to evaluate tectonic models. While the N-trending, right-stepping RGR largely shows orthogonal E-W extension, the NW-striking, oblique Tusas segment preserves W- and SW-trending

slip directions. While a multi-directional extension model is possible, a continuous E-W extension with reactivation of pre-existing weakness can alternatively explain slip direction variations. Initial extension on reactivated faults was recorded by W-trending slickenlines. Subsequently, extension was re-oriented to SW-trending, i.e., pure dip-slip, due to local stress rotation across heterogeneities. Then, the Embudo accommodation zone began to accommodate E-W extension, causing diffuse, SSW-directed slip on the Tusas segment. The early extension along the Tusas segment was abandoned once the Embudo transfer fault formed. This study highlights the significance of obliquity and inherited heterogeneity in the kinematic evolution of rifts.

Contents

CHAPTER 1. POST-BREAKUP MAGMATISM IN NORTHERN GULF OF MEXICO

1. Introduction

Worldwide examples of post-breakup magmatism are geographically and volumetrically minor. One of the best examples is our study area in the northern Gulf of Mexico (GoM), where post-breakup Cretaceous volcanism provides a window into the convective mantle underlying the rifted GoM margin. A rich dataset compiled from studies over the last three decades allows us to evaluate tectono-magmatic process from the deep mantle to the surface.

Igneous activity plays a significant role in the evolution of rifted passive margins. Such magmatism, based on its relative timing to rifting and seafloor spreading, can be classified into four categories: (1) Pre-rift magmatism that precedes rifting, e.g. southwestern Ethiopia (Ebinger and Sleep, 1998), northern Ethiopia, and Yemen (Hofmann et al., 1997; Ukstins et al., 2002). (2) Syn-rift magmatism, which is emplaced during intra-continental rifting, and precedes the onset of seafloor spreading. Most volcanic rifted margins preserve syn-rift igneous rocks, such as the Red-Sea (Menzies et al., 1997), North Atlantic (White et al., 1987), Central Atlantic (Blackburn et al., 2013; Marzoli et al., 1999; White and McKenzie, 1989), northeastern and northern Gulf of Mexico (Heatherington and Mueller, 2003; Stern et al., 2011), and Deccan, India (Hooper, 1990). (3) Syn-breakup magmatism, which immediately follows the cessation of rifting and is coincident with the initial stage of seafloor spreading. Volcanic activity in the South Atlantic (Turner et al., 1994; White and McKenzie, 1989), East Greenland (White and McKenzie, 1989), Northwest Australia (Hopper et al., 1992), and South China Sea (Zhao et al., 2016) are examples of this type. (4) Post-breakup magmatism, which postdates the breakup of continental plates while the rifted margins are already dominated by thermal relaxation and subsidence (McKenzie, 1978;

White and McKenzie, 1989). It has been documented in East Mexico (Ortega-Gutiérrez et al., 2014), Greenland (Meyer and van Wijk, 2007), Newfoundland (Hart and Blusztajn, 2006; Karner and Shillington, 2005), western Ireland (Tate and Dobson, 1988), eastern Gulf of Aden (Lucazeau et al., 2008), offshore Senegal (Hansen et al., 2008), and even possibly the Pacific coast of Antarctica (Hart et al., 1995). Due to its location within a plate, post-breakup magmatism is considered a type of intraplate magmatism.

While the first three types of magmatism are extensively studied around the world (e.g., Burke and Dewey, 1973; Koptev et al., 2015; Meyer and van Wijk, 2007; Storey et al., 1995; van Wijk et al, 2001; White et al., 1987, 2008;), post-breakup magmatism is still enigmatic, in terms of its spatial-temporal distribution, petrogenesis, and tectonic mechanism. Such magmatism is critical, both scientifically and economically, because it carries information regarding the mantle beneath rifted margins and continents, and exerts a potentially strong influence on hydrocarbon and mineral generation on or near passive margins.

Post-breakup magmatic rocks in the northern Gulf of Mexico (GoM) were emplaced during the Cretaceous (ca. 108-65 Ma). They consist of predominantly lamproites, carbonatites, lamprophyres, and a group of alkaline silicate rocks such as nephelinites, alkali basalts, basanites, and phonolites, which are the characteristics of many intraplate igneous provinces. Previous studies of these rocks have produced a sizeable geochemical and geochronological dataset (e.g., Baksi, 1997; Barker et al., 1987; Duke et al., 2014; Eby and Vasconcelos, 2009; Ewing, 2009; Flohr and Ross, 1990; Griffin et al., 2010). This dataset has been used to formulate four families of models for the petrogenesis and/or tectonics of the magmatism, including: 1) Bermuda hotspot (Chu et al., 2013; Cox and Van Arsdale, 2002; Duncan, 1984; Morgan, 1983); 2) edge-driven convection (Ballmer et al., 2015; King and Anderson, 1998; Matton and Jébrak; 2009); 3) reactivation of pre-existing heterogeneities (Eby and Vasconcelos, 2009; Griffin et al, 2008); and 4) deep-seated subduction of the Farallon plate (Duke et al., 2014; McCandless, 1999). However,

a critical evaluation of existing models, particularly in a regional context, is still lacking. Such a review has become possible and necessary thanks to recent progress in geochronology, geochemistry, plate reconstruction, seismic tomography, and experimental petrology. In this contribution, we assess these models based on an integration of multi-disciplinary data of the GoM igneous rocks and propose a new tectono-magmatic model in a plate-scale framework.

2. Regional Geology

The Mesozoic tectonic evolution of the Gulf of Mexico region includes two primary phases: Late Triassic-Early Jurassic (235-174 Ma) continental rifting among the Laurentian, Yucatán block, and African plates, followed by Late Jurassic (ca. 156-145 Ma) seafloor spreading facilitated by counterclockwise rotation of the Yucatán block (e.g., Bird et al., 2005; Burke, 1988; Eddy et al., 2014; Marton and Buffler, 1994; Pindell and Kennan, 2009; Sandwell et al., 2014). Associated with continental rifting is a bimodal magmatism composed of basaltic and rhyolitic rocks during the Jurassic (199-159 Ma) from Florida to Louisiana in southeastern U.S. (Heatherington and Mueller, 2003; Stern et al., 2011).

By ca. 145 Ma, tectonic and magmatic activities ceased in northern GoM once the rifted margin was established (Fig. 1). Subsequent thermal subsidence and rapid growth of carbonate banks dominated the northern GoM margin during the Early Cretaceous (e.g., Galloway, 2008; Snedden et al., 2015; Salvador, 1991; Winker and Buffler, 1988). However, about 40 Myr later, extensive, prolonged igneous activities began in the northern GoM. This igneous activity is traditionally divided into two provinces (Fig. 1): the Arkansas-Jackson Dome igneous province (AIP) that spans Arkansas, Louisiana, and Mississippi (Fig. 2a), and the Balcones-Trans Pecos igneous province (BIP) that extends from central to west Texas (Fig. 2b).

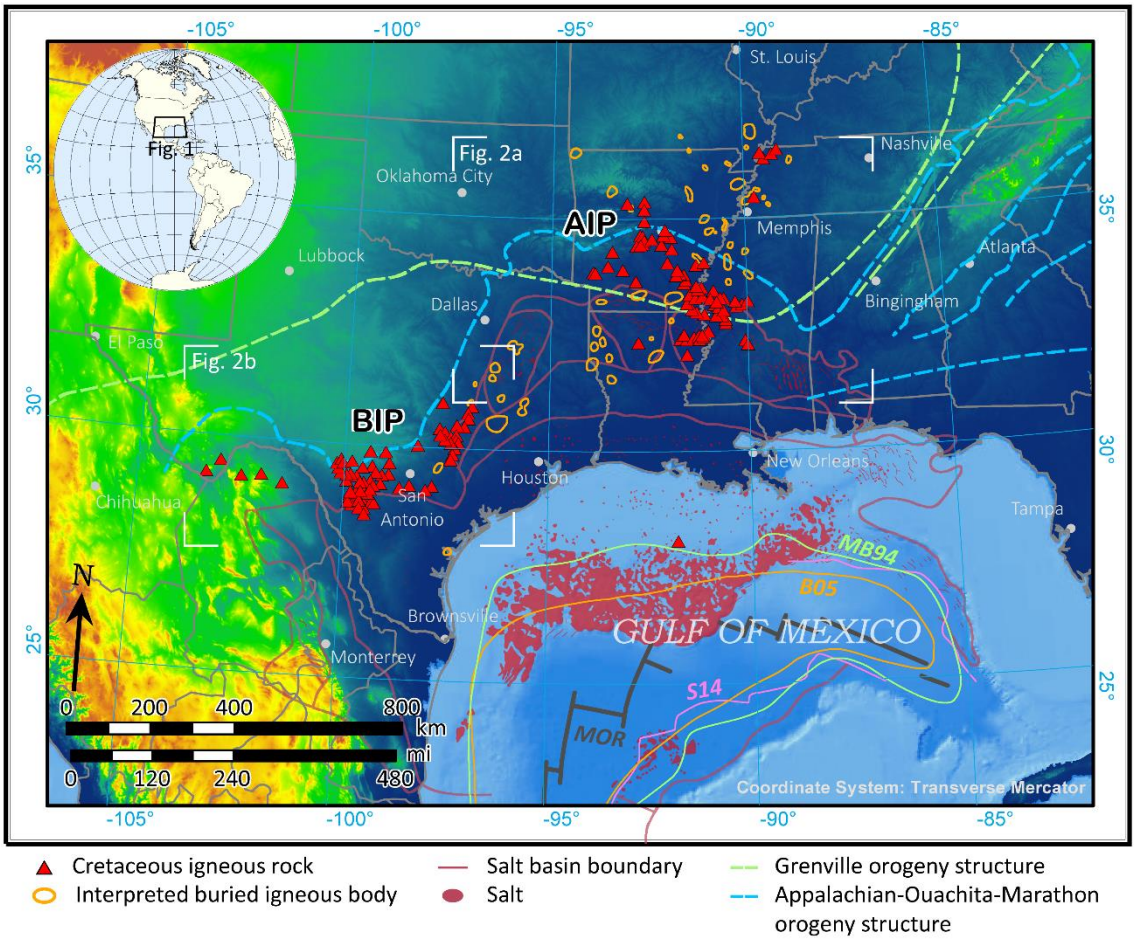

Figure 1 Geographic distribution of Cretaceous igneous rocks and interpreted buried igneous bodies in the northern GoM region. Also shown are the Grenville and Appalachian-Ouachita-Marathon orogenic belts (Thomas, 2006), GoM salt basins and their boundaries (Hudec et al., 2013), Jurassic mid-ocean ridges in the GoM oceanic basin (Sandwell et al., 2014), and three continental-oceanic transition zones proposed by MB98, Marton and Buffler 1994; B05, Bird et al., 2005; and S14, Sandwell et al., 2014. AIP, Arkansas-Jackson Dome igneous province; BIP, Balcones-Trans Pecos igneous province.

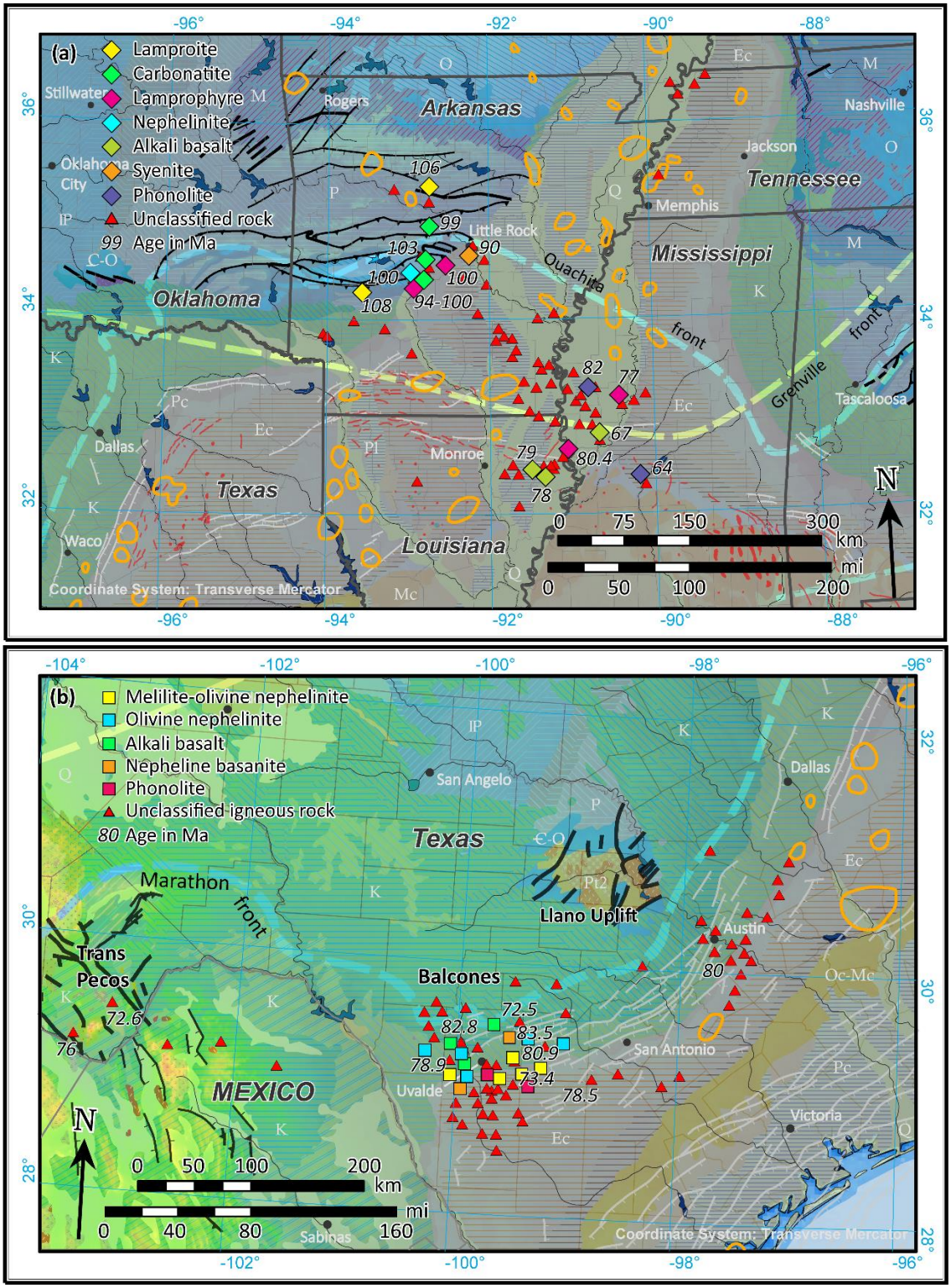

Figure 2 Regional geologic maps of the Arkansas-Jackson Dome (AIP) (a) and Balcones-Trans Pecos (BIP) (b) igneous provinces, showing their locations, rock types, and emplacement ages (in Ma). Base map is simplified from the USGS online map database (https://ngmdb.usgs.gov). Light grey lines in the GoM basins represent normal faults. Black lines are undifferentiated fault traces.

2.1 Lithology and ages

The AIP is emplaced mainly within the Mesoproterozoic (ca. 1.55-1.35 Ga) Granite-Rhyolite Province (e.g., Whitmeyer and Karlstrom, 2007). In central Arkansas (Fig. 2a), the AIP consists of diamond-bearing lamproites (in Prairie Creek, Twin Knobs, and Black Lick), lamproites (Dare Mine Knob), carbonatites and associated ijolites, jacupirangites, nepheline syenites, and phonolites (Magnet Cove and Potash Sulfur Springs), carbonatite dikes (Morrilton and Perryville), and nephiline syenites (Granite Mountain and Saline County), as well as other mafic and felsic rocks (Eby and Vasconcelos, 2009). In the Monroe Uplift and Jackson Dome area in SE Arkansas, NE Louisiana, and west-central Mississippi, subsurface volcanic and hypabyssal rocks have been revealed in many boreholes, and four major groups of igneous rocks can be identified: trachytes, phonolites, basalts, and lamprophyres (cf. Baksi, 1997).

The Prairie Creek, Arkansas lamproites mark the earliest magmatic pulse (108-105 Ma) in the AIP (Fig. 1c) (Eby and Vasconcelos, 2009; Gogineni et al., 1978; Zartman, 1977). These rocks contain xenoliths and xenocrysts that are derived from the Archean subcontinental lithospheric mantle (SCLM), which was metasomatized during two episodes, 1.4-1.5 Ga and 200-300 Ma (Griffin et al., 2011). Eclogitic inclusions are present in the diamonds from the Prairie Creek lamproites (Pantaleo et al., 1979).

Following the lamproites was the emplacement of carbonatites (ca. 103-96 Ma), ijolites (ca. 102-94 Ma), nepheline syenites, olivine syenites, jacupirangites, and phonolites (ca. 100-86 Ma) (Eby and Vasconcelos, 2009; and references therein). Southeastward, volcanism continued during the Coniacian-Campanian into the Monroe Uplift and Jackson Dome area (cf. Baksi, 1997). Geochronologic studies show emplacement ages of ca. 80-77 Ma for lamprophyres, ca. 82-64 Ma for phonolites, 79 Ma for jacupirangites, and ca. 79-67 Ma for alkali basalts (Baksi, 1997; Saunders and Harrelson, 1992). In brief, the AIP has a prolonged period of activity from

Albian to the latest Cretaceous/earliest Paleocene. A weak southward-younging trend may be present based on their spatiotemporal distribution (Table 1).

The BIP was emplaced during the Campanian in south-central and western Texas along the northwestern GoM margin (Fig. 2b). The BIP is characterized by low-volume monogenic igneous centers and lack of large lava flows (Barker et al., 1987; Miggins, 2004; Spencer, 1969). The Balcones segment of BIP is about 400-km long, 100-km wide, and curves from NE-trending near the Travis County to near E-W trending in the Uvalde and Kinney Counties in Texas, following the traces of the Ouachita-Marathon suture. Over 200 igneous bodies can be recognized from aeromagnetic surveys of the Balcones region, but less than 30 have surface exposures (Miggins, 2004). A bimodal pattern characterizes the BIP: olivine nephelinites, melilite olivine nephelinites, alkali basalts, and nepheline basanites were emplaced during 83.5-81 Ma; phonolites and phonotephrites yield younger ages of 78-72 Ma (Barker et al., 1987; Miggins, 2004; Spencer, 1969). Further west, basaltic pyroclastic deposits are present in the Rosillos and Pena Mountains in the Big Bend area of Trans Pecos, Texas. These deposits yield zircon U-Pb ages of ca. 78-73 Ma, suggesting a westward extension of the Balcones segment (Befus et al., 2008; Breyer et al., 2007). No carbonatites or lamproites have been reported in this region to our knowledge.

There is also an "outlier" that does not fall into either of the alkaline provinces, which is a 77-Ma olivine basalt dike discovered in the Alderdice Bank area, offshore Louisiana (Fig.1) (Rezak and Tieh, 1984). We speculate that this dike was carried up and exposed by the seaward-flow and diapir of the Louann salt in the northern GoM margin (e.g., Hudec et al., 2013), but its original position is unknown. Some other igneous bodies have also been interpreted from seismic data in this region, but this is beyond the scope of this study due to their limited publicities.

Extensive igneous activities during the Late Cretaceous were also recorded as volcanic clasts within sedimentary rocks in the northern GoM (Fig.1), as revealed by over 145 drill cores in the Mississippi embayment, Arkansas, Texas, and Oklahoma (e.g., Gogineni et al., 1978;

Heydari et al., 1997). Trachyte, trachybasalt, and phonolite cobbles from the volcaniclastic Woodbine Formation in southwestern Arkansas show $^{40}Ar/^{39}Ar$ ages of ca. 94-92 Ma (Baksi, 1997). The Door Point volcaniclastic rock, which is located 2.2-2.6 km below sea level, offshore Louisiana, yields an age of 82 $\pm$ 8 Ma (dating method not reported, Braunstein and McMichael, 1976; rock type re-classified by Anderson and Snow, 2015).

I have mapped buried igneous bodies by interpreting the first-order features in potential field anomaly maps in the region (Fig. 3). Potential field maps are generated following the methods described in Bird et al. (2005). The gravity anomaly map is composed of onshore Bouguer and offshore satellite-derived free-air gravity anomalies, and the magnetic anomaly map consists of total intensity magnetic anomaly maps in the study area. I have interpreted round-shaped, positive anomalies in both Bouguer gravity and magnetic maps in GoM basins as buried igneous bodies (Bird, 2004; Ewing, 2009). A number of bodies with these characteristics can be interpreted along the Mississippi river valley from Louisiana up to Tennessee. Similarly, we interpret the Sabine Uplift spanning the Texas-Louisiana border as a Cretaceous igneous-cored uplift (Ewing, 2009).

In brief, the northern GoM lamproites, carbonatites, and alkaline magmatism took place ca. 40 Myr after the formation of the GoM oceanic basin, and continued for as long as 45 Myr during the Late Cretaceous. It spans the entire northern and northwestern GoM, but is absent along the Florida margin.

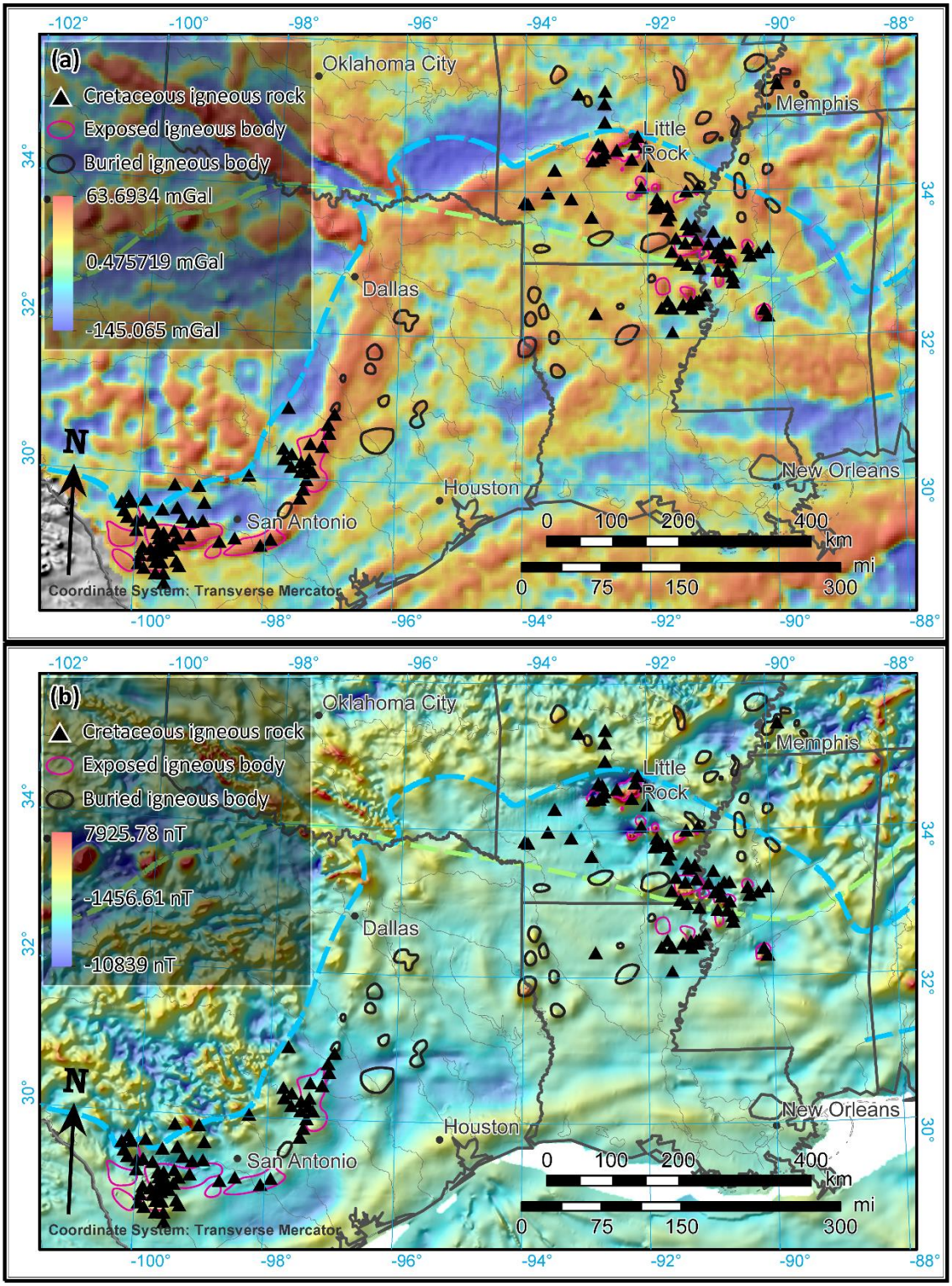

Figure 3 Gravity (a) and magnetic (b) anomaly map of the study region. Potential field data is from DNAG. Map (a) shows onshore Bouguer residual and offshore satellite-derived free-air gravity anomalies, and (b) is a total intensity magnetic anomaly map. The range of anomalies is indicated in the legend of each figure.

2.2 Geochemical characteristics

We compile published data to evaluate the geochemical characteristics of the AIP and BIP rocks. The AIP and BIP rocks, except the Arkansas lamproites, are characterized by silica-undersaturation, high contents of total alkali, incompatible trace element-enrichment, and OIB-like isotopic characteristics. This suite of rocks points to a sub-lithospheric (convective) mantle origin.

2.2.1 Arkansas lamproites

The Prairie Creek, Arkansas lamproites are ultrapotassic (molar K_2O / Na_2O > 3) volcanic rocks. They are low in CaO, Na_2O, and Al_2O_3, high in K_2O/ Al_2O_3 and K_2O/Na_2O, and rich in Mg with Mg# (Mg# = Mg / (Mg + Fe_total) * 100) ranging between 82 and 86 (Figs. 4 and 5) (Alibert and Albarede, 1988; Gogineni et al., 1978). They are highly enriched in incompatible elements including Rb, Ba, Th, U, Nb, Ta, Pb, Zr, Hf, light rare Earth elements (LREE), and Ni, and negative anomalies in Sr relative to Pb and Nd (Fig. 6a and 6b). Primitive mantle-normalized La/Yb ratios ((La/Yb)n) of lamproites range between 45 and 146, with an average of 111 (Alibert and Albarede, 1988; Ausburn, 2006; Baksi, 1997; Lambert et al., 1995). Niobium/Uranium ratios of the lamproites are between 23 and 49 (Alibert and Albarede, 1988; Duke et al., 2014; Lambert et al., 1995), most of which fall in the range of ocean basalts (47 ± 10) (Hofmann, 1986) (Fig. 7a). Their Ce/Pb ratios of 10-25 also partially overlap the ocean island basalt (OIB) values (25 ± 5) (Hofmann, 1986), suggesting an asthenospheric origin. Given the exceedingly enriched incompatible element concentrations in the AIP lamproites, crustal contamination cannot be precluded but does not appear significant.

Isotopic measurements of the Arkansas lamproites (Figs. 7b and 8) show a distinct domain in which, (1) their initial $^{86}Sr/^{87}Sr$ ratios range between 0.70628 and 0.70833 with an average of 0.70747; (2) initial ε_{Nd} (at 106 Ma) between -9.9 and -19.2, with an average of -12.2

and model ages of 1.2-1.75 Ga; (3) Pb isotopes: $^{206}Pb/^{204}Pb$ = 16.618 - 16.819, average 16.763; $^{207}Pb/^{204}Pb$ = 15.339 - 15.360, average 15.350; $^{208}Pb/^{204}Pb$ = 36.574 - 38.063, average 37.037; (4) initial εHf ranges from -12.5 to -21.9, with an average of -19.05 and model ages of 1.32 - 1.75 Ga; and (5) initial γOs between -3.2 and -3.6 with 1.2 Ga model ages (Alibert and Albarede, 1988; Duke et al., 2014; Lambert et al., 1995).

These negative ε_{Nd} and high $^{86}Sr/^{87}Sr$ ratios fall in the lower right domain on the Sr-Nd diagram (Fig. 8a). Their common Pb isotopes plot to the left of the meteorite isochron and above the terrestrial evolution line in the $^{207}Pb/^{204}Pb$ vs. $^{206}Pb/^{204}Pb$ diagram (Fig. 8c). In addition, two out of four analyses (Duke et al., 2014) seem to depart by more than 5 εHf units from the Hf-Nd regression line (Fig. 8f) (Chauvel et al., 2008), which might be a sign of Hf-Nd decoupling.

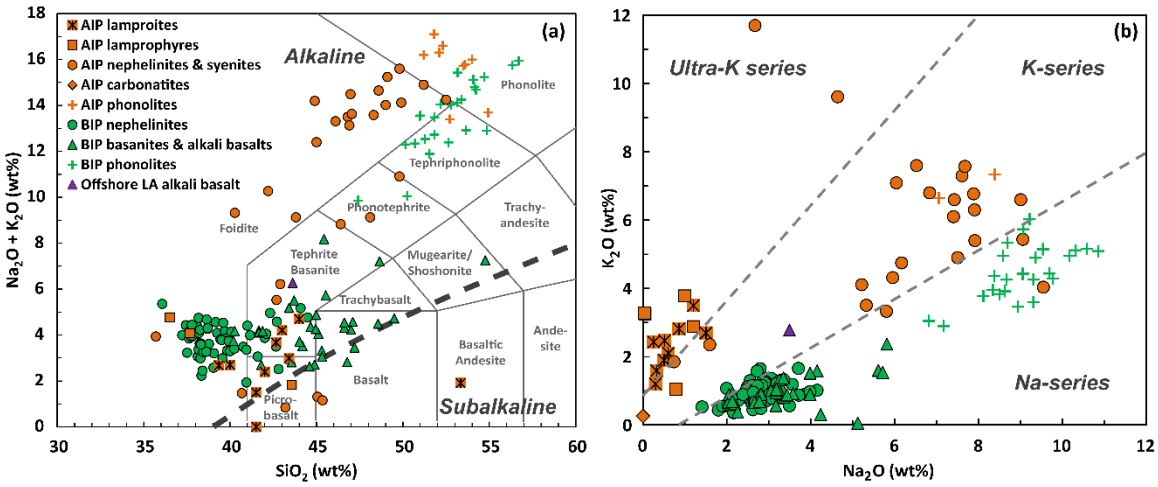

Figure 4 Major elements of the Cretaceous igneous rocks in the northern GoM. (a) Total silica (Na2O + K2O) versus SiO2 diagram. AIP carbonatites have very low SiO2 contents (<5 wt. %) and are not shown in this diagram. Classification after Le Bas et al. (1986). (b) K2O vs. Na_2O. The AIP rocks plot in the potassic and ultrapotassic series fields, while the BIP rocks are located in the Na-series field. Data sources are: AIP: Ausburn, 2006; Flohr and Ross, 1990; Gogineni et al., 1978; Heydari et al 1997; Ledger et al., 1988; Nelson et al., 1988; Salpas et al., 1986; Saunders and Harrelson, 1992; Waldman et al., 1987; BIP: Barker et al., 1987; Befus et al., 2008; Breyer et al., 2007; Griffin, 2008; Wittke and Mack, 1993; Offshore LA (Louisiana): Rezak and Tieh, 1984.

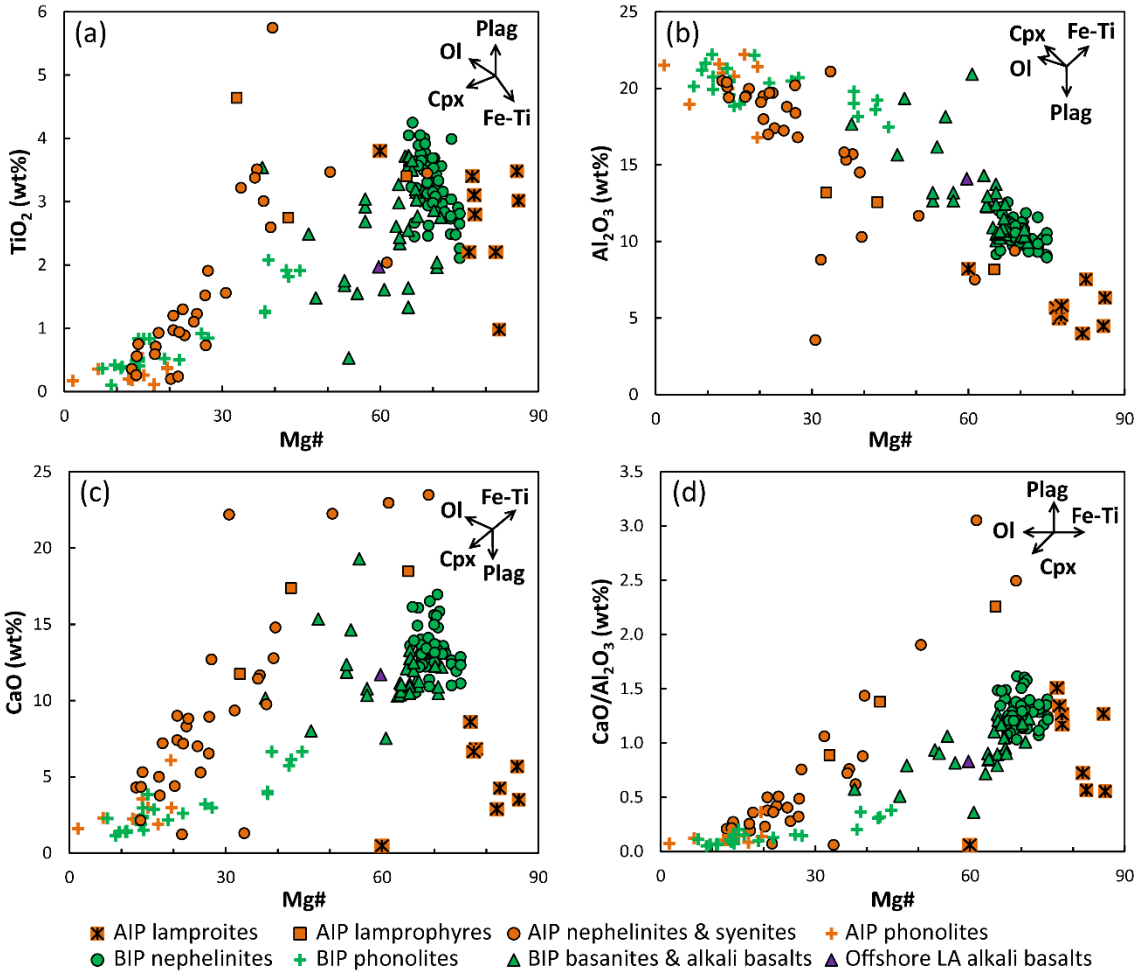

Figure 5 Plots of (a) TiO_2, (b) Al_2O_3, (c) CaO, and (d) CaO/Al_2O_3 versus Mg#. Mg# = 100 ×Mg/(Mg+Fe) (molar). See Fig. 4 for data sources.

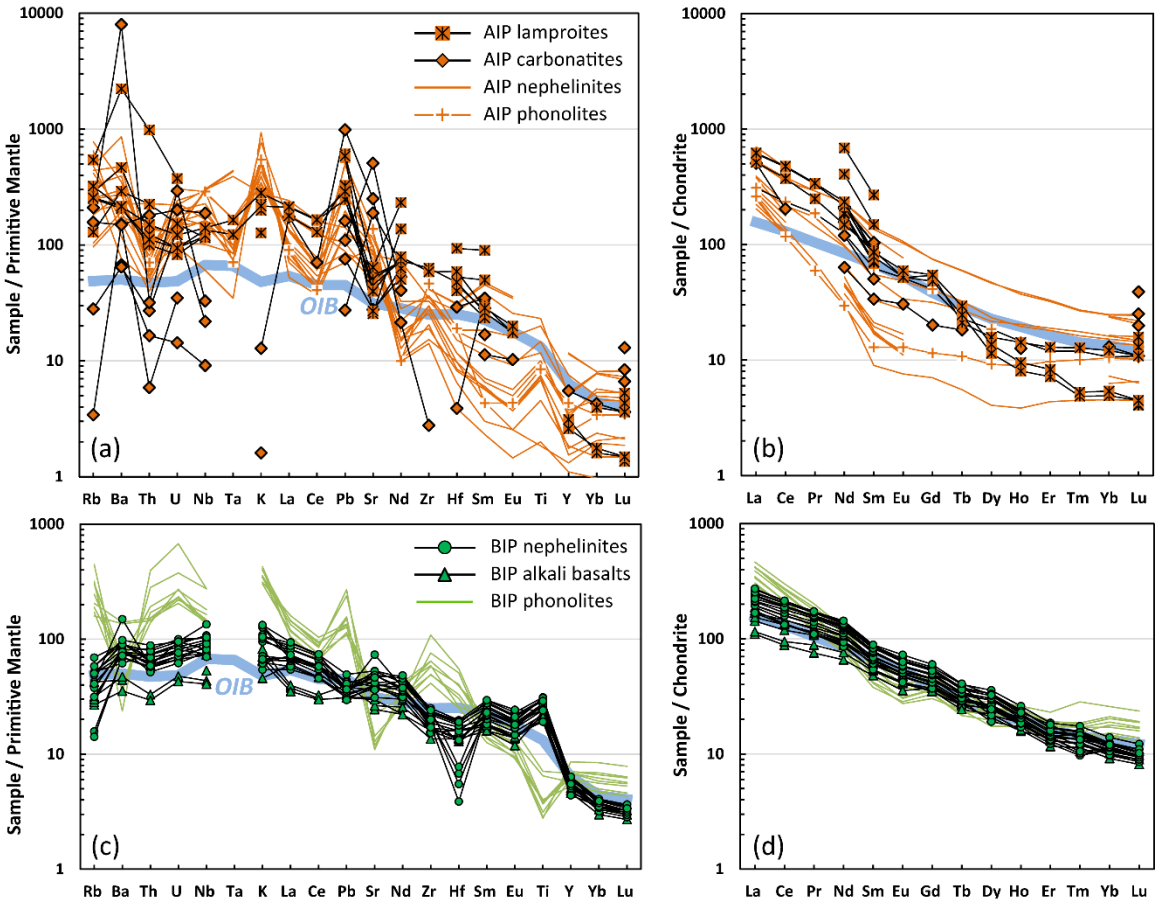

Figure 6 Trace and rare earth element diagrams for the AIP ((a) and (b)) and BIP ((c) and (d)) rocks. Primitive mantle-normalization after Sun and McDonough (1989), and chondrite-normalization after McDonough and Sun (1995). OIB from Sun and McDonough (1989) is shown as light blue line. Data sources are: AIP: Ausburn, 2006; Baksi, 1997; Duke et al., 2014; Flohr and Ross, 1990; Heydari et al., 1997; Lambert et al., 1995; Nelson et al., 1988; Saunders and Harrelson, 1992; BIP: Griffin, 2008.

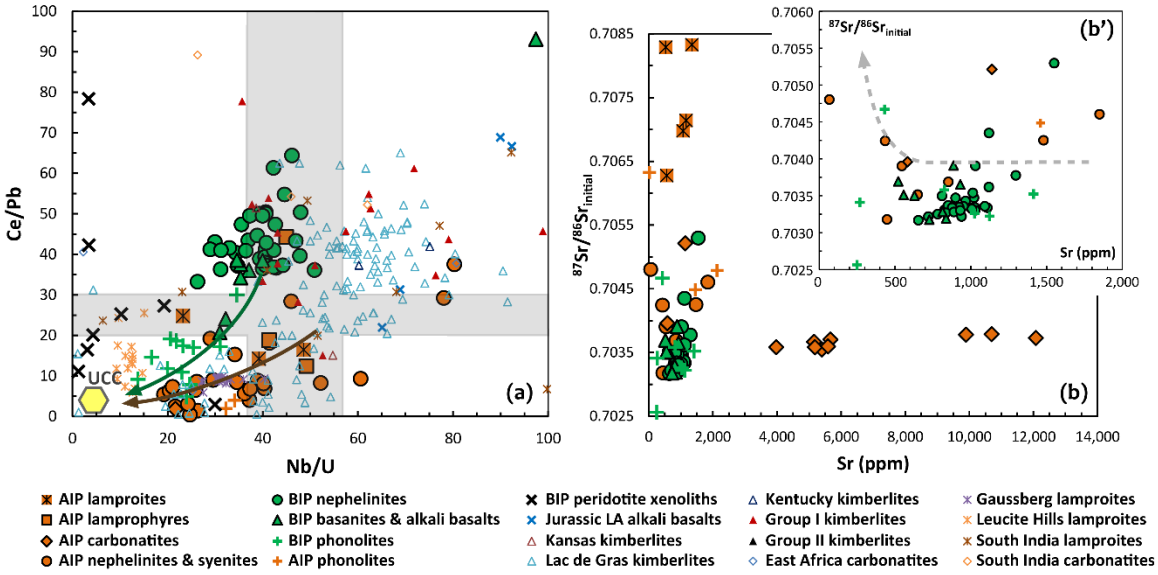

Figure 7 Trace element and isotopic ratio discriminative diagrams. (a) Nb/U vs. Ce/Pb diagram for the AIP and BIP rocks. (b) Sr contents (ppm) vs. initial Sr isotopic ratios for AIP and BIP, and the Insert (b') is a close-up view of the clustered area in (b). The grey area on (a) denotes the Nb/U and Ce/Pb ratios for OIB (Hofmann, 1986), the yellow hexagon represents the upper continental crust (UCC) which has Nb/U and Ce/Pb ratios of 4.4 and 3.7, respectively (Hawkesworth and Kemp, 2006). The brown and green arrows show approximately the assimilation trajectories from the OIB-field to the UCC for AIP and BIP, respectively. Also shown for comparison are the peridotite xenoliths found in BIP volcanic rocks (Young and Lee, 2009), Jurassic syn-rift alkali basalt in Louisiana (Stern et al., 2011), Kansas kimberlites (Alibert and Albarede, 1988), Lac de Gras kimberlites in Northwest Territories (Nowicki et al., 2004, 2008; Tappe et al., 2013), Kentucky kimberlites (Alibert and Albarede, 1988), Group I and II kimberlites (Gaffney et al., 2007; Smith, 1983), East African carbonatites (Nelson et al., 1988), South India carbonatites (Pandit et al., 2016), Gaussberg lamproites (Murphy et al., 2002), Leucite Hills, Wyoming, lamproites (Mirnejad and Bell, 2006), and South India lamproites (Chakrabarti et al., 2007). The grey, dashed line in (b') represents the trend of assimilation-fractional crystallization-liquid immiscibility (AFCLI) model of crustal materials (Ray, 2009).

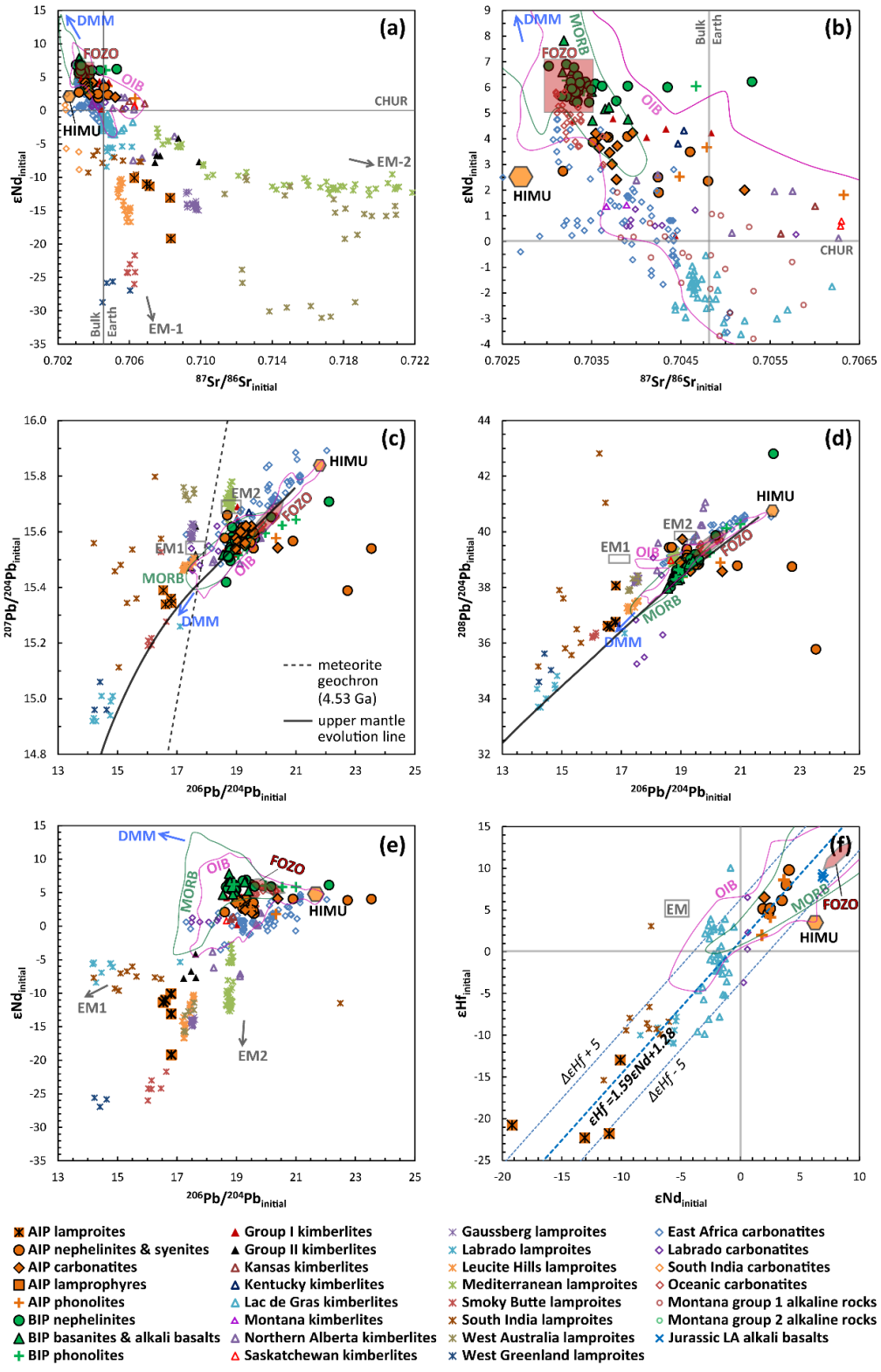

Figure 8 Sr-Nd-Pb-Hf isotopes of the AIP and BIP, with a global compilation of kimberlites, lamproites, and carbonatites. HIMU, FOZO, MORB, OIB, DMM, and EM fields from Stracke et al., 2005; meteorite geochron, Stracke et al., 2005; Hf-Nd mantle array, Chauvel et al., 2008.

2.2.2 Arkansas carbonatites

The Arkansas carbonatites are calcic, carbonate-rich (> 50 wt%) magmatic rocks characterized by high abundances of Ba, Pb, Sr, and LREE, and relatively-depleted Rb, Th, Nb, Zr, and Hf (Fig. 6a). Chrondrite-normalized REE patterns, albeit incomplete, portray a steep LREE and relatively-flat HREE trend with (La/Yb)n ratio of 41 (Fig. 6b) (Duke et al., 2014; Nelson et al., 1988). Their Nb/U ratio is up to 32 (Fig. 7), similar to that of primitive mantle (30; Hofmann, 1986), while the Ce/Pb ratio is only 1.8 (Nelson et al., 1988), possibly due to the excess amount of Pb (70 ppm) by secondary alteration.

Their isotopic systems (Fig. 8) are characterized by unradiogenic initial 86Sr/87Sr (= 0.70355 - 0.70396, with an average of 0.70383), slightly positive εNd (between +2.0 and +4.2, with an average of +3.5 and ca. 360-500 Ma model ages), radiogenic initial Pb isotopes ($^{206}Pb/^{204}Pb$ = 18.971 - 20.389, average 19.328; $^{207}Pb/^{204}Pb$ = 15.542 - 15.621, average 15.575; 208Pb/204Pb = 38.574 - 38.957, average 38.897), and radiogenic Hf isotope (εHf = +6.5) (Duke et al., 2014; Nelson et al., 1988; Tilton et al., 1987). They all plot in the OIB fields on Sr-Nd-Pb-Hf isotope diagrams. A mixture between FOZO and EM, and possibly HIMU mantle reservoirs can be inferred from the isotope diagrams (FOZO, focal zone; EM, enriched mantle; HIMU, high 'μ', $\mu = {}^{238}U/^{204}Pb$; see Hofmann, 1997 for a review of mantle geochemistry nomenclatures). Stable isotope composition from a Magnet Cove sample yields $\delta^{18}O_{SMOW}$ = +7.5 and $\delta^{13}C_{PDB}$ = -5.4, which overlaps the mantle field ($\delta^{18}O_{SMOW}$ range of +5 to +8, $\delta^{13}C_{PDB}$ range of -7 to -5), in contrast to the sedimentary carbonate with higher $\delta^{18}O_{SMOW}$ and $\delta^{13}C_{PDB}$ values (+18 or greater, and > -3, respectively) (Nelson et al., 1988). The Arkansas carbonatites are isotopically similar to many other carbonatites in East Africa, South India, Cape Verde, and Canary Islands, as well as Group I kimberlites, pointing to a sub-lithospheric mantle origin.

2.2.3 AIP alkaline rocks

The AIP alkaline silicate rocks here include lamprophyres, nephelinites, syenites, basanites, and phonolites. They are alkaline-rich, potassic to ultrapotassic (Figs. 4a and 4b), and enriched in incompatible elements (Fig. 6a and 6b). Concentrations of Ba, U, Nb, K, and LREE typically exceed 100 times primitive mantle, whereas relative depletions are present in Rb, Th, Ta, Pb, Nd, Hf, and HREE.

On oxides versus Mg number (Mg# = 100×Mg/(Mg+Fetotal) (molar)) diagrams (Fig. 5), the AIP rocks demonstrate a crystallization series of olivine accompanied and followed by clinopyroxene and plagioclase as the Mg number decreases and silica contents increases. Covariation on major element diagrams (Fig. 5) and sub-parallel incompatible element and REE patterns (Figs. 6a and 6b) indicate fractional crystallization in this igneous system. Crustal assimilation also played a role in the igneous system, as shown by the trend between high Nb/U and Ce/Pb ratios (up to 80 and 44, respectively) in the ocean basalt domain (47±10 and 25±5, respectively; Hofmann et al., 1986) and the smaller values that approach the upper continental crust (4.4 and 3.7; Hawkesworth and Kemp, 2006) (Fig. 7a). Strontium contents vs. initial 87Sr/86Sr ratio plot (Fig. 7b) show that the AIP alkaline silicate rocks were derived from carbonatitic parent magma, and may have experienced an assimilation-fractional crystallization-liquid immiscibility (AFCLI) process in the crust, as shown by the AFCLI trend line (Ray, 2009).

Isotopically, the AIP alkaline rocks display low initial $^{87}Sr/^{86}Sr$ ratios (0.69021 ~ 0.70633, average 0.70285), high εNd (+1.8 ~ +4.1, average +2.9), radiogenic Pb isotopes ($^{206}Pb/^{204}Pb$ = 18.604 ~ 23.537, average 19.786; $^{207}Pb/^{204}Pb$ = 15.389 ~ 15.615, average 15.572; $^{208}Pb/^{204}Pb$ = 35.781 ~ 39.447, average 38.824), and positive εHf (+2.0 ~ +9.8, average +5.9) (Fig. 8) (Duke et al., 2014; Tilton et al., 1987). On Sr-Nd isotope diagrams (Figs. 8a and 8b), they plot in the OIB field and overlap the Arkansas carbonatites. The alkaline rocks and carbonatites also present a mixing trend on Pb-Pb, Nd-Pb, and Hf-Nd isotope diagrams (Figs. 8c-8f).

Together, these isotopes indicate a mixed origin of HIMU, FOZO, and EM components, suggesting a common parental magma with the carbonatites that originated from the sub-lithospheric mantle. In contrast to the earlier-emplaced carbonatites and nephelinites, the younger phonolites show greater variations in isotopic ratios, implying a complicated evolution possibly in an open, contaminating system in the crust (e.g., Bell, 1998).

2.2.4 BIP alkaline rocks

The BIP is composed of a suite of Si-undersaturated, sodic, alkaline igneous rocks (Fig. 4). It displays a bimodal pattern in terms of crystallization ages and geochemistry (Figs. 5, 6c, and 6d). The earlier group consists of olivine nephelinites, nepheline basanites, and alkali basalts, and is ultrabasic to basic, strongly alkaline, and high MgO (> 8 wt%). The younger group consists of phonotephrites and phonolites, with < 1 wt% of MgO and ca. 3-5 Myr younger crystallization age. The Mg number ranges show a decreasing trend with increasing Si contents: melilite olivine nephelinites, Mg# = 66-75; olivine nephelinites, 65-75; nepheline basanites, 63-71; alkali basalts, 53-71; and phonotephrites and phonolites, 7-46. Relationships between various oxides versus Mg number suggest that the BIP series has undergone magmatic differentiation during the emplacement (Fig. 5) (Barker et al., 1987; Griffin, 2008; Wittke and Mack, 1993).

Nephelinites, basanites, and alkali basalts in the BIP have very similar trace and rare earth element concentrations with the OIB, with minor enrichment in Ba, Nb, K, LREE, and Ti, and depletion in Rb, Zr, Hf, Eu, and HREE (Figs. 6c and 6d). The phonolites show a distinct pattern in which Ba, Sr, Ti, Eu are more depleted and Rb, Th, U, Zr, Hf, LREE, and HREE are more enriched than the high Mg# alkaline rocks. Crustal contamination of the phonolites (Mg# < 50) is clearly demonstrated on the Nb/U vs Ce/Pb diagram (Fig. 7a); Griffin (2008) suggests that up to 20% input of the granitic crustal materials may be involved in the BIP magma evolution. In contrast, contamination in most nephelinites and basanites is insignificant, as their Nb/U and

Ce/Pb ratios are still located in the ocean basalt field, and they do not follow the assimilation trend in the 87Sr/86Sr vs Sr content diagram (Fig. 7b).

The BIP shows a slightly different Sr-Nd-Pb isotope system than the AIP rocks (Fig. 8). Their initial 87Sr/86Sr ratios range between 0.70256 and 0.70530, and the average is 0.70346, comparable with the AIP alkaline rocks and carbonatites. Their εNd values are between +4.7 and +7.8, and average at +6.0, higher than AIP's values. The Pb isotopes ($^{206}Pb/^{204}Pb$ = 18.548 - 22.109, average 19.117; $^{207}Pb/^{204}Pb$ = 15.419 - 15.709, average 15.554; $^{208}Pb/^{204}Pb$ = 37.977 - 42.808, average 38.683) are hardly differentiable from the AIP rocks (except the lamproites) (Griffin, 2008; Wittke and Mack, 1993). The BIP rocks plot closely to the FOZO end-member on the Sr-Nd diagram (Figs. 8a and 8b). Their Pb-Pb and Nd-Pb isotopes further show the presence of DMM and HIMU components (Figs. 8c-e). Although the SCLM beneath BIP was metasomatized by arc-like fluids which occurred probably at ca. 1 Ga during the Grenville Orogeny (Young and Lee, 2009), ancient, metasomatized SCLM signature is absent in the BIP rocks. Instead, strong coherence of geochemical, isotopic, and geochronologic affinities among various lithologies suggest a well-mixed source comprising predominantly FOZO as well as HIMU and DMM. The BIP originated from the sub-lithospheric mantle as well.

3. Previous Models

Previous studies have formulated four families of tectonic models to explain the origin of the AIP and/or BIP in northern Gulf of Mexico (Fig. 9).

3.1 Bermuda hotspot model

Before high precision ages became available, K-Ar and Rb-Sr isochron ages of volcanic rocks in central and southern US (Kansas kimberlites and AIP) displayed a possible age progression pattern that led to the hypothesis in which the North America plate passed westward

over the Bermuda hotspot (C13, D86, and M83 in Fig. 9a) (Chu et al., 2013; Cox and Van Arsdale, 2002; Duncan, 1984; Morgan, 1983). However, recent geochronologic studies have clarified the onset of Kansas kimberlites at ca. 109-106 Ma (Blackburn et al., 2008), while AIP magmatism commenced coevally at ca. 108-106 Ma (Eby and Vasconcelos, 2009). No eastward younging trend can be easily inferred between Kansas and Arkansas. Also, the Elliott County, Kentucky kimberlites were predicted to be ca. 70 Ma in a "plume" model by Chu et al. (2013), whereas their initiation age is at least ca. 91 Ma, or even earlier (Alibert and Albarede, 1988; Heaman et al., 2004).

Moreover, the basic assumption of this model, that the Bermuda hotspot is a long-lived stationary plume of hot rock rooted at the core-mantle boundary, is also questionable because: (1) volcanism between the AIP and the Bermuda has not been detected on either continental crust or oceanic crust; (2) elongation direction of the bathymetric swell of the Bermuda Rise is highly oblique, not parallel, to the plate motion; (3) the 660 km discontinuity beneath Bermuda is anomalously 19 ± 5 km deeper than the global average, while a mantle plume should have an elevated 660 km discontinuity (Benoit et al., 2013). In short, the Bermuda hotspot is not a convincing model for the northern GoM igneous rocks.

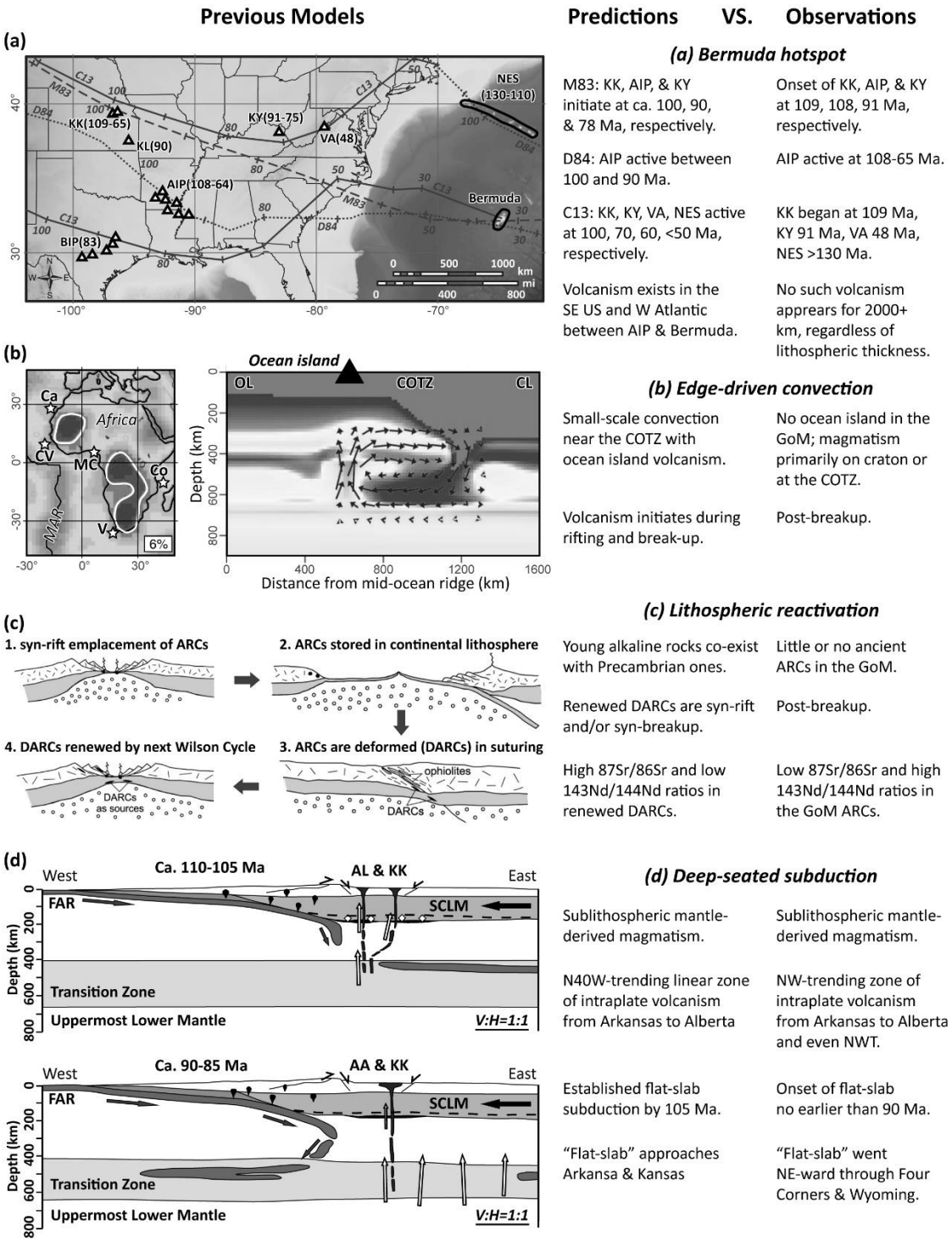

Figure 9 Summary of previous tectonic models, and a comparison of key predictions against observations. AA, Arkansas alkaline rocks; AL, Arkansas lamproites; KK, Kansas kimberlites; KL, Kansas lamproites; KY, Kentucky kimberlites; NES, New England Seamount; VA, Virginia-West Virginia alkaline rocks.COTZ, continent-ocean transition zone; FAR: Farallon plate.

3.2 Edge-driven convection

Matton and Jébrak (2009) propose the AIP is part of the Peri-Atlantic Alkaline Pulse which they suggest resulted from edge-driven convection (EDC). The EDC model, established by King and Anderson (1998), demonstrates that small-scale convective cells can nucleate in the upper mantle at the continent-ocean transition zone, as stimulated by horizontal thermal gradient between the thick continental root and thin oceanic plate (Fig. 9b). The upwelling limb of the convective cell is located underneath the oceanic plate, and the downwelling limb lies beneath the continent root (King, 2007; King and Ritsema, 2000).

A major prediction of the EDC model is that volcanism predominantly occurs within the oceanic plate hundreds of kilometers from the continent-ocean boundary. Some seamount volcanisms have been attributed to this model, including Cape Verde, Canary, Comores, and Vema islands, etc (Benoit et al., 2013; King, 2007; King and Ritsema, 2000). Despite the shallow marine settings in which BIP was emplaced (Barker et al., 1987), there is so far no evidence suggesting abundant Cretaceous volcanism exists within the GoM oceanic basin based on bathymetry, seismic and well data, or gravity surveys by Sandwell et al. (2014). Also, the EDC model predicts syn- rift to syn-breakup magmatism, which also violates the post-breakup nature of the igneous rocks in this region. We therefore suggest that the EDC model is not applicable in this region.

3.3 Lithospheric reactivation

It has long been noticed that intraplate alkaline magmatism tends to be located along preexisting zones of weakness, such as suture zones that penetrate the entire lithosphere, allowing asthenospheric sources of magma to be tapped (Phipps, 1988; Sykes, 1978). Indeed, two Wilson Cycles took place along the eastern US and northern GoM margin since the Proterozoic, including the Grenville orogeny during the assembly of Rodinia, followed by the opening of the

Iapetus Ocean, and then the Appalachia-Ouachita-Marathon orogeny during the assembly of Pangea, and finally, opening of the Atlantic and the Gulf of Mexico (Thomas, 2006). Locally, the distribution of these igneous bodies broadly coincides with the Ouachita-Marathon suture (Fig. 1). This led to hypotheses invoking lithospheric reactivation to cause alkaline magmatism (e.g., Baksi, 1997; Eby and Vasconcelos, 2009; Griffin et al., 2010; Phipps, 1988). However, this model is debatable on the timing, tectonic process, and geochemistry between predictions and observations.

The "ARCs-DARCs" model proposed by Burke et al. (2003) is probably the most persuasive "reactivation" model (Fig. 9c). In this model, alkaline rocks and carbonatites (ARCs) are emplaced in the lithosphere during continental rifting, resulting from decompression melting of elevated convective mantle. Once continents converge again, the ARCs become deformed ARCs (DARCs), preserved in suture zones. Then, the DARCs "hibernate" in the lithosphere, until they are remobilized when a new continental rifting phase begins (Burke et al., 2003). This model provides appealing interpretations for the ARCs and DARCs in the Malawi rift in eastern Africa (Ashwal et al., 2007), Kola Peninsula, Russia and Seiland, Norway (Burke et al., 2007), Ontario, Canada (Burke et al., 2008), and southern West Greenland (Tappe et al., 2009). However, it predicts syn-rift and/or syn-breakup magmatism, rather than post-breakup magmatism. The fact that crustal basement is not rich in alkalic rocks in this region (Dunn, 2002) does not favor the ARCs-DARCs model as well. Even if there exists some ancient DARCs beneath Arkansas, the "renewed DARCs" should display more radiogenic $^{87}Sr/^{86}Sr$ ratio and negative εNd value, as radiogenic isotopes accumulate with time. Moreover, decompression melting of DARCs during rejuvenation would also cause partial melting of continental crust as a by-product, because minimum melts of granitoids forms at temperatures lower than that of alkaline rocks and carbonatites (Burke et al., 2008). Few Cretaceous felsic igneous rocks are found in this region. Therefore, the ARCs-DARCs model seems unlikely to work here.

Baksi (1997) suggests that depositional loading flexed the lithosphere and induced lithospheric-scale fracture zones that function as conduits for alkaline melts beneath Arkansas. However, as pointed out by Young and Lee (2009), this mechanism is not sufficient to cause melting due to the lack of decompression of the mantle. Also, if such mechanism is viable, similar magmatism would have continued and even enhanced during the Cenozoic due to higher rates and greater amounts of sediment accumulation in the GoM (Blum and Pecha, 2014; Galloway, 2008), and we would also expect alkaline rocks in other passive margins with huge sediment wedges such as the Bengal, Indus and Amazon fans, where no such magmatism has been observed.

Decompression melting within the lithosphere is unlikely to be the primary cause for the AIP and BIP rocks. Provided metasomatized SCLM has existed for 1 Gyr or longer beneath Arkansas and Texas, the question is how they survive the Wilson cycles (Thomas, 2006) and melt only during a period of tectonic quiescence in the mid- to Late Cretaceous? Also, there are only small amounts of Jurassic syn-rift or syn-breakup volcanism in the northern and northwestern GoM (Stern et al., 2011), three or more orders of magnitude less than the post-breakup Cretaceous magmatism. How could the lithosphere alone produce more melts during thermal relaxation than during continental rifting? These outstanding questions rule out the North American lithosphere as either an ultimate driver or a primary source. While compositions and pre-existing structures in the lithosphere play an undeniable role in the emplacement of magmas, the lithospheric reactivation model is unlikely to be the driver for the northern GoM magmatism.

3.4 Deep, low-angle subduction

Previous studies have proposed that deep subduction of oceanic lithosphere is a primary driver for intraplate volcanism (Fig. 9d) (e.g., Currie and Beaumont, 2011; McCandless, 1999; Ringwood et al., 1992; Sharp, 1974; Stern et al., 2016; Tappert et al., 2009). McCandless (1999)

suggest that a weak westward-younging trend exists from eastern North America (Quebec, Ontario, and Michigan), through the central portion of the U.S. and Canada, including the Arkansas alkaline province, to the western U.S. and northwest Canada, due to dehydration of the deeply-subducted Farallon plate.

In their numerical models, Currie and Beaumont (2011) argued that the Farallon oceanic plate subducted at a low angle and had travelled 1400 km eastward along the base of the North American plate by ca. 100 Ma. Duke et al. (2014) recognized a N40 °W-trending linearity of kimberlite-carbonatite magmatism from Mississippi to Alberta, paralleling the active margin along the western North America, that were emplaced in four pulses between ca. 109 and 48 Ma. They correlate this linear trend with the fragmentation of subducted Farallon and Kula slabs, and proposed that partial melts from carbonated garnet lherzolite passively upwelled along the slab edges when the slabs penetrated the mantle transition zone (MTZ) (Duke et al., 2014).

The subduction model is appealing because it provides a conceivable explanation for the coeval, sub-lithospheric mantle-derived volcanism in the Cretaceous across the North American plate. Also, the parallelism between intraplate volcanism and convergent boundary highlights a potential linkage at plate scales. In this context, the slab geometry in Currie and Beaumont (2011) and Duke et al. (2014) is worth discussing. The conceptual tectonic model in Duke et al. (2014) is 2.7 times vertically exaggerated. Restoring it to a 1-to-1 ratio of the vertical and horizontal scales (Fig. 8d, modified from Figs. 6-1 and 6-3 in Duke et al., 2014) results in a very long, flat geometry of the subducting plate, similar to the model setup in Currie and Beaumont (2011). Such a geometry would result in a slab that becomes flat ~100 Ma, reaching farther east than the region affected by the Laramide orogeny , which is restricted to the western US during ca. 88-35 Ma (e.g. Coney and Reynolds, 1977; Copeland et al., in press; Liu et al., 2010). If low-angle subduction occurred as early as 100 Ma, arc magmatism and crustal shortening structures would have reached far beyond the North American Cordilleran orogeny, at odds with numerous

geological observations (e.g., Coney and Reynolds, 1977; DeCelles and Graham, 2015; Humphreys, 2009; Paterson and Ducea, 2015; Yonkee and Weil, 2015). In short, a modified subduction model may explain Cretaceous northern Gulf of Mexico magmatism. In the following sections I propose a tectonic and petrogenetic model which is inspired by Currie and Beaumont (2011) and Duke et al. (2014).

4. Northern Gulf of Mexico Magmatism in a Regional Context

4.1 Mesozoic-Cenozoic intraplate magmatism in North America

Cretaceous post-breakup magmatism in the northern GoM has a potential tectono-magmatic correlation with other mid-Cretaceous-early Eocene intraplate volcanism in North America. We compiled Mezosoic to Cenozoic carbonatites, lamproites, alkaline rocks, and kimberlites in North America (Fig. 10), and notice that these rocks can be broadly categorized into three groups: (1) an East province in eastern Canada and US; (2) a West province located within the Cordilleran orogeny; and (3) a Central province, extending from Arctic Canada to the northern GoM, and possibly to the southeastern US.

The East province contains Jurassic to Early Cretaceous kimberlites and carbonatites (Fig. 10) that spread from the Hudson Bay region in Canada to the New England seamount in offshore northeastern US. Their spatial-temporal distribution clearly shows an eastward younging trend, which is ascribed to the Great Meteor hotspot track. This can be envisaged by the North American plate passing over the margin of the long-lived, relatively-stable African large low shear velocity province (LLSVP, also known as “TUZO”) (Fig. 11) (Burke, 2011; Heaman et al., 2015; Torsvik et al., 2010, 2014).

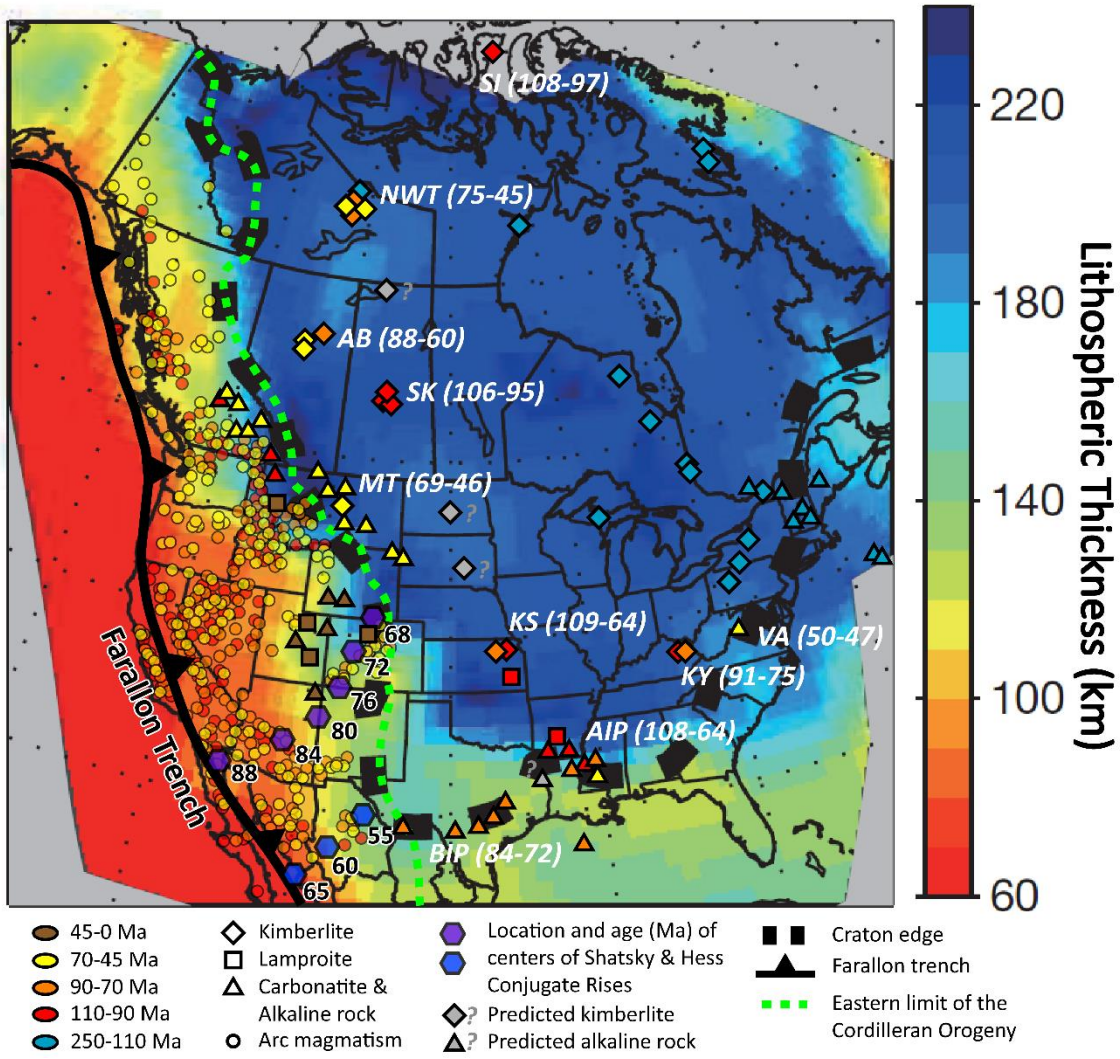

Figure 10 Map of the Mesozoic and Cenozoic carbonatites, lamproites, alkaline rocks, and kimberlites in North America. Base map is lithospheric thickness map from Yuan and Romanowicz (2010). Cretaceous-Eocene intraplate magmatic provinces are labelled, and the numbers in brackets are their age ranges. Also shown are (1) eastern limit of the Cordilleran orogeny; (2) estimated Farallon and/or Kula trench along the west margin of North American plate prior to the Basin-and-Range extension (Saleeby, 2003; Shephard et al., 2014); (3) relative locations of the centers of the Shatsky and Hess conjugate rises modelled by Liu et al., 2010, which clearly postdate most intraplate volcanism in this study; (4) arc magmatism at 110-90, 90-70, 70-50 Ma (circles filled in red, orange, and yellow, respectively) in western North America (data downloaded from NavDat.org). We also plot some predicted kimberlites occurrences in North and South Dakota, and Saskatchewan-Northwest Territories border, as well as predicted alkaline rocks that core the Sabine uplift on Texas-Louisiana border. KS, Kansas kimberlites and lamproites; KY, Kentucky kimberlites; MT, Montana-Wyoming kimberlites and alkaline suites; AB, Northern Alberta kimberlites; NWT, Northwest Territories kimberlites; SK, Saskatchewan kimberlites; BC, Southeastern British Columbia carbonatites and alkaline rocks; SI, Somerset Island kimberlites; VA, Virginia-West Virginia alkaline province.

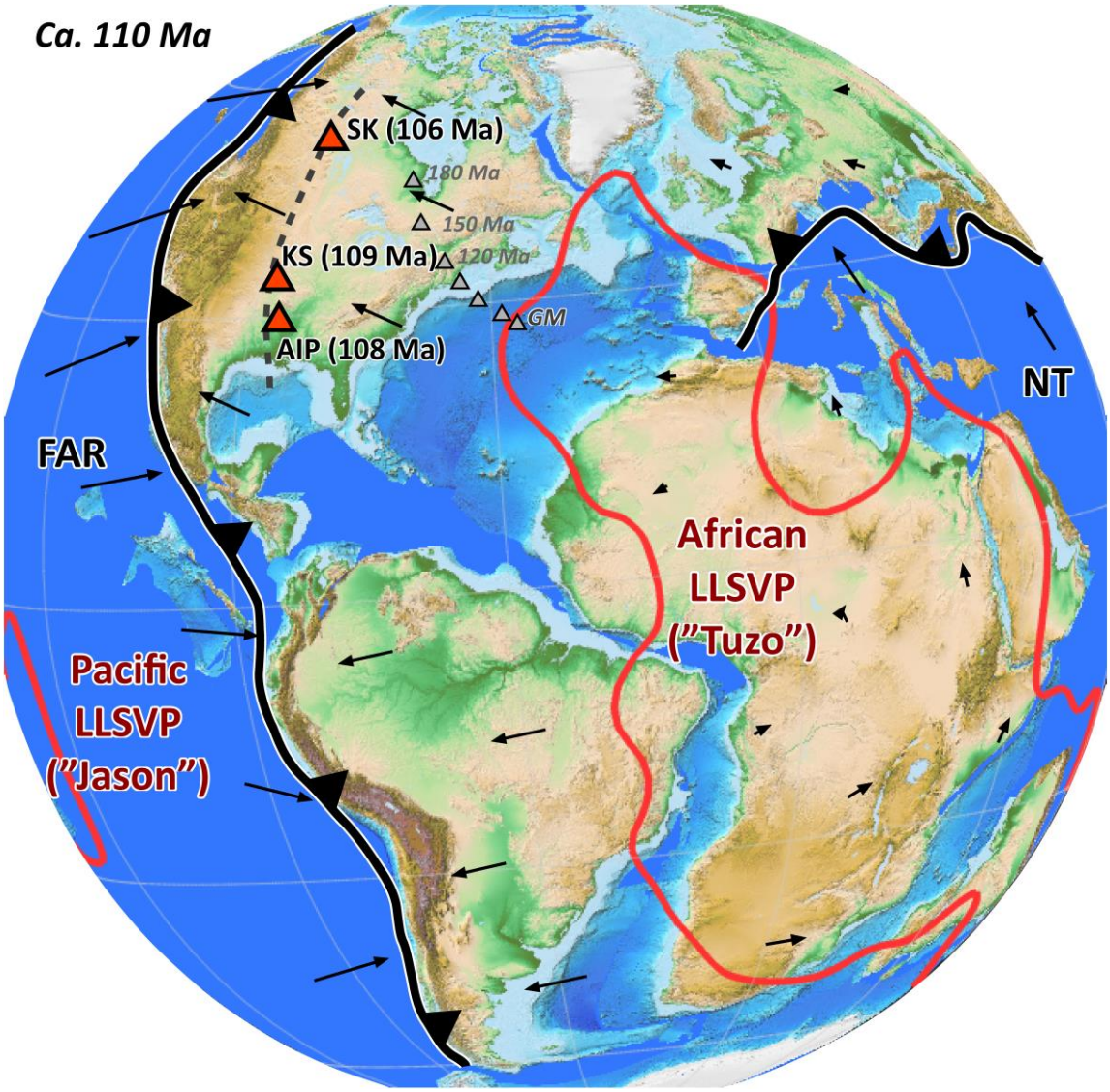

Figure 11 Plate reconstruction of the western hemisphere at 110 Ma based on Seton et al. (2012) and Shephard et al. (2013). Orange triangles denote the locations of the earliest volcanism in each igneous province: Magnet Cove lamproites in Arkansas (AIP), Riley Co kimberlite in Kansas (KS), and Fort a la Corne kimberlites in Saskatchewan (SK). Ages in brackets show the onset timing of the volcanism. Thick, black curves denote the Farallon (FAR) trench along the west margin of the Americas and the Neo-Tethyan (NT) trench along the southern margin of Eurasia. The grey, dashed line in central North America outlines the leading edge of the proposed stagnant Farallon slab. Red lines bound the surface projection of the African and Pacific large low shear velocity provinces (LLSVPs, "Tuzo" and "Jason", respectively) at the core-mantle boundary (Burke, 2011; Torsvik et al., 2014). Grey triangles represent the Great Meteor hotspot track in the eastern North America (cf. Heaman et al., 2000, 2004), which is interpreted to be generated from the African LLSVP. Note the significant difference in spatial-temporal distributions of the Great Meteor hotspot track from the central North American volcanism.

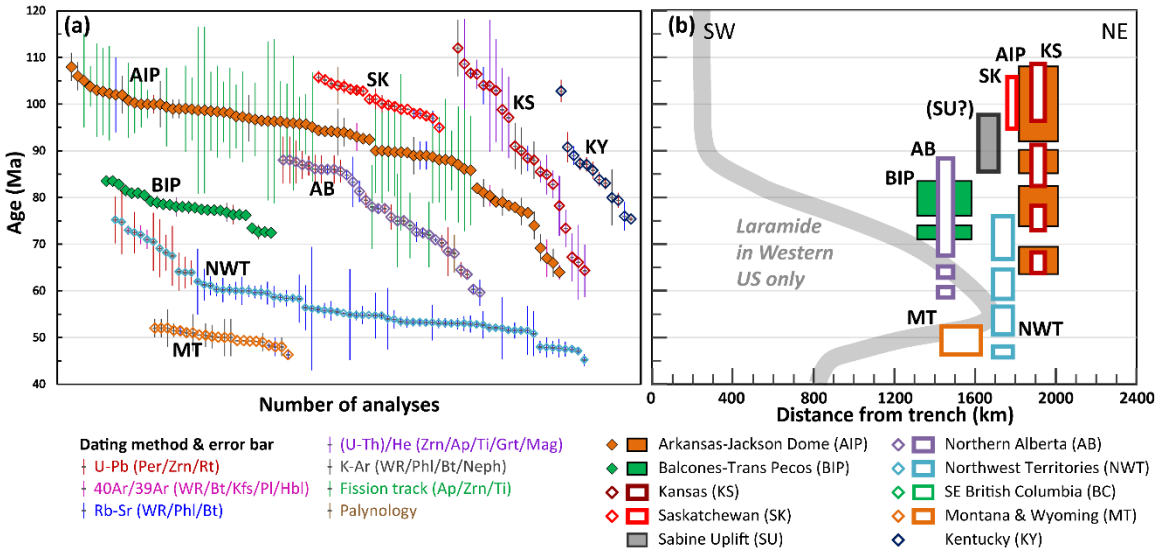

Figure 12 Summary of published geochronologic dates of the AIP and BIP rocks, as well as other intraplate magmatic provinces in North American mid-continent from mid-Cretaceous to Eocene. (a) Published geochronologic data of each igneous province, arranged in decreasing order from left to right. Dating methods are shown by different colors of the error bar (2 sigma). Note that this figure (a) does not intend to show any spatial relationships among different igneous provinces. Data sources are same as the Figure 10. Abbreviations: Ap, apatite; Bt, biotite; Grt, garnet; Hbl, hornblende; Kfs, K-feldspar; Mag, magnetite; Neph, nepheline, Per, perovskite; Phl, phlogopite; Pl, plagioclase; Rt, rutile; Ti, Titanite; WR, whole rock; Zrn, zircon. (b) Time span of the intraplate igneous provinces and their distances from the Farallon/Kula trench along the west margin of North America. Thick grey curve in (b) is an outline of the Laramide-related deformation and magmatism, which is constricted in the western US only (modified from Copeland et al., in press, and references therein). Note that the onset timing of the Arkansas-Jackson Dome, Kansas, and Sasckatchewan igneous provinces clearly predates the Laramide orogeny and associated flat-slab subduction. Geographically, most of these provinces are not related to the Laramid Orogeny, either, except for the Montana alkaline province. Note that the Elliott County, Kentucky, kimberlite province is not plotted on (b) since it is ca. 3000 km from the Farallon trench. We predict that the Sabine Uplift (SU) is cored by alkaline rocks and abridges the AIP and BIP, and plot it as a grey box.

The western province within the Cordilleran orogeny domain is characterized by a mixed age pattern in convergent margin settings (Fig. 10). Alkaline rocks and lamproites on the Colorado Plateau, which are all younger than 45 Ma, are generated by removal of the Farallon flat-slab and/or Basin-and-Range extension (e.g., DeCelles et al., 2009). Alkaline rocks and carbonatites in British Columbia and northwestern Montana yield Late Cretaceous to Eocene

ages, and may record a complex history of arc magmatism and metamorphism related to Farallon/Kula subduction (Millonig et al., 2012).

The central province consists predominantly of Cretaceous-Eocene intraplate volcanic rocks. Heaman et al. (2004) named it the "Cretaceous Corridor" based on kimberlite distributions, which is supported by our compilation in Fig. 10. The Cretaceous Corridor igneous rocks span the mid-continental North America, including, from north to south, the Lac de Gras and Ekati kimberlites in Northwest Territories (NWT, 75-45 Ma), the Buffalo Head Hills and Birch Mountain kimberlites in north-central Alberta (AB, 88-60 Ma), the Fort à la Corne kimberlites in Saskatchewan (SK, 106-95 Ma), the Great Plain alkaline province that spans southernmost Alberta, central Montana, northeast Wyoming and western South Dakota (MT, 69-46 Ma), the Riley County kimberlites and Woodson/Wilson County lamproites in Kansas (KS, 109-64 Ma), the AIP in Arkansas, Louisiana, and Mississippi (108-64 Ma) and the BIP in Texas (84-72 Ma) (Fig. 12) (for references, see figure captions).

The central province also includes (1) the Somerset Island kimberlites in Arctic Canada (SI, 108-97 Ma), which are products of the Cretaceous High Arctic large igneous province (Heaman et al., 2004); (2) the Late Cretaceous kimberlites in Elliott County, Kentucky (KY, 91-75 Ma), which is suggested to result from a mantle plume (Chu et al., 2013), although this hypothesis is questionable as discussed in previous section; and (3) an Eocene alkaline province on the border of Virginia and West Virginia (VA, 50-47 Ma) which may be caused by a localized lithospheric delamination (Mazza et al., 2014).

Plate reconstruction shows that by 110 Ma, the "Cretaceous Corridor" igneous rocks were already thousands of kilometers from the African LLSVP (Fig. 11) (Shephard et al., 2013). We found no evidence of an east-younging age progression pattern associated with them, and therefore suggest that they are not correlated with African LLSVP-derived plumes. Instead, these igneous rocks are aligned within a NW-trending linear belt that is ca. 1300-1900 km away from

the convergent margin along western North America, indicating a potential link to the Farallon subduction factory (Figs. 10 and 11; for data references see the caption of Figure 10) (Currie and Beaumont, 2011; Duke et al., 2014; Heaman et al., 2004, 2015).

4.2 Origin of the Cretaceous Corridor magmatism

The genetic relationships among kimberlite, carbonatite, and alkaline rocks have long been investigated (e.g., Canil and Scarfe, 1990; Dalton and Presnall, 1998). Some melting experiments lend supports to a primary carbonatite-kimberlite melt continuum (e.g., Brey et al., 2008; Dalton and Presnall, 1998; Gudfinnsson and Presnall, 2005); others propose a hybrid, heterogeneous carbonate-silicate ("proto-kimberlite") magma as the primary source from which carbonatite melt is separated (e.g., Brooker, 1998; Kiseeva et al., 2013). In either case, it is reasonable to consider the intraplate igneous rocks across the mid-continent of North America as a whole when exploring their tectonic-magmatic mechanism.

A common characteristic of the "Cretaceous Corridor" igneous rocks is significant involvement of sub-lithospheric mantle in their origins. This is illustrated by their lithology and Sr-Nd isotopes (Figs. 8a and 8b), pristine kimberlites in Kansas, Saskatchewan, Alberta, Northwest Territories, Montana, and Kentucky all plot between the FOZO and EM-I or EM-II components in the OIB domain, showing a convective mantle origin.

The Prairie Creek, Arkansas lamproites were conventionally interpreted as partial melts of garnet lherzolites in the metasomatized SCLM, because of their highly enriched incompatible elements, radiogenic Sr isotopes and low εNd values (Gogineni et al., 1978; Lambert et al., 1995). Nevertheless, Pb isotopes of the lamproites challenge the SCLM origin. Worldwide, intraplate lamproites including the Arkansas, Gaussberg, Leucite Hills, Smoky Butte, West Australia, and West Greenland ("Group I" lamproites by Foley et al., 1987) all show unusual Pb isotopic ratios that plot to the left of the meteorite isochron and above the terrestrial evolution line in the

207Pb/204Pb vs. 206Pb/204Pb diagram (Fig. 8c; data sources in the figure caption), whereas average marine sediments and MORBs plot to the right of the meteorite isochron, which requires a hidden Pb reservoir on the other side of the isochron. To solve this so-called "first terrestrial Pb paradox", Murphy et al., (2002, 2003) proposed a three-stage model for the origin of the Pb isotope signature in lamproites and other OIBs: (1) continental-derived sediment subduction to the MTZ or lower mantle, followed by (2) the mantle mineral assemblages stored as an isolated reservoir for ~2 Gyr, until finally (3) mantle upwelling entrains this isolated "lamproitic" reservoir and generates lamproites. High-pressure experiments on marine mud and metapelite at 16-23 GPa support this model by demonstrating that the source of lamproites may contain an EM1-type reservoir of ancient, recycled (subducted), K-hollandite-bearing continental sediments at the MTZ depths (Rapp et al., 2008). Moreover, the Arkansas lamproites appear to display Hf-Nd decoupling (Fig. 8f), although limited current data samples (four analyses) are not sufficient to confirm this speculation. If it exists, it can be also explained by long-term storage and isolation of ancient subducted sediments in the MTZ (Tappe et al., 2013). In short, we ascribe the Arkansas lamproites as derivations from the "lamproitic" reservoir in the MTZ, as described by Murphy et al. (2003) and Rapp et al. (2008).

The AIP carbonatites, lamprophyres, and associated alkaline rocks hold OIB-like signature in their trace element, radiogenic isotope and stable isotope systems. They are isotopically similar to many other carbonatites in East Africa, South India, Cape Verde, and Canary Islands, as well as oceanic island basalts and Group I kimberlites worldwide, and they usually plot close to the HIMU-EM1 mixing trend as defined by OIBs (Fig. 8a and 8b), pointing to a sub-lithospheric mantle origin (Bell and Tilton, 2001; Bell and Simonetti, 2010). The BIP nephilinites and syenites also are derived from the convective mantle, based on trace elements and Sr-Nd-Pb isotopes as presented in Fig. 8 and Section 2.2.4 (Griffin, 2008; Wittke and Mack, 1993).

An engaging discovery is the discovery of mantle transition zone diamonds in the Lac de Gras kimberlites, Northwest Territories (Davies et al., 2004a). In addition, extreme Nd-Hf isotope decoupling in the kimberlites led Tappe et al. (2013) to propose that the presence of ancient, OIB-bearing, subducted oceanic crust in the mantle transition zone is responsible for the mixing of isotopically distinct melt components (Tappe et al., 2013). Eastward subduction of the Farallon plate during the Late Cretaceous could have induced faster convective flow and facilitated the entrainment of recycled materials from the MTZ into the upwelling kimberlitic melts (Tappe et al., 2013).

Moreover, diamonds from the Buffalo Head Hills kimberlite field in northern Alberta also contain a collection of deeply-derived mineral inclusions, such as majoritic garnet, ultradeep ferropericlase, peridotitic fosterite, and eclogitic and websteritic clinopyroxene (Davies et al., 2004b). The diamonds have low nitrogen concentrations, and their inclusions show a wide range of carbon isotope values ($\delta^{13}C$ between -2.6‰ and -20.6‰) with two peaks at ca. -5‰ and -10‰ (Davies et al., 2004b). This implies a mixed source including mantle carbon and organic carbon, indicating the presence of recycled oceanic crust in the MTZ or uppermost lower mantle (Cartigny, 2005; Davies et al., 2004b; Walter et al., 2011).

The kimberlites, carbonatites, and Group 1 alkaline rocks in Montana (as defined by Duke et al., 2009) also plot along the mantle array on Sr-Nd isotope diagram and closely to the bulk silicate Earth-chondrite intersection, suggesting a dominant asthenospheric origin (Duke et al., 2009; O'Brien et al., 1991, 1995) (Fig. 8b). The Group 2 and 3 alkaline rocks in Montana, despite being largely derived from partial melting of mantle lithosphere, show an increasing trend of an asthenospheric component, due to continuous heating from the upwelling asthenosphere (Dudas, 1991; Duke et al., 2009).

Because the "Cretaceous Corridor" igneous rocks share a common origin from the sub-lithospheric mantle, any model that attempts to explain the AIP, BIP, and other "Cretaceous

Corridor" rocks needs to address their timing (mid-Cretaceous to early Eocene), location (intraplate), lifespan (ca. 20-40 Myr), and source (sub-lithospheric mantle) in a tectonically-viable regime. The MTZ, in particular, plays a key role.

5. Stagnant Slab Model

I propose a "stagnant slab" model to explain the northern GoM post-breakup magmatism that also has implications for other intraplate volcanism across central North America. The model consists of four major steps:

(1) The Farallon slab subducts eastward at a moderate angle while the trench retreats westward. Dehydration and decarbonation takes place in the subduction factory.

(2) Subducted Farallon slab stagnates in the mantle transition zone (MTZ). Leading edge of the slab reaches 1000-2000 km inboard from the trench, and undergoes decarbonation and dehydration. The transition zone mantle surrounding the slabs becomes heterogeneous.

(3) As the stalled slab breaks into fragments and descends into the lower mantle, slab fragments induce gravitational instabilities and passive upwelling from the MTZ depth. The upwelling entrains the ancient "lamproitic" and newly-generated carbonatitic melts and rises from the MTZ to the base of the lithosphere.

(4) The buoyant upwelling mantle experiences decompression melting and exploits lithospheric weaknesses during ascent. As the upwelling interacts with overriding lithosphere of varied thicknesses and compositions, kimberlites, carbonatites, and alkaline rocks are produced in different settings.

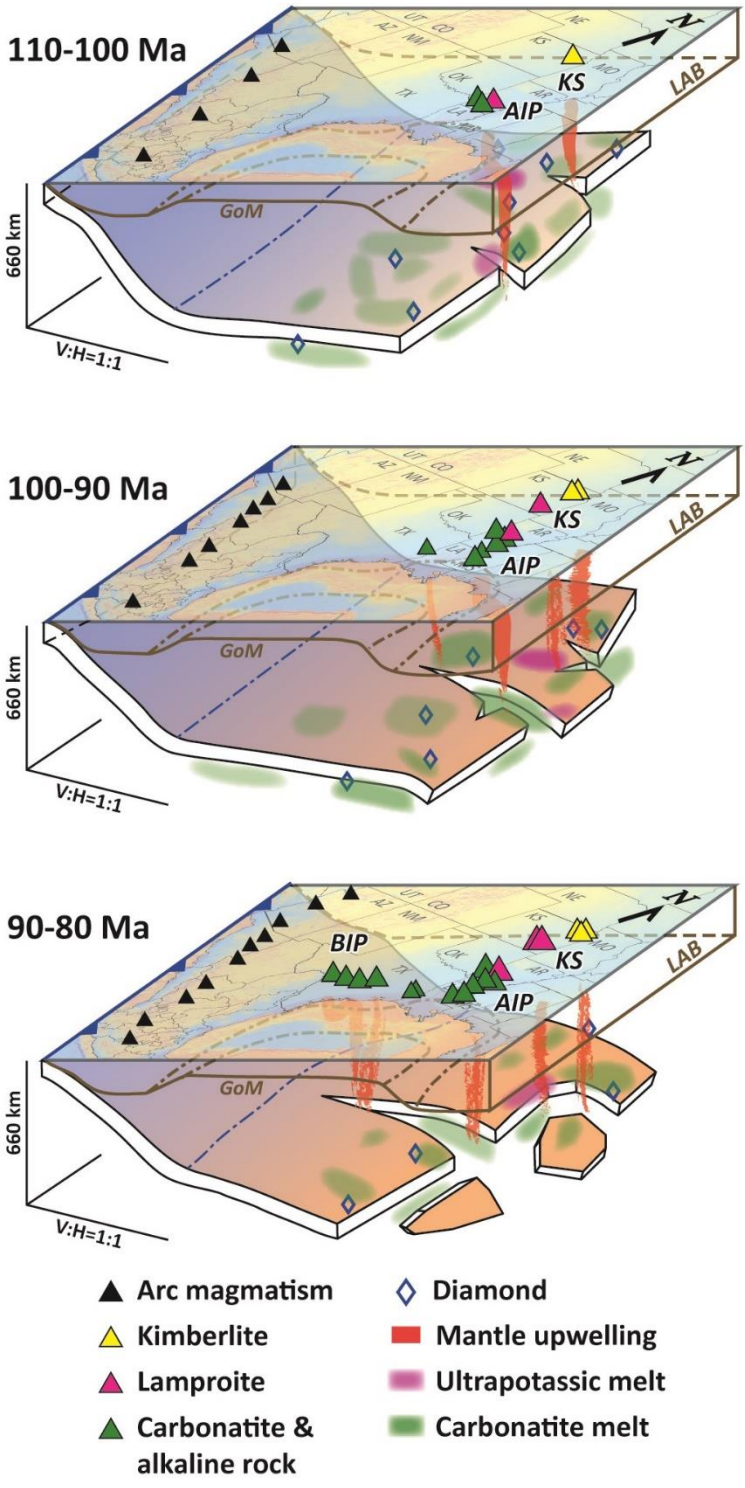

Figure 13 Three-dimensional block diagrams illustrating the geometry and geological processes of the stagnant slab model. View is towards the northwest, looking across the northern Gulf of Mexico to the Four Corners area. This figure schematically shows a series of processes including normal subduction, stagnation, dehydration, decarbonation, redox freezing, slab fragmentation, instability-induced upwelling, redox melting, and emplacement in the overlying plate.

5.1 Step 1: Farallon subduction during the Early Cretaceous

My model is built upon the widely-accepted conception of eastward subduction of the Farallon oceanic plate since, at least, the Early Cretaceous (e.g., Bird, 1988; Coney and Reynolds, 1977; DeCelles and Graham, 2015; Liu et al., 2010; Yonkee and Weil, 2015). An alternative model that advocates a westward Panthalassic (or Angayucham-Mezcalera) subduction prior to the eastward Farallon subduction has been proposed (Hilderbrand, 2009; Sigloch and Mihalynuk, 2013). A comprehensive review that evaluates these two models, unfortunately, is beyond the scope of this paper.

To the south of 50˚N, the Farallon plate has been subducting eastward continuously since at least 140 Ma or even earlier (e.g., DeCelles, 2004; Dickinson, 2004; Engebretson et al., 1985; Shephard et al., 2013). North of 50˚N, by 140 Ma, the eastward Farallon subduction is also established, following the closure of the Cache Creek Ocean and accretion of the Wrangellia superterrane onto the Laurentian continent (e.g. Shephard et al., 2013). Given an averaged orthogonal convergence rate of ca. 7 cm/yr (Müller et al., 2016), there can be 1750 km-long Farallon slab subducted beneath the North American plate within 25 Myr, i.e., from 135 Ma to 110 Ma. This satisfies the spatial requirements for a stagnant slab geometry (Fig. 13).

At 130-100 Ma, the subducting Farallon plate is ca. 70-90 Myr old according to recent plate reconstruction models by Seton et al. (2012) and Müller et al. (2016). Present-day subducting plates with similar ages typically dip 50˚±5˚ in subduction zones (Syracuse et al., 2010). This narrow range of subduction angle reflects a relatively cold, stable thermal status of the slab. Also, Andean-type arc magmatism and retroarc deformation are confined to within 300 km from the active margin, from the Coast Mountains in British Columbia to Sierra Nevada, California and Peninsular Ranges in Baja California (e.g., DeCelles, 2004; DeCelles and Graham, 2015; Dickinson, 2004; Paterson and Ducea, 2015). We therefore infer that the dip of the Farallon slab during the Early-Cretaceous is ca. 50˚, i.e. an intermediate subduction angle.

We assume that Farallon oceanic crust is altered by hot hydrothermal fluids and carbonate precipitation in fractures (Shilobreeva et al., 2011); therefore it stores water and carbon prior to its arrival in the Farallon trench. In the subduction zone, the "wet" Farallon slab can release more than 95 wt% of its water to the mantle wedge and overriding plate, leaving the residual slab "damp" (Dixon et al., 2002). The remaining small amount (up to 4 wt%) of water is carried to sub-arc depths via ultra-high pressure mineral phases and/or nominally anhydrous silicates, assisted by its relatively cold temperature and fast subduction rate (e.g. Schmidt and Poli, 2014; van Keken et al., 2011). In the meantime, at least 40% of carbon in the altered oceanic crust is released by decarbonation processes via carbonate dissolution in fluids (Dasgupta and Hirschmann, 2010) and hydrous carbonatitic liquid (Poli, 2015). In a cold subduction regime, altered oceanic gabbro can store H_2O and CO_2 in hydrous silicate and carbonate minerals (lawsonite + dolomite + magnesite) and carry them to sub-arc depths (Fig.14) (Poli, 2015). In a warm thermal regime of subduction, altered gabbro loses carbon into the mantle wedge by generating hydrous carbonatitic liquid from carbonate-rich aqueous vapor (Poli, 2015). Carbonated metapelite, which represents the oceanic sediments atop the slab, melts at ca. 6-9 GPa, or 200-280 km, because its melting curve has a negative Clapeyron slope at this depth which makes intersection with the subduction slab easier (Fig. 14) (Grassi and Schmidt, 2011). The remaining carbon and water are transported to the deep upper mantle by carbonated oceanic crust (eclogite) (e.g., Hammouda, 2003).

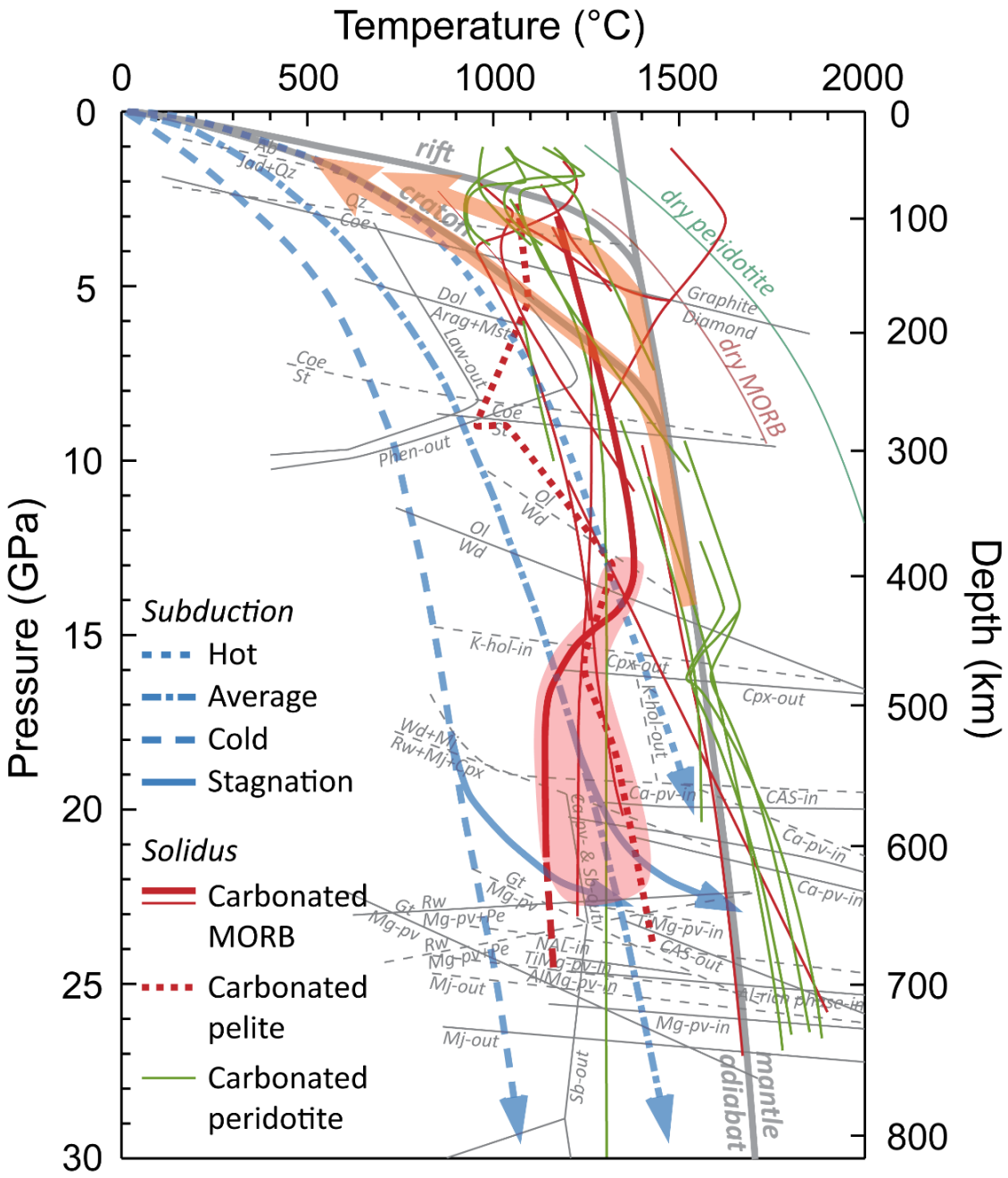

Figure 14 Integration of melting curves of carbonated oceanic crust (MORB), oceanic sediment (pelite), and peridotite, compared with P-T paths of hot, moderate, and cold oceanic slab subduction, solidi of dry MORB and peridotite, and phase boundaries. Solidi of carbonated MORB (thin, red curves) and carbonated peridotite (thin, green curves) are from Hammouda & Litasov (2015) and references therein; thick, red curve is the solidus of carbonated oceanic crust from Thomson et al. (2016); red, dotted curve is the solidus of carbonated pelites from Grassi & Schmidt (2011). Phase boundaries are from Litasov et al. (2013), Karato (2015), and references therein. Upwelling paths are shown as orange curves. Subduced slabs with average temperature can intersect the melting curves, producing carbonatitic melts in the MTZ.

5.2 Step 2: Stagnation, decarbonation, and dehydration in the mantle transition zone

Modern-day geophysical observations lend support to my hypothesized stagnation geometry of the Farallon slab. Global and regional seismic tomography studies reveal that a subducted slab can stagnate above, within, or below the MTZ that is bounded between two seismic discontinuities at 410-km and 660-km ("d410" and "d660" hereafter, respectively) (e.g., Fukao et al., 1992, 2001; Fukao and Obayashi, 2013; Zhao et al., 2009). The depth range for slab stagnation also broadly corresponds to the Bullen transition region (400-1000 km) (cf. Fukao et al., 2001). Statistically, older, colder, denser oceanic slabs tend to stagnate within or around the MTZ, whereas younger, warmer oceanic slabs buckle and thicken more readily, facilitating fast penetration through the d660 (Fukao and Obayashi, 2013; Goes et al. 2008; King et al, 2015). Several mechanisms play a crucial role in slab stagnation, including the endothermic phase change at the d660 (e.g., Litasov and Ohtani, 2005; Tackley et al., 1993), abrupt viscosity increase by 1 to 3 orders of magnitude from upper to lower mantle (Bunge et al., 1997; Karato and Wu, 1993; Panero et al., 2015), density crossovers between eclogite and peridotite (Hirose et al., 1999), and slow diffusion of the low-density metastable pyroxene to majorite-garnet in cold slabs (Agrusta et al., 2014; King et al., 2015; van Mierlo et al., 2013). Rapid trench retreat also provides a preferable tectonic environment for the stagnation (Billen, 2010; Christensen, 1996; Goes et al., 2008). Therefore, it is feasible to envision the stagnation of the Farallon slab during Early to mid-Cretaceous.

Stagnated slabs undergo decarbonation in the MTZ. Figure 14 shows a compilation of solidi of carbonated peridotite and carbonated eclogite (modified from Hammouda and Keshav, 2015 and references therein; Thomson et al., 2016). The carbonated eclogite solidi are systematically lower than the carbonated peridotite solidi. Particularly, most slabs, especially the stagnated ones, will intersect a portion of negative or near-zero dT/dP on the melting curve of carbonated eclogite at the MTZ depths (red, thick curve in Fig. 14), leading to substantial release

of the remaining carbon from the slabs to the surrounding mantle (Thomson et al., 2016). Subsequently, the expelled carbonatite melt is mixed into the mantle and may either be reduced to diamond through a "redox freezing" reaction, due to the reducing environment in deep mantle (Rohrbach and Schmidt, 2011), or be preserved as carbonatitic melts, since the melting curves of Na2CO3 and CaCO3 almost overlap the mantle geotherm at the MTZ pressures (Li et al., 2016). The diamonds that contain transition zone mineral inclusions in the Northwest Territories and Alberta kimberlites have probably grown in this way.

Dehydration also takes place in "damp" slabs. Water solubility of the transition zone minerals (i.e., wadsleyite and ringwoodite) is an order of magnitude higher than that in the upper and lower mantle (see Hirschmann, 2006 and references therein). This forms the foundation of the "transition-zone water-filter" model (Bercovici and Karato, 2003; Karato et al., 2006) which predicts two scenarios for ascending mantle materials of different upwelling rates and/or temperatures: (1) the MTZ filters out water and incompatible elements into dense, hydrous, alkaline melts atop the d410 when ambient mantle rises up slowly, leaving depleted mantle that fuels MORBs, or, (2) the transition zone water filter can be surpassed if the upwelling is either hot or fast, thus, upwelling preserves enriched, OIB-like signature and geochemical heterogeneity. During the stagnation stage, dense, hydrous, alkaline melts accumulate and cause local convections around the slabs (Richard and Bercovici, 2009); but in general, because of their slightly-higher density than the surrounding mantle, these melts tend to be sequestered atop the d410 (Jing and Karato, 2009; Matsukage et al., 2005), until perturbed by an intense upwelling.

This stage is characterized by slab stagnation, decarbonation, and dehydration in the MTZ (Fig. 13). Carbonatite and alkaline melts coexist at the MTZ depths, occasionally with the presence of a "lamproitic" component (i.e., an EM1-type reservoir of ancient, recycled (subducted), K-hollandite-bearing continental sediments), forming heterogeneous mantle in the MTZ.

5.3 Step 3: Sinking slab-induced instabilities and upwelling

Most stagnated slabs will eventually sink into the lower mantle, as the low-density, metastable pyroxene gradually becomes denser majorite-garnet as the slab warms (Agrusta et al., 2014; King et al., 2015; van Mierlo et al., 2013). Slabs can also tear apart along directions that are parallel, perpendicular, or oblique to the trench (Obayashi et al., 2009; Wortel and Spakman, 2000). Stagnant slabs become convectively unstable after tens of million years of stagnation due to heating and preexisting heterogeneities. As the denser, eclogitic slabs separate from the harzburgitic slabs and sink into the lower mantle, Rayleigh-Taylor instabilities are induced, and passive upwelling ensues along slab toes and edges (Fig. 13) (Motoki and Ballmer, 2015).

Upwelling entrains not only the hydrous alkaline melts beneath the d660 and atop the d410, but also the diamonds "frozen" in the mantle around slabs, and any "lamproitic" component in the MTZ. Redox melting, an inverse reaction to the redox freezing, transforms diamonds back to carbonatitic melts when the upwelling crosses the MTZ (Rohrbach and Schmidt, 2011). About 1 wt% of carbonatitic melt is estimated to exist in such upwellings (Rohrbach and Schmidt, 2011), which absorb incompatible elements and become highly enriched. The upwelling is possibly accelerated from an "ordinary" ascending rate of 10s of centimeters per year (Gerya and Yuen, 2003) to a very fast rate on the order 10-100 m/yr (Connolly et al., 2009). Buoyant decompression melting can accelerate the upwelling by building a positive feedback between upward motion and increased buoyance of the mantle upwelling (Raddick et al., 2002). The extremely low viscosity (10-3-10-2 Pa s) and low density (ca. 2050-3200 kg/m^3) of carbonatite melts facilitates rapid upwelling (cf. Hammouda and Keshav, 2015).

This ascending mantle, with very low degree of partially-molten, heterogeneous, highly enriched melts, upwells along the mantle adiabat and arrives at the base of the overriding lithosphere (Fig. 12).

5.4 Step 4: Magma emplacement in the lithosphere

While we favor a deep (MTZ) origin for the "Cretaceous Corridor" igneous rocks from GoM to NWT, we acknowledge that the North American lithosphere plays a significant role in guiding the emplacement and controlling the presence and absence of certain rock types.

5.4.1 Lithology controlled by lithospheric thickness and composition

A phenominal observation in Fig. 10 is that lithospheric thickness appears to exert a first-order control on the presence or absence of certain rock types. The map in Fig. 10 shows that kimberlites, particularly diamondiferous ones, are emplaced in the thickest cratonic lithosphere, whereas carbonatites and alkaline rocks are emplaced near cratonic edges separating thicker lithosphere from thinner lithosphere. The apparent thickness control on composition and lithology has been demonstrated in oceanic island basalts (Humphreys and Niu, 2009), mantle plume-related volcanism in eastern Australia (Davies et al. 2015), and the North Atlantic Igneous Province (Hole and Millett, 2016).

Many petrologic experiments have shown a continuum between kimberlitic and carbonatitic melt compositions, suggesting petrogenetic links between kimberlites and carbonatites in the mantle source with different melt fractions (<1% and <0.5%, respectively) (Dalton and Presnall, 1998; Hirose, 1997; Gudfinnsson and Presnall, 2005). The discovery of carbonatitic inclusions that are quenched in xenoliths from the Lac de Gras kimberlites, Northwestern Territories provides direct evidence for the carbonatitic origin of kimberlites (Van Achterbergh et al., 2002).

Provided a shared source, how does the continental lithosphere control the final rock types? According to Russell et al. (2012), kimberlites are formed from carbonatitic melts that assimilate orthopyroxene while rising through the cratonic lithosphere. Cratons usually contain a higher fraction (~15-30%) of orthopyroxene and thicker lithospheric mantle (ca. 90-120 km or

greater) than other lithosphere; thus, the carbonatitic melts moving through them have more opportunities to release dissolved CO2 thoroughly, and generate kimberlites with violent eruptions. By contrast, carbonatitic melts will be preserved and emplaced as carbonatites if the lithosphere is thinner in thickness (such as on a cratonic edge) or poor in orthopyroxene content, due to insufficient assimilation reactions.

Furthermore, the "carbonate ledge" at ca. 100 km depth with negative or flat dT/dP slopes (Fig. 14) can prevent carbonatite magma from reaching the surface, unless the ascent rate is either very fast or hot enough to overcome the reaction at the carbonate ledge (Hammouda and Keshav, 2015, and references therein). In thick cratons, the assimilation reaction accelerates the magma to an extremely rapid rate of ca. 20 m/s (Wilson and Head Iii, 2007); therefore, the carbonate ledge can be surpassed, and kimberlites dominated the entire igneous provinces from Northwest Terriroties to Kansas. On the contrary, carbonatites are present in the early stage of AIP magmatism but absent in the late stage, possibly because the thinner lithosphere failed to accelerate the magma fast enough to escape the ledge after the early, fast and/or hot, pulses. As the orthopyroxene was consumed, some carbonatite melts, especially the younger ones, became alkaline silicate in composition, and gave rise to the alkaline rocks. For BIP, the thickness of the lithosphere is 100 km or less, based on two independent studies on mantle xenoliths geochemistry and Sp receiver functions (Ainsworth et al., 2014; Young and Lee, 2009); therefore, the reactions at the carbonate ledge likely took place at the very bottom of the lithosphere and totally degassed the carbonatite melts, leaving only alkaline melts to form the carbonatite-free BIP rocks on surface.

5.4.2 Emplacement guided by lithospheric structures

Locally, the AIP and BIP are proximal to the Ouachita-Marathon suture along the northern GoM (Cox and Van Arsdale, 2002; Griffin et al., 2010). While the reactivation model

for their genesis has been ruled out, lithospheric structures still play an undeniable role in their emplacement.

Relief of the lithosphere-asthenosphere boundary can guide buoyant upwelling material to flow laterally toward thinner lithosphere (Sleep, 2008). We suggest that the BIP, which is characterized by an arcuate shape and coeval emplacement along its strike, is emplaced under this scenario: upwelling mantle reached the base of the Llano uplift in central Texas where lithosphere is ca. 120 km thick, and flowed radially and laterally to the south, southeast, and east, to the outskirt of the Llano Uplift where lithosphere is less than 100 km thick (Ainsworth et al., 2014; Young and Lee, 2009). The AIP, which shows a gentle southward younging trend on map view, also suggests the occurrence of lateral flow from thick to thin lithosphere (Schaeffer and Lebedev, 2014). Moreover, almost all diamondiferous kimberlite fields in Canada overlie areas of steep slopes at the base of thick, cratonic lithospherie (Faure et al., 2011), consistent with Sleep's (2008) model.

In addition, a recent seismic tomography study in the New Madrid seismic zone in the Reelfoot rift, southeastern U.S. imaged a low velocity anomaly that bends into the rift at the base of lithosphere (Figs. 13 and 14 in Chen et al., 2014). Some round-shaped gravity high anomalies in the subsurface have been interpreted as igneous bodies of unknown ages, potentially derived from this upwelling (e.g., Ewing, 2009). Forte et al. (2007) also suggested that the seismicity in the New Madrid seismic zone could be induced by localized passive upwelling induced by sinking Farallon slabs. While this study focuses on the Cretaceous magmatism and tectonics, it is possible that small-scale convection in the upper mantle continues to modern day, triggered by younger, smaller Farallon fragments that are currently stagnant in the MTZ, as imaged and interpreted by Sigloch (2011).

Once magma starts to infiltrate the lithosphere and rise, its ascent is guided by pre-existing lithospheric discontinuities. Spark et al. (2006) suggested that magma exploits fractures

in lithosphere and ascends as dike networks. Particularly, for carbonatite magmas whose viscosities are extremely low, pre-existing lithospheric structures should exert a strong control on their paths from the mantle to the surface. Younger melts could rise to the surface with less interaction with country rocks by taking advantage of the conduit formed by the earlier melts, which explains the increasing contribution of sub-lithospheric mantle components in the AIP as well as the Great Plain alkaline province in Montana and adjacent areas (Duke et al., 2014).

Therefore, lithospheric structures play an important role in guiding magma emplacement in the overriding lithosphere, although they have little to do with the original genesis of the magma.

6. Two-dimensional Kinematic Reconstruction along 30 ℕ

If the stagnant slab exists, we would expect to see the once-stagnated slab in the lower mantle, east of the Laramide-age Farallon slab. East-dipping high velocity anomalies at ca. 660-1800 km depths beneath central and eastern US, annotated as "m" by Shephard et al. (2013) (Fig. 15), are commonly interpreted as remnants of subducted Farallon slab (e.g., Grand, 2002; Schmandt and Lin, 2014; Van der Hilst et al., 1997). Further east and deeper, a flat-lying high velocity anomaly at ca. 1600-2200 km depth beneath the East Coast of the U.S. (ca. 30˚N, 45˚W-70˚W) has been detected by various seismic tomography models (Fig. 14, 0 Ma) (Grand, 2002; Li et al., 2008; Ritsema et al., 2011; Simmons et al., 2010;). We interpret that this anomaly, annotated as "p" by Shephard et al. (2013), represents the stagnated Farallon slab that subducted in Early Cretaceous, and the anomaly "m" is the younger, Laramide-age Farallon slab. In this case, sinking rate of "p" in the lower mantle would be 8.5-14 mm/yr on average, assuming the initial penetration through the d660 occurred at ca. 110 Ma. This value is consistent with the average slab sinking rate of 12 ±3 mm/yr (van der Meer et al., 2010) or 13 ±3 mm/yr (Butterworth et al., 2014) in the lower mantle.

I use this interpreted stagnant slab and the plate reconstruction model by Shephard et al. (2014) to build a two-dimensional kinematic model for the Farallon subduction and North America drifting. Although the relative convergence orientation is mainly NE-SW, I present a kinematic model along an E-W profile in order to compare it with the same seismic profiles in Shephard et al. (2014). We believe this is viable to capture the first-order characteristics. Also, because the seismic signal of the "p" anomaly beneath Canada is blurry, and also because this study focuses on the northern GoM, we draw the E-W profile along 30 ℃N, between 130 ℃W and 30 ℃W (Fig. 15).

At 130 Ma, a portion of the subducted Farallon slab had stagnated in the MTZ, and was experiencing decarbonation and dehydration. The width of the stagnant slab continued to increase as the trench retreated westward and more slab settled in the MTZ. Abundant carbon and some amount of water were expelled from the slab into the surrounding mantle. A fragment of slab penetrated the d660 at ca. 110 Ma, created gravitational instabilities around its edge, and induced upwelling. Based on the complex physical and chemical processes described above, fragmentation of the slab ultimately triggered the formation of the Arkansas lamproites and carbonatites, as well as the kimberlites in Riley County, Kansas and the Forte a la Corne field, Saskatchewan (Fig. 15 and 13).

As the cracks propagated, stagnant slabs broke into smaller fragments and sank into the lower mantle. This could generate either (1) a focused kimberlite field such as the Kansas and Saskatchewan ones, if the slab tear keeps relatively stationary with the overriding plate; or (2) a westward migrating igneous pattern, as seen in the northern GoM, if the slab tear propagates towards the trench at a faster rate than the retreating trench. These two scenarios are illustrated beneath the northern GoM and Kansas in Fig. 13. The latter is further shown in Fig. 14 for northern GoM from 110 Ma to 70 Ma. The Sabine uplift, which records uplift and erosion in mid-

Cenomanian-Turonian (Snedden et al., 2015), is predicted to be emplaced by alkaline igneous rocks at ca. 95-85 Ma, given a westward migration trend of the AIP-BIP magmatism.

After ca. 80 Ma, the arrival of the Shatsky Conjugate Rise followed by the Hess Conjugate Rise (Liu et al., 2010) altered the subducted slab geometry, and in turn, eliminated the slab tearing in the MTZ, and terminated the BIP magmatism (Fig. 12). The flat-slab subduction hardly affected Canada and provided sufficient time and space for stagnation and decarbonation, leading to a longer history of kimberlite volcanism and a more prolific period for diamond growth (Fig. 10 and 12) (Faure et al., 2011).

As the younger slab entered the MTZ, long-term stagnation became less likely, since young, warm slabs tend to penetrate into the lower mantle because of faster diffusion of metastable pyroxene to majorite-garnet (e.g., Goes et al. 2008; King et al, 2015). The younger Farallon slabs display a tilted geometry from deep upper mantle to lower mantle at present with only minor stagnation at present(Fig. 14) (Bunge and Grande, 2000; Grand, 2002; Li et al., 2008; Sigloch, 2011; Simmons et al., 2010). While the slab sinking-induced dehydration melting atop the d410 and below the d660 and small-scale convection in the upper mantle have been taking place (Chen et al., 2014; Schmandt et al., 2011, 2014), the "Cretaceous Corridor" intraplate magmatism overall migrated westward and eventually terminated in the Eocene due to the lack of sufficient stagnation in the MTZ.

If the interpretation above is valid, how long did stagnation last? The flat-lying "p" anomaly is 1900-2300 km long. Given a plate convergent rate of 60-80 mm/yr, with an assumption that no significant shortening strain occurs within the slab due to rapid trench retreat, it takes ca. 24-38 Myr to achieve the observed geometry. This matches the estimated timescale of 30-40 Myr by King et al. (2015), and is consistent with the maximal timespan of 50 Myr for a hydrated slab to completely dry out (Richard et al., 2006).

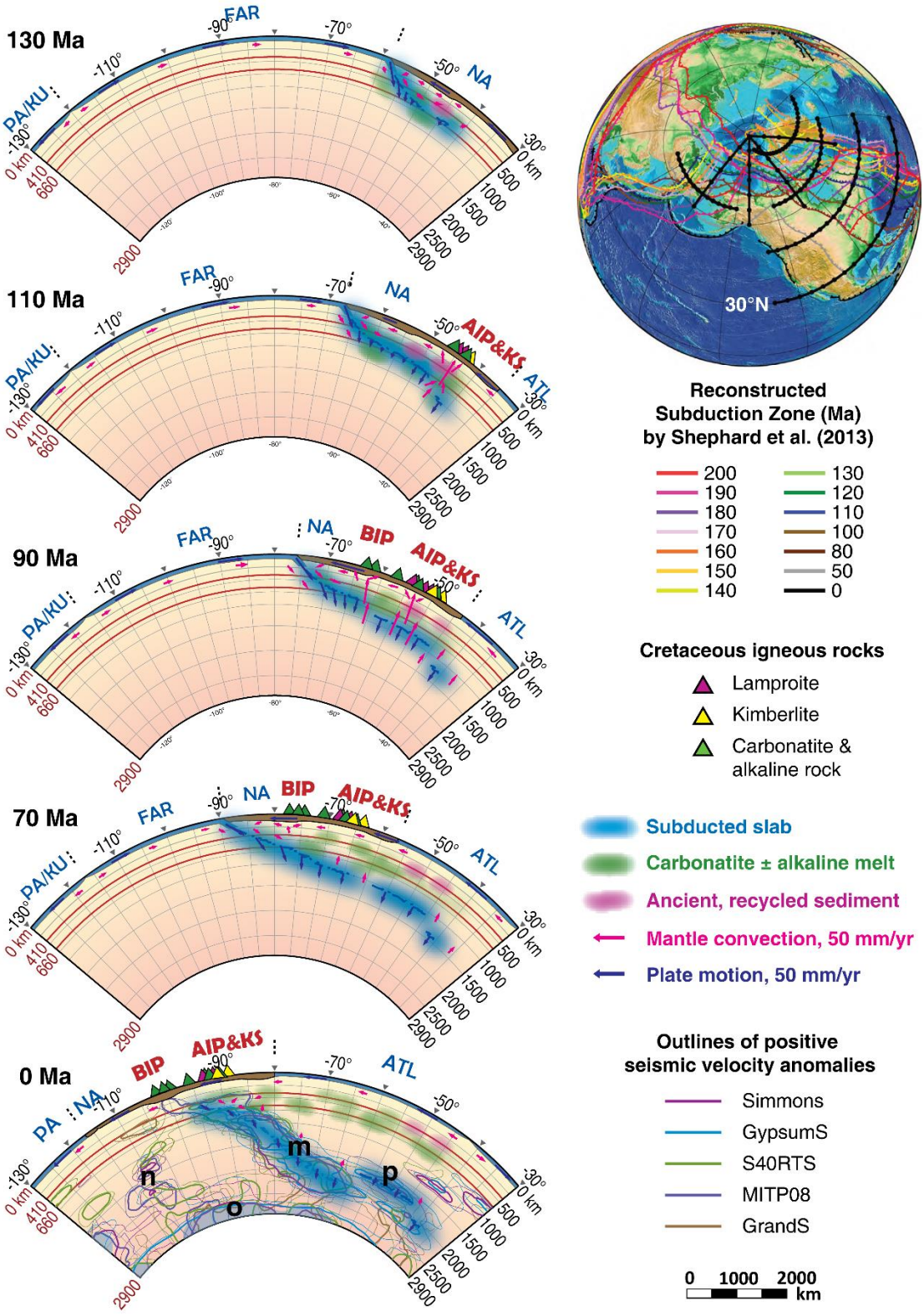

Figure 15 Kinematic model of the Farallon slab motion in the mantle along 30 ℕ between 130 ℚ and 30 ℚ at 130 Ma, 110 Ma, 90 Ma, 70 Ma, and present.

The once-stagnated slab hypothesis is supported by high electrical conductivity in the transition zone and the uppermost lower mantle. At such depths, electrical conductivity is higher beneath the offshore East Coast of the US (ca. 50˚W-80˚W) than that beneath the continental North America (ca. 80˚W-110˚W) (Kelbert et al., 2009). H_2O and CO_2 are the main contributors for the elevated electrical conductivities in or around the MTZ (Gaillard et al., 2008; Huang et al., 2005; Karato, 2011; Kelbert et al., 2009). Greater electrical conductivity suggests a reservoir of higher abundance of hydrous and/or carbonatitic melts, which could result from a longer period of stagnation; this may be the case for the MTZ beneath the offshore East Coast. By contrast, the slightly-lower electrical conductivity beneath the continental US implies limited decarbonation and dehydration in the MTZ because younger, warmer Farallon slab travelled through the MTZ without significant stop.

7. Implications

7.1 Albian-Turonian paleogeography in the northern GoM

Dynamic topography models have suggested an eastward migration and widening of the depocenters (without uplift) from south Texas to Mississippi during the Late Cretaceous and early Paleogene (e.g., Flament et al., 2014; Liu, 2014). However, sedimentary records and paleogeography reconstructions demonstrate a contradictory scenario of highs and lows in the GoM region.

By the end of the Early Cretaceous, lithospheric thinning and thermal contraction resulted in a deep oceanic basin surrounded by continental shelves (Galloway, 2008; Snedden et al., 2015). From late Albian to Coniacian (ca. 107-86.3 Ma), however, numerous unconformities appeared in the northern GoM stratigraphy, most of which appear to be tectonically controlled (Ewing, 2009).

The Monroe uplift, cored by alkaline igneous rocks near Arkansas-Louisiana-Mississippi borders, has no Paluxy-Washita (late Albian to mid-Cenomanian, ca. 107-96 Ma) or Eagle Ford-Tuscaloosa (mid-Cenomanian-Turonian, 96-85.6 Ma) supersequence strata due to uplift and erosion (Ewing, 2009; Snedden et al., 2015). Further west, the Sabine uplift on Texas-Louisiana border, preserves the older Paluxy-Washita but lacks the younger Eagle Ford-Tuscaloosa supersequence strata (Snedden et al., 2015). In onshore areas (East Texas and northern Louisiana), the base of the Eagle Ford-Tuscaloosa supersequence coincides with the Mid-Cretaceous Unconformity (Dohmen, 2002), which might result from a tectonic uplift that altered the Tuscaloosa drainage system during the Cenomanian to Turonian (Snedden et al., 2015). Other uplifts, such as the LaSalle Arch, Adams County High-Wiggins Arch, Angelina-Caldwell Flexure, and San Marcos Arch, also influenced the Cenomanian-Turonian depositional environment.

These mid-Cretaceous uplifts are, on first order, characterized by a westward migration trend, a few hundred meters of uplift, and ca. 10-20 Myr timespan for each uplift. The Albian-Turonian uplifts and unconformities in the northern GoM can be readily explained by this model (Fig. 12). While the sinking oceanic slabs caused long-wavelength subsidence, small-scale upwelling induced at slab edges can result in local surface uplifts.

7.2 Post-breakup magmatism and other intraplate magmatism worldwide

It is not expected that one uniform model will be able to explain all post-breakup magmatism on rifted passive margins. Karner and Shillington (2005) suggested that this type of magmatism may result when a rifted passive margin overrides a deep mantle plume. Examples include the Newfoundland margin (Karner and Shillington, 2005), and possibly the South China Sea margin in Hainan island (Wei and Chen, 2016). Another possible mechanism is edge-driven convection and/or plate motion-induced asthenospheric shear flow (Conrad et al., 2011; King and

Anderson, 1998). Volcanism in southeastern Australia (Davies and Rawlinson, 2014), eastern Gulf of Aden (Lucazeau et al., 2008), and Cape Verde and Canary islands (King and Ritsema, 2000) can possibly be explained by this type of mechanism. A third mechanism, advocated by this study, proposes that subduction and slab fragmentation can be the ultimate driver of post-breakup magmatism on passive margins as well as other intraplate volcanism (Duke et al., 2014; Ringwood et al., 1992; Stern et al., 2016; Tappert et al.. 2009). Because of the scientific and economic values of passive margins, further investigation is needed on post-breakup magmatism.

Intraplate magmatism triggered by stagnated slabs is found in other regions. In central Europe and the Mediterranean region, Cenozoic intraplate volcanism is primarily OIB-like alkaline basalt with HIMU-signatures, and their locations overlap the edge of stagnant slabs (cf. Faccenna et al., 2010). Faccenna et al. (2010) proposed a "wet plume" model, which highlights dehydration at the leading edge of stagnant slabs as the source for focused upwelling. Dehydration alone, however, may not be able to provide persistent upwelling, because the density contrast between the melt and the surrounding mantle rocks at the MTZ depths is highly sensitive to the water content (Jing and Karato, 2009). We suggest that some mechanism to induce instabilities is needed in the wet plume model.

Beneath northeast China and adjacent areas, remnant Pacific slabs lying within the MTZ have reached as far as 2400 km from the Ryukyu trench, causing a number of active, OIB-like, alkaline volcanic rocks (e.g. Wang et al., 2015; Zhao et al., 2009). In terms of the subduction, stagnation, dehydration, and decarbonation processes, the Pacific slab beneath northeast China may be a modern analog for the Farallon slab beneath the North America during the Cretaceous. These two intraplate volcanic systems differ in their final rock types, which can be attributed to the lithospheric thickness control. While the interior of the North American plate stayed intact during the Farallon subduction, the North China Craton experienced substantial extension, heating, and hydration during the Mesozoic and Cenozoic Pacific subduction, resulting in a

thinned lithosphere (thickness < 140 km, even as thin as 60-70 km) (Chen et al., 2008), leading to predominant alkaline rocks with little or no kimberlites emplaced in the crust.

7.3 Potential kimberlites in North America and future directions

To my knowledge, no kimberlite has been reported in the "Cretaceous Corridor' between Nebraska and North Dakota, and between central Saskatchewan and southeastern Northwest Terriroties. It has been suggested that the subducted Farallon plate influenced the overriding lithosphere in this region during the Late Cretaceous (Mitrovica et al., 1989; Liu et al., 2011). With a thick continental lithosphere (Schaeffer and Lebedev, 2014; Whitmeyer and Karlstrom, 2007; Yuan and Romanowicz, 2010), Cretaceous-Eocene kimberlites may exist in this region, and subsequently been eroded during the burial phase of the Western Interior Seaway in Cretaceous. Therefore, my model may imply potential occurrence of kimberlites and possible plays for diamond explorations along the Arkansas-Kansas-Saskatchewan-Northwest Territories zone aided by high-resolution potential field surveys (Fig. 9). As pointed out by Pavlis et al. (2012), to really understand the subducted Farallon/Kula system, we need three-dimensional visualization system and four-dimensional kinematic and dynamic model. Similar to Wu et al. (2016) study for Southeast Asia, a deliberate model that reconstructs the subducted slabs beneath North America is desired.

Moreover, it is important to fully utilize inclusions from radiogenic and stable isotope geochemistry. Whether or not the AIP lamproites and carbonatites contain deep mantle-derived mineral inclusions is critical to the model proposed in this study. Isotope geochemistry and inclusions from the kimberlites and lamproites in Kansas, Saskatchewan and Alberta will further characterize the heterogeneous mantle source. The Elliott kimberlite in Kentucky, as an unexplainable phenomenon in this model, also demands further research on its petrogenesis and tectonic significance.

8. Conclusions

I have examined the nature and emplacement mechanisms of the post-breakup magmatism in the northern Gulf of Mexico region, and propose a new tectonic and petrogenetic model at a plate scale. We conclude that:

1. The post-breakup magmatism initiated in south-central Arkansas long after the cessation of GoM seafloor spreading, and extended to a vast area including Mississippi, Louisiana, South and West Texas, as well as offshore Louisiana area. The two largest components, the Arkansas-Jackson Dome (108-64 Ma) and the Balcones-Trans Pecos (84-72 Ma) igneous provinces are both derived from the sub-lithospheric mantle, with OIB-like geochemical signatures.

2. Previous models, including the Bermuda hotspot, edge-driven convection, lithospheric reactivation, and deep, low-angle subduction, are all at odds with observations.

3. Placing the GoM magmatism into a regional framework leads to an outstanding "Cretaceous Corridor" across the North America continent from the Gulf of Mexico to Northwest Territories. Their linearity suggests a related genetics and a strong connection with the Farallon subduction.

4. I propose a stagnant slab model to explain the tectonic and petrogenetic mechanism for the GoM magmatism, which also generally portrays other kimberlites and lamproites in the Cretaceous Corridor. This model consists of four steps: (1) normal subduction of the Farallon slab; (2) slab stagnation, decarbonation, and dehydration in the mantle transition zone; (3) sinking slab-induced upwelling and entrainment of heterogeneous mantle; and (4) emplacement in the overriding plate controlled by lithospheric thickness, composition, and discontinuities.

5. We provide a two-dimensional kinematic model to justify the new model. To fully testify this model and explore the relationship between the deep subduction and intraplate

volcanism, a three-dimensional reconstruction of subducted slabs beneath the North America is needed.

CHAPTER 2. OBLIQUE RIFT, OBLIQUE SLIP? STRUCTURAL ANALYSIS ON THE EARLY-STAGE EXTENSION OF THE RIO GRANDE RIFT IN NORTHERN NEW MEXICO

1. Introduction

How continental rifts initiate and develop has been a subject of debate for decades. Due to protracted deformation history since the onset of plate tectonics, continental crust is characterized by anisotropy and heterogeneity, both mechanically and compositionally. Inherited weak zones within the lithosphere can be reactivated repeatedly during the succeeding tectonic cycles (e.g., Thomas, 2006). Therefore, it is not uncommon to find a continental rift under the influence or control of pre-existing structures (e.g., Autin et al., 2013; D'Agostino et al., 1998; Versfelt and Rosendahl, 1989). Oblique rift, whose axial trend is at an angle to the direction of extension, is more pervasive than orthogonal rift on Earth (e.g., Philippon and Corti, 2016). With the presence of pre-existing weak zones, oblique rifts become very complex in terms of their fault pattern (geometry), strain paths (kinematics), and stress fields (dynamics) (e.g., Agostini et al., 2009; Bellahsen and Daniel, 2005; Corti, 2008; van Wijk, 2005). Outstanding questions in oblique rift studies often include: do varying geometry and kinematics of faults record multi-directional extension, or continuous, single-phase extension? How do pre-existing heterogeneities influence the rift evolution? What are the roles of border faults, internal faults, and transfer fault, in building an oblique rift?

The Rio Grande Rift (RGR) in the southwestern US offers an excellent natural laboratory to study the structures of orthogonal and oblique rifts under the influence of pre-existing crustal heterogeneities (Fig. 16). It is unique among continental rifts because it is part of a broad (> 1200

km) region of extended lithosphere and anomalous upper mantle that includes the Basin and Range province and the Colorado Plateau, driven by plate tectonic forces (e.g., Atwater and Stock, 1998; Dickinson, 2002; McQuarrie and Oskin, 2010; Perry et al., 1988; Wernicke and Snow, 1988). A wide variety of geological and geophysical studies have been conducted in and around the RGR, resulting in a good understanding of the tectonics, sedimentation, and magmatism of the RGR (e.g., Chapin and Cather, 1994; Ingersoll, 2001; Kelley and Duncan, 1986; Perry et al., 1988; Wilson et al., 2005; Drenth et al., 2013). While consensus has been reached regarding the most recent kinematics of the RGR extension, i.e., near E-W orientation, perpendicular to the N-trending RGR (Berglund et al., 2012; Morgan et al., 1986), debates still exist on its Tertiary extension direction. Competing kinematic models include (1) sinistral shear (Cather et al., 2006; Kelley, 1982), (2) dextral shear (Wawrzyniec et al., 2002), (3) clockwise rotation of the Colorado Plateau (Chapin and Cather, 1994), and (4) a multi-directional extension involving a clockwise rotation from NE-SW to NWW-SEE orientation (Morgan et al., 1986; Zoback et al., 1981). Kinematics of the Rio Grande rifting is crucial to constrain geodynamic models for the western US. This study uses field-based measurements of fault slip data in the Tusas Mountains segment and the adjacent Abiquiu embayment, compared with regional extension data and analog experiment results, to study the extension history of the RGR and the roles of reactivation in oblique rift evolution.

2. Geological Background

Crystalline basement rocks in northern and central New Mexico recorded intense and complex deformation history that consisted of three major tectonic events prior to the Cenozoic Rio Grande rifting. The earliest events occurred during the Proterozoic, characterized by the assembly the Mazatzal and Yavapai orogenic belts followed by a major ca. 1.4 Ga tectonic and metamorphic event (e.g., Amato et al., 2008; Daniel et al., 2013; Karlstrom et al., 1997;

Whitmeyer and Karlstrom, 2007; Williams, 1991). In the Tusas Mountains area, the 1.4 Ga Mesoproterozoic shortening event created top-to-the-northeast (in present-day geographic coordinate system) ductile shear zones and numerous folds (Aronoff et al., 2016; Williams et al., 1999). The Mesoproterozoic supracrustal Vadito Group (mainly metavolcanic and metasedimentary schists and gneisses) and the overlying Hondo Group (primarily the Ortega quartzites) in northern New Mexico were pervasively foliated and metamorphosed at lower to mid-crustal level (Aronoff et al., 2016). Following the Precambrian deformation, the second crustal shortening event is the Ancestral Rocky orogeny during the late Paleozoic (e.g., Kluth, 1986; Ye et al., 1996), and pre-existing structures played a key role in this reactivated structure in Colorado and New Mexico (e.g., Dickinson and Lawton, 2003; Marshak et al., 2000). The Late Cretaceous to Eocene Laramide orogeny is the latest shortening event, and again, Laramide-related thrusts took advantage of pre-existing crustal weaknesses, generating basement uplifts in the Sangre de Cristo, Brazos-Tusas, Nacimiento, and Picuris Mountains (e.g., Cather et al., 2006; Erslev, 2001; Yin and Ingersoll, 1997). These basement uplifts are exposed in the footwall blocks of rift-bounding normal faults during the Oligocene-to-present Rio Grande rifting (Kelley and Chapin, 1995; Kelley and Duncan, 1986). Because the RGR basically follows structural grains in the basement rocks, reactivation is considered an important contributor in the RGR deformation (Chapin and Cather, 1994; Karlstrom et al., 1999).

The Rio Grande Rift ranges from Leadville, Colorado, through New Mexico, US, to Chihuahua, Mexico. Its northern and central portions separates the Colorado Plateau to the west from the Great Plain to the east, and are characterized by N-trending, narrow, asymmetric axial basins (the San Luis, Espanola, and Albuquerque basins), bounded by basement uplifts (the Sangre de Cristo, Tusas, Nacimiento, and Sandia mountains), shallow embayments (the Abiquiu, Culebra, Santa Fe, and Hagan), and accommodation/transfer zones (the Embudo and Santo Domingo) (Fig. 16). In general, geologic records of the early RGR extension, such as

deformation, deposition, and low-temperature thermochronologic ages, were preserved in the rift-bounding uplifts and embayments, whereas younger extension since the mid-Miocene has migrated basinward, forming the narrow, axial half-grabens (e.g., Baldridge et al., 1994; Chapin and Cather, 1994; Ingersoll et al., 1990; Kelley, 1979; Kelley and Duncan, 1986; Ricketts et al., 2016). The southern RGR, south of Socorro, New Mexico, is distinct from the central and northern RGR by local high-strain extension, low-angle normal faulting, and shallow rift basins (e.g., Morgan et al., 1986).

The Tusas Mountains segment and Abiquiu embayment on the west flank of the RGR in north-central New Mexico are unique structures in the RGR because of their obliquity. Obliquity is defined as the angle between the normal to the rift trend and regional extension direction. They are bounded by oblique border faults. Normal faults in the Tusas follow the foliations, axial surfaces, and fractures within the Proterozoic basement rocks, suggesting a strong control from the pre-existing mechanical heterogeneities (Fig. 17). The Cañones fault zone is the western boundary of the Abiquiu embayment, and is rooted on a Laramide monocline where a blind thrust has been reactivated (Liu and Murphy, 2013).

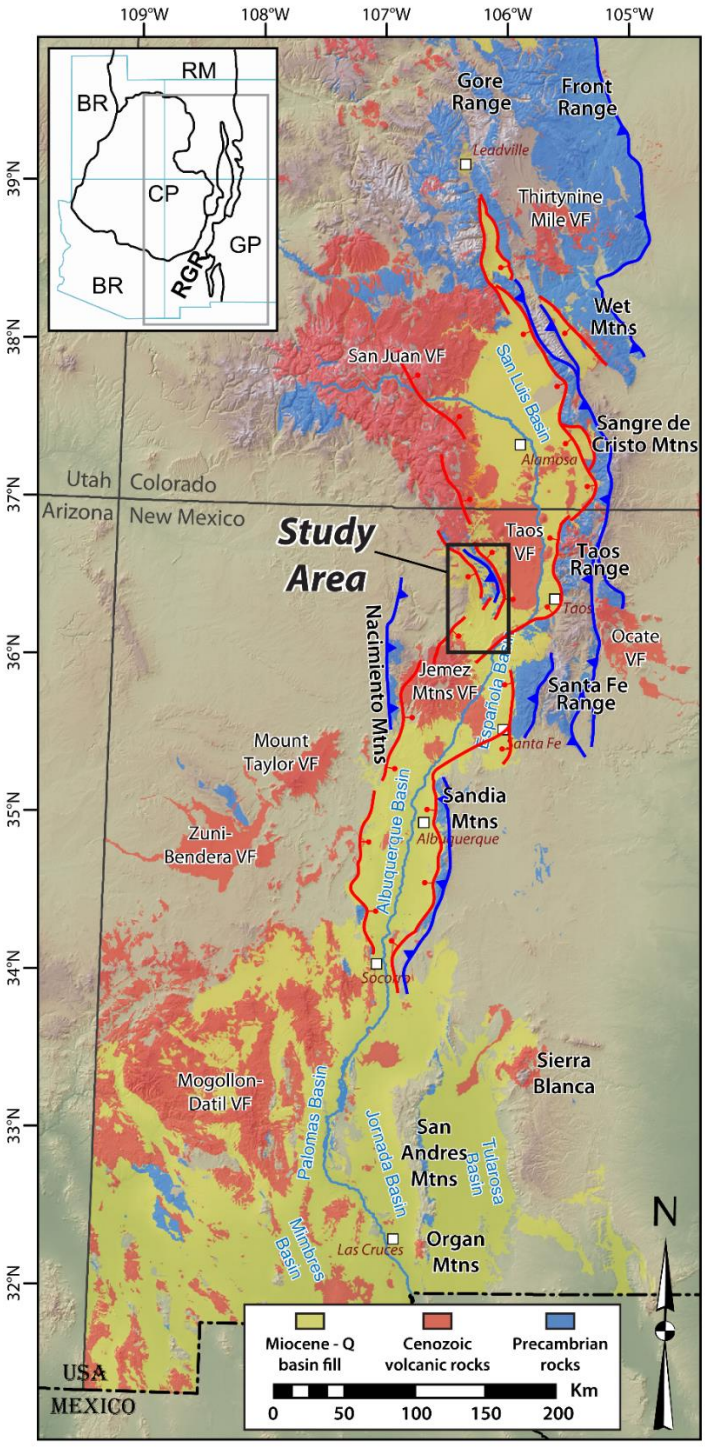

Figure 16 Tectonic map of the northern and central Rio Grande rift. Modified after Ricketts et al. (2016). Inserted index map shows boundaries of major tectonic units in southwestern US, including the Basin and Range (BR), Colorado Plateau (CP), Rocky Mountains (RM), Great Plains (GP), and Rio Grande rift (RGR). Laramide, basement-involved reverse faults are shown as blue lines with teeth in the hanging-wall block; RGR normal faults are red lines with ball-and-bar in the hanging-wall block VF, volcanic field.

Timing of the onset of Rio Grande rifting is not well-constrained, due to the distributed nature of early rifting and subsequent burial. In the southern RGR, extension may have begun by ca. 35-36 Ma (Cather, 1990; Mack et al., 1994). Roughly-coeval cooling ages by low-temperature thermochronologic dating have been obtained along the rift flanks, suggesting that a major, simultaneous exhumation and normal faulting along the RGR began at ca. 25 Ma (Landman and Flowers, 2013; Ricketts et al., 2016). In the Tusas Mountains and Abiquiu embayment area, early rifting was demonstrated by the syn-kinematic Ritito Conglomerate during the Oligocene (Baldridge et al., 1994; Kelley et al., 2013). The Cañones fault is also inferred to be active from late Oligocene to 20 Ma or younger (Kelley et al., 2013; Maldonado et al., 2013). Following that, the Abiquiu Formation in the Abiquiu embayment and its approximate equivalent units, the Esquibel and Cordito members of the Los Pinos Formation in the Tusas Mountains, were deposited during the late Oligocene – early Miocene time (Aby et al., 2011; Ingersoll, 2001; Ingersoll et al., 1990). Subsequently, the Tesuque Formation in the Abiquiu embayment and the Espanola basin and its equivalent Los Pinos formation in the Tusas Mountains were deposited during the Miocene, accompanied by basinward migration of extensional strains and depositional centers (e.g., Aldrich and Dethier, 1990; Baldridge et al., 1994; Ingersoll et al., 1990).

As the RGR extension continued and accelerated during the mid- to late Miocene, the Embudo transfer zone has been active since at least ca. 7 Ma, relaying E-W extension strains between the east-tilted San Luis basin to the north and the west-tilted Espanola basin to the south (Chapin and Cather, 1994; Koning et al., 2004b). This NE-trending antithetic transfer zone accommodates predominantly sinistral strike-slip movement (Aldrich et al., 1986; Muehlberger, 1979). Active deformation is distributed in a wide area around its northeastern and southwestern tips, whereas strain localization has occurred in the central portion of the Embudo fault (Bradford, 1992; Kelson et al., 2004; Koning et al., 2004b), suggesting an ongoing development from

distributed to localized strain along this transfer zone (Faulds and Varga, 1998; Koning et al., 2004b).

3. Field Investigation and Results

3.1 Methods

We conducted field mapping to locate and trace RGR-related normal faults in the Tusas Mountains and Abiquiu embayment region aided by published geologic maps from the New Mexico Bureau of Geology and Mineral Resources (Fig. 17). Litho-tectonic units, contact, faults, folds, and representative attitudes are compiled from the authors' field investigations and published geologic maps from the US Geological Survey and the New Mexico Bureau of Geology and Mineral Resources (Aby et al., 2010, 2012; Kelley et al., 2005; Kempter et al., 2005, 2007, 2008; Koning, 2004; Koning et al., 2004, 2005a, 2005b, 2006, 2007, 2008; Maldonado, 2008; Manley, 1982; Manley and Wobus, 1982; Scholle, 2003; Wobus and Manley, 1982).

At each station, we examined faults and fractures in fault core and damage zone to look for kinematic indicators, such as striations, steps, crescentic markings, trailed materials, and fractures, to infer the relative motion of missing block (Doblas, 1998; Petit, 1987). We measured several slickenlines on each fault surface, in order to obtain the mean attitude of slip directions. Slickenline rakes vary by no more than a few degrees, confirming the notion that they are insensitive to perturbations from small-scale asperities on fault surfaces (Kirkpatrick and Brodsky, 2014). Thus, slickenline measurements can be used to infer kinematics of faults at outcrop- and regional-scale.

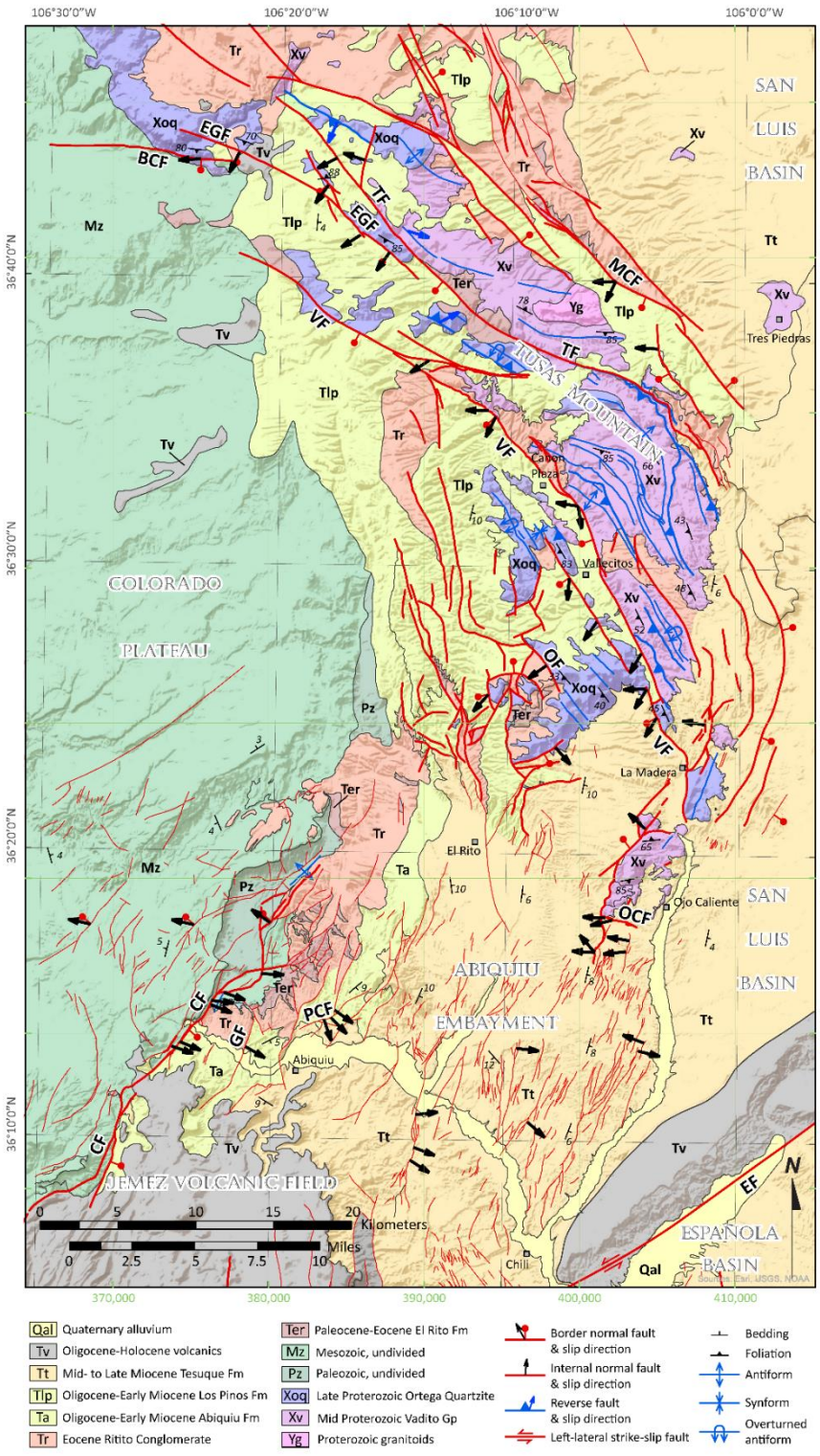

Figure 17 Geologic map of the Tusas Mountains and Abiquiu embayment in northern New Mexico. Abbreviations: BCF, Brazos Cliff fault; CF, Cañones fault; EF, Embudo fault; EGF, East Gavilan fault; GF, Garcia fault; MCF, Mule Canyon fault; OCF, Ojo Caliente fault; OF, Ortega fault; PCF, Plaza Colorada fault; TF, Tusas fault; VF, Vallecitos fault.

In the Tusas Mountains, we also identified the remnant primary structure (such as trough beds) and the lineation of metamorphic minerals (kyanite and sillimanite mainly) in the host metamorphic rocks, in order to rule out those apparent normal faults that are actually overturned reverse faults formed by the earlier orogenic events. The rest normal faults are extension-related, as their slickenlines are not parallel to the kyanite- or sillimanite-defined lineation. Fault surfaces are frequently parallel to the foliations. In the Abiquiu embayment, slickensides in sedimentary rocks are more obvious, because most of them were enhanced by syn-kinematic coatings, usually composed of calcite and hematite.

3.2 Slip on the border faults

Normal faults in the Tusas Mountains are parallel to the foliation in the exposed Proterozoic rocks (Fig. 18). In the northern part of the mapping area, foliations, as well as fold axial surfaces, are generally NW- to NWW-striking, steeply SW-dipping. In most fault stations, the RGR-border normal faults are sub-parallel to the foliation (Fig. 17), while fractures associated with these faults have a more dispersed orientation (Figs. 17 and 18). Southward, the Tusas Mountains turn to roughly N30 ºW-striking, and the normal faults follow the change. The southernmost exposure of the Tusas Mountains basement near Ojo Caliente is at a high angle to the majority of the Tusas.

We plot the fault surfaces and the mean slickenline on each fault onto a lower-hemisphere, equal-area stereographic projection (Figs. 19a, c, and e). We also plot the rakes of the slickenlines into a rose diagram in order to visualize the statistics of dip-slip and oblique slip on fault surfaces (Figs. 4b, d, andf). First, we convert all the rakes (as acute angles with sense of direction) measured from the field to the “right-hand rule” format. In this format, one faces along the fault strike and places the dip direction to the right-hand side. Slickenlines that indicate different kinematics can thus be shown as a single value between 0 °and 360 °. If the missing

block moved left-laterally, the slickenline has about 0 °of rake in right-hand rule format. For normal faulting, the rake is 90 °; dextral faulting, 180 °; and reverse faulting, 270 °. In this format, slip directions in terms of rake become mathematically comparable between a synthetic and an antithetic fault pair. The second step is to treat the rakes as strikes of vertical planes, which can be plotted in a rose diagram. In this rose diagram, "North" becomes sinistral faulting; East now represents normal faulting; South, dextral; and West, reverse. Using the rose diagram to show the statistics of slickenline rakes is convenient in any stereonet program, easy to interpret for structural geologists, and seamless for visualizing dextral shearing with either minor normal or reverse motion.

Slickenline kinematic indicators obtained from the Tusas Mountains normal faults can be classified into two groups (Fig. 19a and b). One group records WNW-ESE extension with dextral-normal oblique rakes. The other group is characterized by almost pure dip-slip, SW-trending normal faulting.

Oblique border faults also bound the west margin of the Abiquiu embayment. They are predominantly NE-striking, and dipping to either SE or NW. The polarity reversal along the rift margin is probably caused by the reactivation of pre-existing Laramide monoclines and faults that accommodated either top-to-the-NW or top-to-the-SE shortening, respectively (Hamilton, 2009). The overall extension direction is near WNW-ESE (Fig. 19c), although dip-slip and normal-sinistral slip both occur along this fault. The left-lateral component of motion characterizes the displacement on the Canones fault (Baldridge et al., 1994; this study).

3.3 Slip on the internal faults

Internal faults in the Abiquiu embayment are mainly N20 °E-striking (Figs. 17 and 18e). These faults accommodated almost pure dip-slip extension. A highly-oblique normal fault, the Plaza Colorada fault north of Abiquiu, strikes ca. N70 °E and also accommodated pure dip-slip.

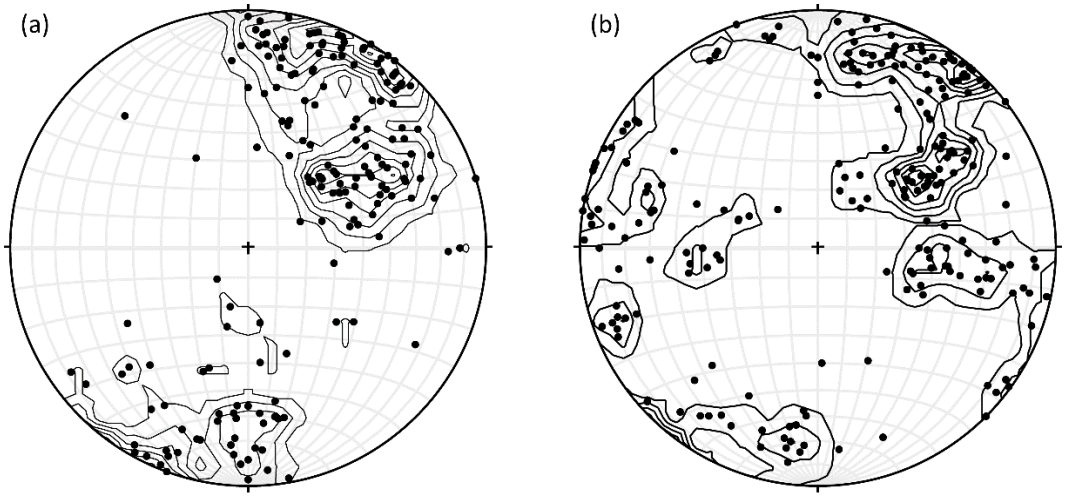

Figure 18 Lower-hemisphere, equal-area stereographic projections of the poles to foliations (a) and fractures and faults (b) in the Tusas Mountains. Contour interval is 1%. The distribution of poles to the fractures and faults is more dispersed than that of foliations, mainly due to minor fractures that have high angles regional trend of the foliations.

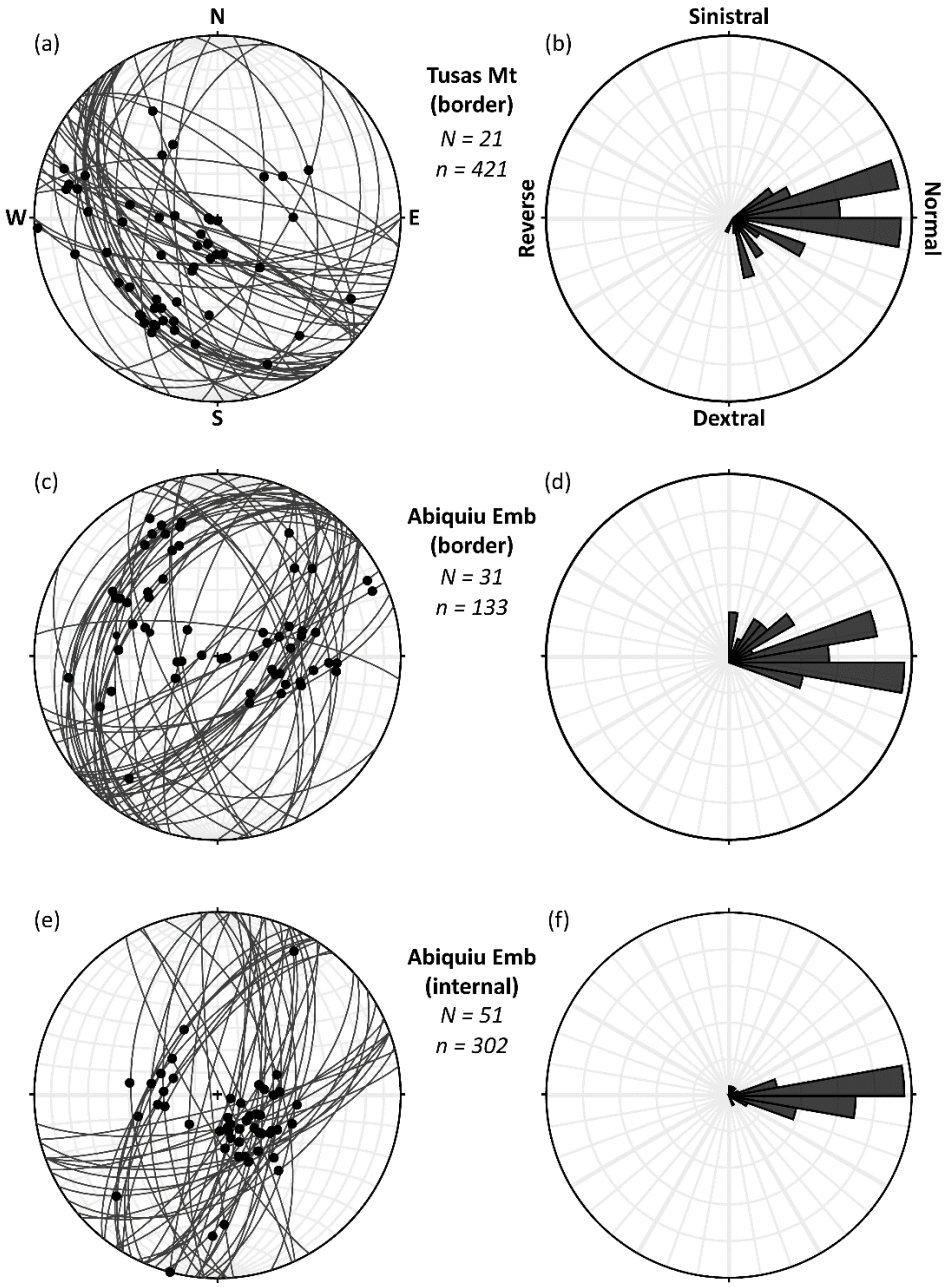

Figure 19 Attitudes of faults and associated slickenlines of the RGR-related border faults in the Tusas Mountain (a & b) and Abiquiu embayment (c & d), and attitudes of internal faults within the Abiquiu embayment (e & f). Figures on the left column are lower-hemisphere, equal-area stereographic projections, and figures on the right side are rose diagrams plotted with the rakes of slickenlines in a right-hand rule format. Four "end-members" of this rose diagram, dextral, normal, sinistral, and reverse movement, are annotated. See section 3.2 for more details. For each tectonic domain, the uppercase "N" means the number of fault measurement stations, and the lowercase "n" is the total number of slickenlines measured from the fault stations.

4. Discussions

The direction, amount, and timing of displacement on faults are fundamental parameters for a tectonic model. Although no low-temperature thermochronology age has been published in the Tusas Mountains, this study still provides some qualitative constraints to tectonic models of the RGR. Wawrzyniec et al. (2002) argued that quasi-continuous dextral shearing along the western margin of North American plate stretched the RGR along the NW-direction. However, the slip data in Wawrzyniec et al. (2002) is rather dispersed, and among the six minor-fault localities, only one that is adjacent to the Villa Grove transfer zone between the San Luis basin and Arkansas graben is directly related to the Rio Grande rifting (Wawrzyniec et al., 2002). Due to the oblique tendency of transfer zones, it is questionable whether this study can represent the direction or history of the RGR extension.

Chapin and Cather (1994) proposed that a vertical-axis clockwise rotation of 1.0 to 1.5 ° of the Colorado Plateau around a pole in northeast Utah facilitated the Rio Grande rifting. This model predicts varying extension directions, from SSW-trending in the San Luis basin to SWW-trending in the Albuquerque basin, and it requires identical kinematics between rift basins and their bounding transfer zones. However, fault slip measurements on border and internal faults in this study as well as the Espanola and northern Albuquerque basins (Minor et al., 2013) are not compatible with this model. In a recent, GPS-based study, the pole of the Colorado Plateau clockwise rotation was relocated to south-central Wyoming (Kreemer et al., 2010). Nevertheless, such a pole may not persist during the Neogene extension in a changing dynamics of the North America. Below we discuss another two models.

4.1 Model 1: Clockwise rotation of extension direction

We group the sinistral shear model (Kelley, 1982) into the clockwise rotational extension model (Fig. 20) (Ebinger et al., 2013; Morgan et al., 1986; Zoback et al., 1981), because sinistral

shear component was present on north-striking normal faults of Miocene age, and became indistinguishable on younger (latest Miocene to Holocene) faults in the RGR (Cather et al., 2006). Based on the orientation of dikes, Aldrich et al. (1986) found that NE-SW-oriented least principal horizontal stress was predominantly present south of Albuquerque before 23 Ma. In northern New Mexico, the least principal horizontal stress was near E-W or NWW-SEE in the Colorado Plateau, and near N-S in the Great Plain. A dike whose age was confined between 23 and 26 Ma in the San Luis basin led Aldrich et al. (1986) to speculate a SW-directed least principal horizontal stress during the earliest stage of the RGR extension. Younger dikes, including a N10°E-trending, 20-Ma dike from the footwall blocks of the Cañones fault (Maldonado et al., 2013) and other younger ones (Aldrich et al., 1986), indicate a near E-W, or slightly NWW-SEE direction of extension.

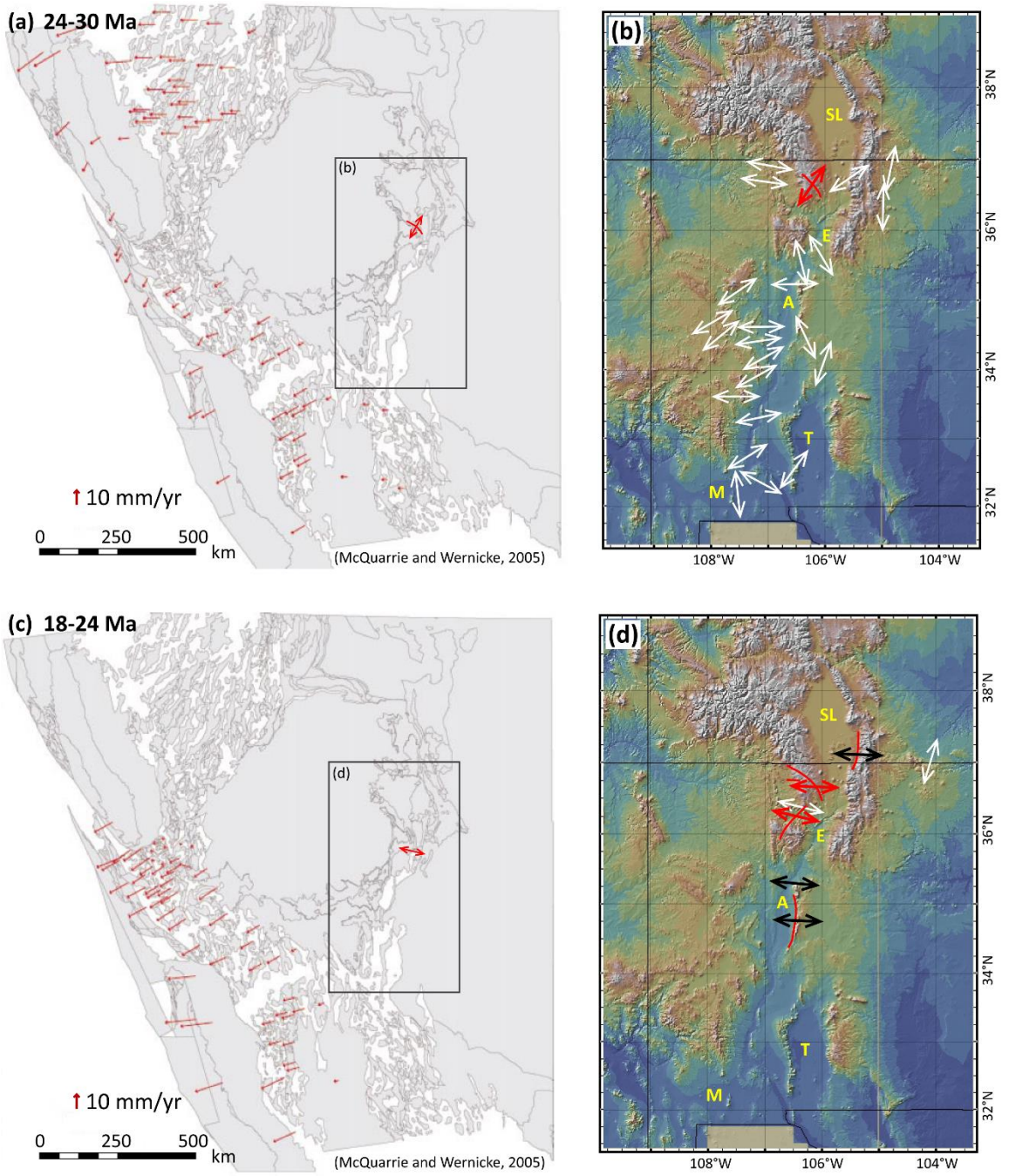

Figure 20 Model 1, Early-stage extension of the Rio Grande rift. (a) NE-SW extension in the Tusas Mountains in a reconstruction model for the Basin and Range between 24 and 30 Ma (McQuarrie and Wernicke, 2005). (b) Extension directions in the RGR and adjacent areas. Red arrows show the fault slip direction. White arrows show the inferred direction of least principal horizontal stress during 24-30 Ma (Aldrich et al., 1986). (c) Near E-W or slightly WNW-ESE extension in northern New Mexico, superimposed on the Basin and Range reconstruction model at 18-24 Ma (McQuarrie and Wernicke, 2005). (d) Extension directions in the RGR and adjacent areas during 18-24 Ma. Black arrows show the coeval, near E-W extension on the border faults of the San Luis, Santo Domingo, and Albuquerque basins (Bradford, 1992; Minor et al., 2013).

4.2 Model 2: Slip re-orientation in a continuous E-W extension regime

In this section, we explore an alternative hypothesis to explain the pure dip-slip and extension history in the oblique Tusas Mountains segment.

Some recent studies recognized an interesting phenomenon on the kinematics of oblique rifting with the presence of pre-existing weak zones in the lithosphere. In the western branch of East African Rift System, rift orientation varies from NE-striking in the north, to N-striking in the central, and NW-striking in the south, while slip directions based on seismic focal mechanisms show predominantly pure dip-slip, i.e., perpendicular to the local trend of border faults, along the rift (Ebinger, 1989; Yang and Chen, 2010). Similar observation is found in the Main Ethiopian Rift, whose NE-striking oblique border faults also preserve orthogonal slip (Corti, 2009). Both rifts are characterized by reactivation of Precambrian mobile belts that surround stable cratons (Versfelt, and Rosendahl, 1989). Centrifuge-based analog experiments are able to reproduce the pure dip-slip on oblique faults (i.e., slip re-orientation) (Fig. 21): when pre-existing weak zone is present in the crust, oblique extension results in pure dip-slip displacement on faults that strike obliquely to the extension direction (Corti et al., 2013; Philippon et al., 2015). As the obliquity increases, the border faults develop strikes between the weak zone trend and the orthogonal to the extension direction, whereas the internal faults growing above the stretched weak zone are always orthogonal to the extension direction (Philippon et al., 2015). With the presence of inherited weakness, two sets of faults with different preferred orientations co-exist in a continuous, oblique extension system.

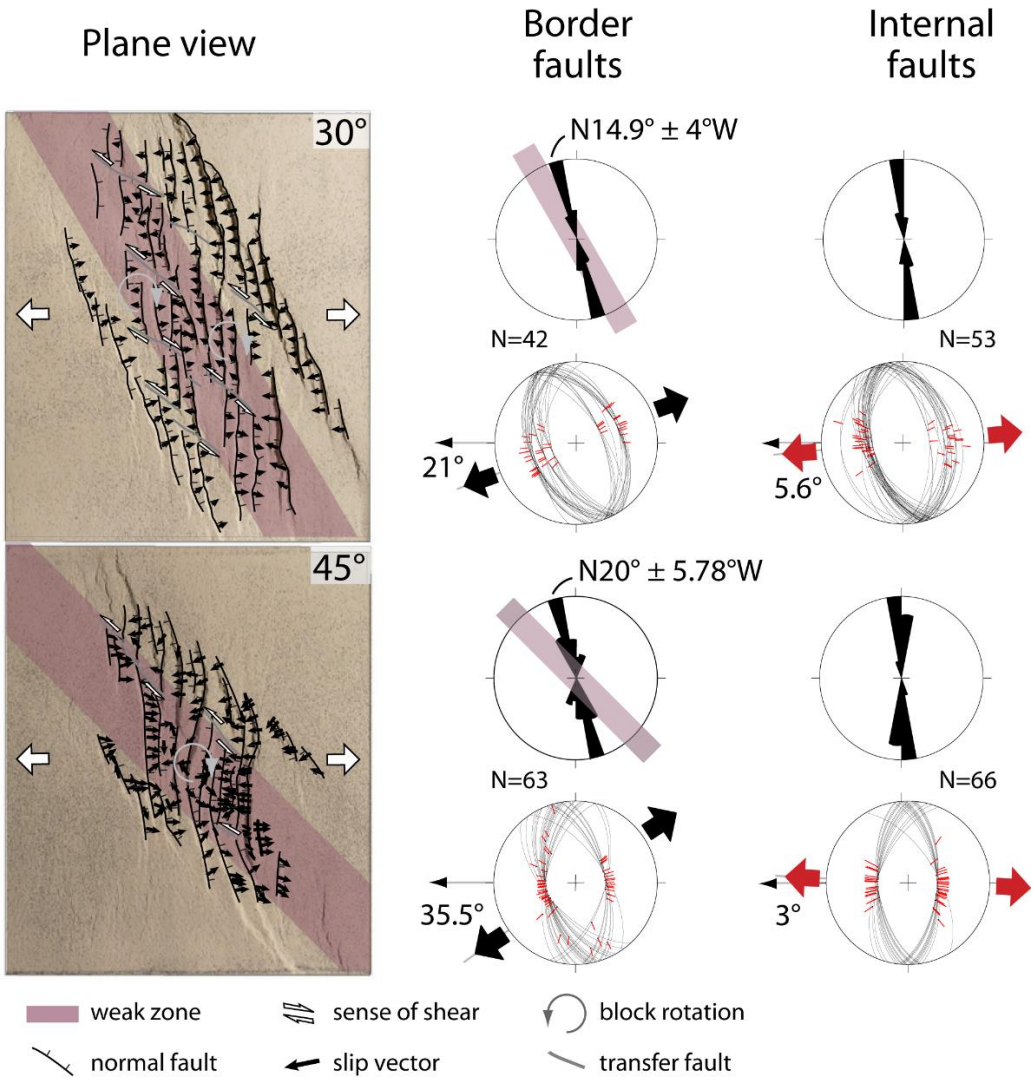

Figure 21 Analog experiments that show slip re-orientation on oblique border faults, as a comparison to the Tusas Mountains segment. Modified from Philippon et al. (2015), to illustrate Model 2, an alternative model to explain purely-orthogonal extension in the oblique Tusas segment. The left panel includes two experiment results in plain view, with different obliquities. In the right panel, stereonet plots for the border faults and internal faults in each experiment show that: (1) preferred strike of the border faults is nearly half of the obliquity; (2) preferred strike of the internal faults is largely normal to the regional extension direction; (3) slips on both the border and internal faults are predominantly pure dip-slip, resulting in two sets of slip directions

What causes the slip re-orientation is stress rotation. It is well-known that stress field rotates near the surface of the Earth, in order to re-orient the minimal principal stress (σ3) to be

perpendicular to the free surface, because shear stress is zero along any free surface (e.g., Fossen, 2010; Zoback, 1992). Similarly, stress re-orientation also takes place in the lithosphere near heterogeneities: when a weak layer is present, σ3 tends to adjust to perpendicular to it, and the maximal principal stress (σ1) tends to be parallel to it; a strong layer, on the other hand, deviates the local stress field in an opposite way, in which σ1 tends to become orthogonal and σ3 parallel to the strong layer (Morley, 2010 and references therein). Combined regional and local stress fields can thus locally activate pre-existing weakness whose orientation is not favored by far-field forces. Considerable stress rotation of σ1 towards unfavorably oriented weak fault can happen, but is restricted in the fault core with highly anisotropic rocks, under conditions of elevated pore fluid pressure (Faulkner et al., 2006; Healy, 2008).

During the Oligocene to early Miocene, stress field in northern New Mexico might be different from that in the southern RGR and southern Basin and Range (e.g., Aldrich et al., 1986; Zoback et al., 1981). If the near E-W oriented least principal horizontal stress persisted from late Oligocen to Miocene across the northern and central RGR, a continuous, near E-W extension model thus becomes possible. In this case, initiation of the northern and central RGR in each segment is characterized by E-W movement. The NW-striking Tusas segment, therefore, would accommodate the W-trending, normal-dextral motion on the SW-dipping faults. As the W-trending, oblique faulting strain accumulated, frictional weakening mechanism began to play a substantial role in faulting along fine-grained, well-connected, phyllosilicate-rich foliations (Collettini et al., 2009). Such process could cause the oblique faults in the Tusas Mountains sufficiently weak, rotate the stress field in the fault cores, and generate pure dip-slips. In the meantime, other border faults, including the Canones, Brazos Cliff, and Ojo Caliente, if still active, would accommodate near E-W-trending oblique slip because of their high shear strength or high obliquity.

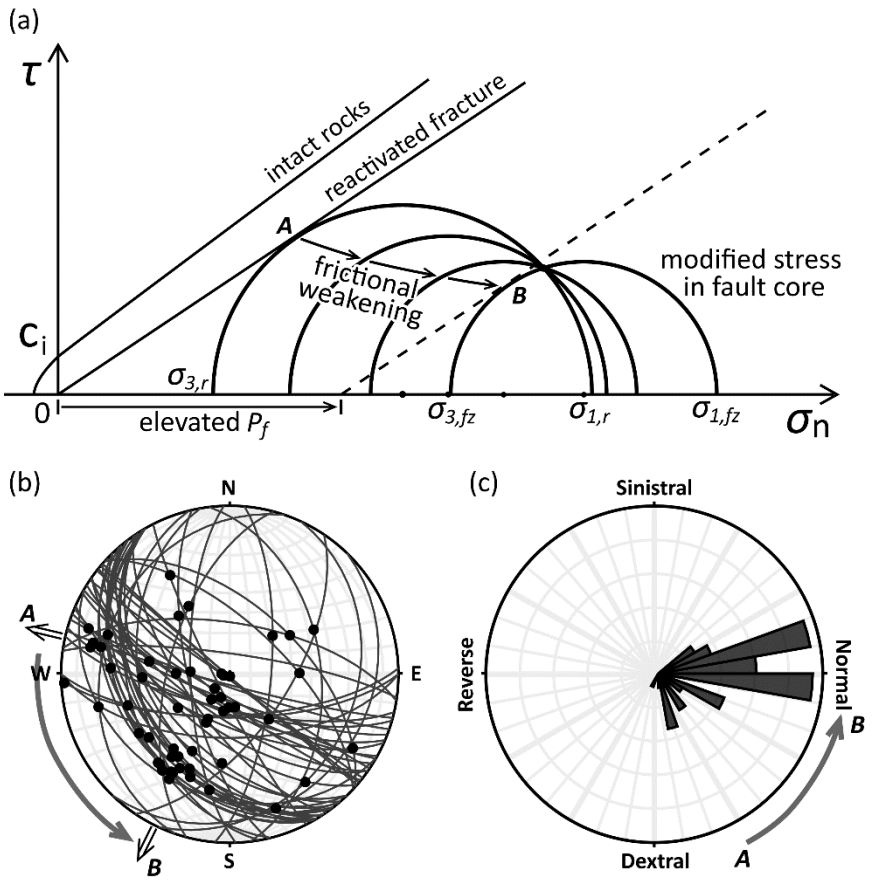

Figure 22 Stress rotation, pore fluid pressure increase, and frictional weakening processes in the fault core of reactivated crustal faults as illustrated in the Mohr's diagram (a), stereographic projection (b), and rose diagram of rakes under the right-hand rule (c). Mohr circle partially modified from Faulkner et al. (2006), to show the evolution of slip direction on oblique, reactivated faults during initial rifting. A local, counterclockwise rotation is predicted in fault kinematics (b), accompanied with an increase of orthogonal component in fault motion, i.e., rakes approach 90 °(c).

Structure and kinematics of internal faults are also consistent with this continuous near E-W extension model. The majority of internal faults in the Abiquiu embayment (this study), as well as those in the Espanola basin and Albuquerque basin (Minor et al., 2013) strike nearly north-south, contain 90 °±15 °rakes, and show a diffused map pattern. Even along the NEE-striking Plaza Colorada-Plaza Blanca fault northeast of Abiquiu, displacement is still pure dip-slip.

Pure dip-slip in internal faults is caused by their weak cohesion. According to the net slip-length scaling relationship (e.g., Kim and Sanderson, 2005; Schlische et al., 1996), these internal faults, whose surface traces are on the order of 102-103 m, usually accommodate 10s to 100s m of displacement. My field observation supports this estimated range, because most faults cut through same stratigraphic unit (either the Abiquiu Formation, or the Tesuque Formation of the Santa Fe Group) (Fig. 17). The internal faults in the Albuquerque basin also demonstrate an uppermost crustal origin, as they only tap the brines in sedimentary layers, not the underlying basement rocks (Williams et al., 2015). The Abiquiu and Tesuque Formations are not well-consolidated; some sections are even poorly-consolidated. These sediments/sedimentary rocks are not cohesive enough to support oblique component of slips, and therefore only experience pure dip-slip under continuous E-W extension, even though the fault strike varies. The overlying rift-rill sediments may be detached from the underlying basement rocks.

After a period of diffuse extension and transtension, strain is localized on master border faults of each basin and transfer faults between these basins. This is also accompanied by basinward migration of deposition centers in the San Luis, Espanola, and Albuquerque basins, forming half-graben geometry and transfer zones in-between (Baldridge et al., 1994; Chapin and Cather, 1994; Morgan et al., 1986).

A comparable case comes from the NE-trending Santo Domingo basin, which is an accommodation zone between the en echelon, right-stepping Espanola and Albuquerque basins. Unlike the Embudo fault zone on which most strain has been localized, transtensional strain is still distributed across the Santo Domingo basin. The oblique South San Francisco border fault that separates the Sandia Mountain from the Santo Domingo basin recorded a clockwise rotation of slip directions, from W-trending, normal-sinistral slip, to NW-trending, pure dip-slip, and finally, to N-trending, normal-dextral slip (Minor et al., 2013). A tectonic model that invokes multi-directional extension at regional scale is unlikely; otherwise one would find more NW- and

N-directed extension in other portion of the Rio Grande rift. A continuous E-W extension combined with pre-existing heterogeneities, instead, can readily explain the slip vector variation on the South San Francisco border fault. The W-trending, normal-sinistral slip marked the onset of oblique rifting; the subsequent pure dip-slip resulted from complete reactivation and stress re-orientation. The youngest, N-trending slip recorded the diffuse transtention in this accommodation zone.

5. Conclusions

Fault slickenline measurements in the oblique Tusas Mountain segment and Abiquiu embayment on the western flank of the Rio Grande rift show that the oblique border normal faults in both area recorded near E-W extension during the early stage of the Rio Grande rifting. Another set of movement was recorded as almost pure dip-slip on the oblique border faults in the Tusas Mountains segment. Internal faults in the Abiquiu embayment are primarily near N-striking, and accommodated E-W extension.

An assessment of kinematic models for the RGR extension show that the quasi-continuous dextral shear model can hardly reproduce the displacement observed on the RGR normal fauls, and the Colorado rotation model is also not fully satisfactory. Another two models, the clockwise rotation and the continuous E-W extension, can both explain available data, and are both testable. How to explain the extension in the oblique Tusas Mountains segment lies in the center of the debate. Extension model that invokes a clockwise rotation works better if the pure dip-slip in the Tusas Mountains fault predates the E-W oblique slip. Alternatively, because of the strong influence of pre-existing heterogeneities, the border faults in the Tusas may trigger slip re-orientation due to local stress rotation in the weak fault core. If this is the case, a continuous, near E-W extension history can already explain the orthogonal and oblique extension in the northern and central Rio Grande rift. Future study on the timing and amount of normal faulting in the

Tusas Mountains is needed, because this segment bears different geodynamic implications for the extension tectonics in southwestern North America.

References

Aby, S. B., Kempter, K., Karlstrom, K. E., 2012. Geologic map of the Cañon Plaza quadrangle, Rio Arriba County, New Mexico. New Mexico Bureau of Geology and Mineral Resources Open-file Geologic Map 221, scale 1:24,000.

Aby, S. B., Kempter, K., Koning, D., 2011. Recent mapping of the Oligo-Miocene Los Pinos Formation and associated units in the Tusas Mountains, New Mexico. New Mexico Geological Society Guidebook, 62nd Field Conference, Geology of the Tusas Mountains-Ojo Caliente, 275-280.

Aby, S., Karlstrom, K., Koning, D., Kempter, K., 2010. Geologic map of the Las Tablas quadrangle, Rio Arriba County, New Mexico. New Mexico Bureau of Geology and Mineral Resources Open-file Geologic Map 200, scale 1:24,000.

Agostini, A., Corti, G., Zeoli, A., Mulugeta, G., 2009. Evolution, pattern, and partitioning of deformation during oblique continental rifting: Inferences from lithospheric-scale centrifuge models. Geochemistry, Geophysics, Geosystems, 10(11), Q11015, doi:10.1029/2009GC002676.

Agrusta, R., Hunen, J., Goes, S., 2014. The effect of metastable pyroxene on the slab dynamics. Geophysical research letters, 41(24), 8800-8808.

Ainsworth, R., Pulliam, J., Gurrola, H., Evanzia, D., 2014. Sp receiver function imaging of a passive margin: Transect across Texas's Gulf Coastal Plain. Earth and Planetary Science Letters, 402, 138-147.

Aldrich, M. J., Chapin, C. E., Laughlin, A. W., 1986. Stress history and tectonic development of the Rio Grande rift, New Mexico. Journal of Geophysical Research: Solid Earth, 91(B6), 6199-6211.

Aldrich, M. J., Dethier, D. P., 1990. Stratigraphic and tectonic evolution of the northern Española basin, Rio Grande rift, New Mexico. Geological Society of America Bulletin, 102(12), 1695-1705.

Alibert, C., Albarede, F., 1988. Relationships between mineralogical, chemical, and isotopic properties of some North American kimberlites. Journal of Geophysical Research: Solid Earth, 93(B7), 7643-7671.

Amato, J. M., Boullion, A. O., Serna, A. M., Sanders, A. E., Farmer, G. L., Gehrels, G. E., Wooden, J. L., 2008. Evolution of the Mazatzal province and the timing of the Mazatzal orogeny: Insights from U-Pb geochronology and geochemistry of igneous and metasedimentary rocks in southern New Mexico. Geological Society of America Bulletin, 120(3-4), 328-346.

Anderson, P. Z., Snow, J. E., 2015. Door Point: volcano in the Gulf. Geological Society of America Abstracts with Programs. 47(7), 811.

Arne, D. C., 1992. Evidence from Apatite Fission-Track Analysis for Regional Cretaceous Cooling in the Ouachita Mountain Fold Belt and Arkoma Basin of Arkansas: Geologic Note (1. AAPG Bulletin, 76(3), 392-402.

Aronoff, R. F., Andronicos, C. L., Vervoort, J. D., Hunter, R. A., 2016. Redefining the metamorphic history of the oldest rocks in the southern Rocky Mountains. Geological Society of America Bulletin, B31455-1.

Ashwal, L.D., Armstrong, R.A., Roberts, R.J., Schmitz, M.D., Corfu, F., Hetherington, C.J., Burke, K., Gerber, M., 2007. Geochronology of zircon megacrysts from nepheline-bearing gneisses as constraints on tectonic setting: implications for resetting of the U-Pb and Lu-Hf isotopic systems. Contributions to Mineralogy and Petrology, 153(4), 389-403.

Atwater, T., Stock, J., 1998. Pacific-North America plate tectonics of the Neogene southwestern United States: an update. International Geology Review, 40(5), 375-402.

Ausburn, K. R., 2006. Geology, mineralogy, and petrology of the contact zone, southern Magnet Cove igneous complex, Hot Spring County, Arkansas. M.S. thesis, Stephen F. Austin State University, Texas, USA, 166 p.

Autin, J., Bellahsen, N., Leroy, S., Husson, L., Beslier, M. O., d'Acremont, E., 2013. The role of structural inheritance in oblique rifting: insights from analogue models and application to the Gulf of Aden. Tectonophysics, 607, 51-64.

Baksi, A. K., 1997. The timing of Late Cretaceous alkalic igneous activity in the northern Gulf of Mexico basin, southeastern USA. The Journal of Geology, 105(5), 629-644.

Baldridge, W.S., Ferguson, J.F., Braile, L.W., Wang, B., Eckhardt, K., Evans, D., Schultz, C., Gilpin, B., Jiracek, G.R., Biehler, S., 1994. The western margin of the Rio Grande Rift in northern New Mexico: An aborted boundary?. Geological Society of America Bulletin, 106(12), 1538-1551.

Ballmer, M. D., Conrad, C. P., Smith, E. I., Johnsen, R., 2015. Intraplate volcanism at the edges of the Colorado Plateau sustained by a combination of triggered edge-driven convection and shear-driven upwelling. Geochemistry, Geophysics, Geosystems, 16(2), 366-379.

Barker, D. S., Mitchell, R. H., McKay, D., 1987. Late Cretaceous nephelinite to phonolite magmatism in the Balcones province, Texas. Geological Society of America Special Papers, 215, 293-304.

Befus, K. S., Hanson, R. E., Lehman, T. M., Griffin, W. R., 2008. Cretaceous basaltic phreatomagmatic volcanism in west Texas: maar complex at Pena Mountain, Big Bend National park. Journal of Volcanology and Geothermal Research, 173(3), 245-264.

Befus, K. S., Hanson, R. E., Lehman, T. M., Griffin, W. R., 2008. Cretaceous basaltic phreatomagmatic volcanism in west Texas: maar complex at Pena Mountain, Big Bend National park. Journal of Volcanology and Geothermal Research, 173(3), 245-264.

Bell, K., 1998. Radiogenic isotope constraints on relationships between carbonatites and associated silicate rocks—a brief review. Journal of Petrology, 39(11-12), 1987-1996.

Bell, K., Blenkinsop, J., 1987. Nd and Sr isotopic compositions of East African carbonatites: implications for mantle heterogeneity. Geology, 15(2), 99-102.

Bell, K., Peterson, T., 1991. Nd and Sr isotope systematics of Shombole volcano, East Africa, and the links between nephelinites, phonolites, and carbonatites. Geology, 19(6), 582-585.

Bell, K., Simonetti, A., 1996. Carbonatite magmatism and plume activity: implications from the Nd, Pb and Sr isotope systematics of Oldoinyo Lengai. Journal of Petrology, 37(6), 1321-1339.

Bell, K., Simonetti, A., 2010. Source of parental melts to carbonatites-critical isotopic constraints. Mineralogy and Petrology, 98(1-4), 77-89.

Bell, K., Tilton, G. R., 2001. Nd, Pb and Sr isotopic compositions of East African carbonatites: evidence for mantle mixing and plume inhomogeneity. Journal of Petrology, 42(10), 1927-1945.

Bellahsen, N., Daniel, J. M., 2005. Fault reactivation control on normal fault growth: an experimental study. Journal of Structural Geology, 27(4), 769-780.

Benoit, M., H., Long, M. D., King, S. D., 2013. Anomalously thin transition zone and apparently isotropic upper mantle beneath Bermuda: Evidence for upwelling. Geochemistry, Geophysics, Geosystems, 14(10), 4282-4291, doi:10.1002/ggge.20277.

Bercovici, D., Karato, S., 2003. Whole-mantle convection and the transition zone water filter. Nature, 425, 39-44.

Berglund, H. T., Sheehan, A. F., Murray, M. H., Roy, M., Lowry, A. R., Nerem, R. S., Blume, F., 2012. Distributed deformation across the Rio Grande rift, Great Plains, and Colorado plateau. Geology, 40(1), 23-26.

Billen, M. I., 2010. Slab dynamics in the transition zone. Physics of the Earth and planetary interiors, 183(1), 296-308.

Bird, D. E., 2004. Jurassic tectonics of the Gulf of Mexico and central Atlantic Ocean. Ph.D. Dissertation, University of Houston, Texas, USA, 173 p.

Bird, D. E., Burke, K., Hall, S. A., Casey, J. F., 2005. Gulf of Mexico tectonic history: Hotspot tracks, crustal boundaries, and early salt distribution. AAPG bulletin, 89(3), 311-328.

Bird, P., 1998. Kinematic history of the Laramide orogeny in latitudes 35 °-49 °N, western United States. Tectonics, 17(5), 780-801.

Blackburn, T. J., Stockli, D. F., Carlson, R. W., Berendsen, P., 2008. (U-Th)/He dating of kimberlites—A case study from north-eastern Kansas. Earth and Planetary Science Letters, 275(1), 111-120.

Blackburn, T.J., Olsen, P.E., Bowring, S.A., McLean, N.M., Kent, D.V., Puffer, J., McHone, G., Rasbury, E.T., Et-Touhami, M., 2013. Zircon U-Pb geochronology links the end-Triassic extinction with the Central Atlantic Magmatic Province. Science, 340(6135), 941-945.

Blum, M., Pecha, M., 2014. Mid-Cretaceous to Paleocene North American drainage reorganization from detrital zircons. Geology, 42(7), 607-610.

Bradford, S. C., 1992. Kinematics of an accommodation zone in the Rio Grande rift: the Embudo fault zone, northern New Mexico. Master of Science thesis, the Ohio State University, 177p.

Braunstein, J., McMichael, C. E., 1976. Door Point: a buried volcano in southeast Louisiana. Gulf Coast Association of Geological Societies Transactions, 26, 79-80.

Brey, G. P., Bulatov, V. K., Girnis, A. V., Lahaye, Y., 2008. Experimental melting of carbonated peridotite at 6-10 GPa. Journal of Petrology, 49(4), 797-821.

Breyer, J. A., Busbey III, A. B., Hanson, R. E., Befus, K. E., Griffin, W. R., Hargrove, U. S., Bergman, S. C., 2007. Evidence for Late Cretaceous Volcanism in Trans-Pecos Texas. The Journal of geology, 115(2), 243-251.

Brooker, R. A., 1998. The effect of CO2 saturation on immiscibility between silicate and carbonate liquids: an experimental study. Journal of Petrology, 39(11-12), 1905-1915.

Bunge, H. P., Grand, S. P., 2000. Mesozoic plate-motion history below the northeast Pacific Ocean from seismic images of the subducted Farallon slab. Nature, 405(6784), 337-340.

Bunge, H. P., Richards, M. A., Baumgardner, J. R., 1997. A sensitivity study of three-dimensional spherical mantle convection at 108 Rayleigh number: Effects of depth-dependent viscosity, heating mode, and an endothermic phase change. Journal of Geophysical Research: Solid Earth (1978-2012), 102(B6), 11991-12007.

Burke, K., 1988. Tectonic evolution of the Caribbean. Annual Review of Earth and Planetary Sciences, 16, 201-230.

Burke, K., 2011. Plate tectonics, the Wilson Cycle, and mantle plumes: geodynamics from the top. Annual Review of Earth and Planetary Sciences, 39, 1-29.

Burke, K., Ashwal, L.D., Webb, S., 2003. New way to map old sutures using deformed alkaline rocks and carbonatites. Geology, 31(5), 391-394.

Burke, K., Dewey, J. F., 1973. Plume-generated triple junctions: key indicators in applying plate tectonics to old rocks. The Journal of Geology, 406-433.

Burke, K., Khan, S. D., Mart, R. W., 2008. Grenville Province and Monteregian carbonatite and nepheline syenite distribution related to rifting, collision, and plume passage. Geology, 36(12), 983-986.

Burke, K., Roberts, D., Ashwal, L.D., 2007. Alkaline rocks and carbonatites of northwestern Russia and northern Norway: Linked Wilson cycle records extending over two billion years: Tectonics, 26, TC4015, doi: 10.1029/2006TC002052.

Butterworth, N.P., Talsma, A.S., Müller, R.D., Seton, M., Bunge, H.P., Schuberth, B.S.A., Shephard, G.E., Heine, C., 2014. Geological, tomographic, kinematic and geodynamic constraints on the dynamics of sinking slabs. Journal of Geodynamics, 73, 1-13.

Canil, D. and Scarfe, C., 1990. Phase relations in peridotite + CO2 system to 12 GPa: implications for kimberlites and carbonate stability in the Earth's upper mantle. Journal of Geophysical Research 95, 15805-15816.

Cartigny, P., 2005. Stable isotopes and the origin of diamond. Elements, 1(2), 79-84.

Cather, S. M., 1990. Stress and volcanism in the northern Mogollon-Datil volcanic field, New Mexico: Effects of the post-Laramide tectonic transition. Geological Society of America Bulletin, 102(11), 1447-1458.

Cather, S. M., Karlstrom, K. E., Timmons, J. M., & Heizler, M. T., 2006. Palinspastic reconstruction of Proterozoic basement-related aeromagnetic features in north-central New Mexico: Implications for Mesoproterozoic to late Cenozoic tectonism. Geosphere, 2(6), 299-323.

Chakrabarti, R., Basu, A. R., Paul, D. K., 2007. Nd-Hf-Sr-Pb isotopes and trace element geochemistry of Proterozoic lamproites from southern India: subducted komatiite in the source. Chemical Geology, 236(3), 291-302.

Chapin, C. E., Cather, S. M., 1994. Tectonic setting of the axial basins of the northern and central Rio Grande rift. Geological Society of America Special Papers, 291, 5-26.

Chauvel, C., Lewin, E., Carpentier, M., Arndt, N. T., Marini, J. C., 2008. Role of recycled oceanic basalt and sediment in generating the Hf-Nd mantle array. Nature geoscience, 1(1), 64-67.

Chen, C., Zhao, D., Wu, S., 2014. Crust and upper mantle structure of the New Madrid Seismic Zone: insight into intraplate earthquakes. Physics of the Earth and Planetary Interiors, 230, 1-14.

Chen, L., Tao, W., Zhao, L., Zheng, T., 2008. Distinct lateral variation of lithospheric thickness in the Northeastern North China Craton. Earth and Planetary Science Letters, 267(1), 56-68.

Chen, W., Simonetti, A., 2013. In-situ determination of major and trace elements in calcite and apatite, and U-Pb ages of apatite from the Oka carbonatite complex: Insights into a complex crystallization history. Chemical Geology, 353, 151-172.

Christensen, U. R., 1996. The influence of trench migration on slab penetration into the lower mantle. Earth and Planetary Science Letters, 140(1), 27-39.

Chu, R., Leng, W., Helmberger, D. V., Gurnis, M., 2013. Hidden hotspot track beneath the eastern United States. Nature Geoscience, 6(11), 963-966.

Collettini, C., Niemeijer, A., Viti, C., & Marone, C., 2009. Fault zone fabric and fault weakness. Nature, 462(7275), 907-910.

Coney, P. J., Reynolds, S. J., 1977. Cordilleran benioff zones. Nature, 270, 403-406.

Connolly, J. A., Schmidt, M. W., Solferino, G., Bagdassarov, N., 2009. Permeability of asthenospheric mantle and melt extraction rates at mid-ocean ridges. Nature, 462(7270), 209-212.

Conrad, C. P., Bianco, T. A., Smith, E. I., Wessel, P., 2011. Patterns of intraplate volcanism controlled by asthenospheric shear. Nature Geoscience, 4(5), 317-321.

Copeland, P., Currie, C., Lawton, T., Murphy, M. A., in press)

Corti, G., 2008. Control of rift obliquity on the evolution and segmentation of the main Ethiopian rift. Nature Geoscience, 1(4), 258-262.

Corti, G., 2009. Continental rift evolution: from rift initiation to incipient break-up in the Main Ethiopian Rift, East Africa. Earth-Science Reviews, 96(1), 1-53.

Corti, G., Philippon, M., Sani, F., Keir, D., Kidane, T., 2013. Re-orientation of the extension direction and pure extensional faulting at oblique rift margins: comparison between the Main Ethiopian Rift and laboratory experiments. Terra Nova, 25(5), 396-404.

Cox, R. T., Van Arsdale, R. B., 2002. The Mississippi Embayment, North America: a first order continental structure generated by the Cretaceous superplume mantle event. Journal of Geodynamics, 34(2), 163-176.

Creaser, R. A., Grütter, H., Carlson, J., Crawford, B., 2004. Macrocrystal phlogopite Rb-Sr dates for the Ekati property kimberlites, Slave Province, Canada: evidence for multiple intrusive episodes in the Paleocene and Eocene. Lithos, 76(1), 399-414.

Cullers, R. L., Ramakrishnan, S., Berendsen, P., Griffin, T., 1985. Geochemistry and petrogenesis of lamproites, late Cretaceous age, Woodson County, Kansas, USA. Geochimica et Cosmochimica Acta, 49(6), 1383-1402.

Currie, C. A., Beaumont, C., 2011. Are diamond-bearing Cretaceous kimberlites related to low-angle subduction beneath western North America?. Earth and Planetary Science Letters, 303(1), 59-70.

D'Agostino, N., Chamot-Rooke, N., Funiciello, R., Jolivet, L., Speranza, F., 1998. The role of pre-existing thrust faults and topography on the styles of extension in the Gran Sasso range (central Italy. Tectonophysics, 292(3), 229-254.

Dalton, J. A. and Presnall, D. C., 1998. Carbonatitic melts along the solidus of model lherzolite in the system CaO-MgO-Al2O3-SiO2-CO2. Contributions to Mineralogy and Petrology 131, 123-135.

Daniel, C. G., Pfeifer, L. S., Jones, J. V., McFarlane, C. M., 2013. Detrital zircon evidence for non-Laurentian provenance, Mesoproterozoic (ca. 1490-1450 Ma) deposition and orogenesis in a reconstructed orogenic belt, northern New Mexico, USA: Defining the Picuris orogeny. Geological Society of America Bulletin, 125(9-10), 1423-1441.

Dasgupta, R., Hirschmann, M. M., 2010. The deep carbon cycle and melting in Earth's interior. Earth and Planetary Science Letters, 298(1), 1-13.

Davies, D. R., Rawlinson, N., 2014. On the origin of recent intraplate volcanism in Australia. Geology, 42(12), 1031-1034.

Davies, D. R., Rawlinson, N., Iaffaldano, G., Campbell, I. H., 2015. Lithospheric controls on magma composition along Earth's longest continental hotspot track. Nature, 525(7570), 511-514.

Davies, R. M., Griffin, W. L., O'Reilly, S. Y., Doyle, B. J., 2004a. Mineral inclusions and geochemical characteristics of microdiamonds from the DO27, A154, A21, A418, DO18, DD17 and Ranch Lake kimberlites at Lac de Gras, Slave Craton, Canada. Lithos, 77(1), 39-55.

Davies, R. M., Griffin, W. L., O'Reilly, S. Y., McCandless, T. E., 2004b. Inclusions in diamonds from the K14 and K10 kimberlites, Buffalo Hills, Alberta, Canada: diamond growth in a plume?. Lithos, 77(1), 99-111.

DeCelles, P. G., 2004. Late Jurassic to Eocene evolution of the Cordilleran thrust belt and foreland basin system, western USA. American Journal of Science, 304(2), 105-168.

DeCelles, P. G., Ducea, M. N., Kapp, P., Zandt, G., 2009. Cyclicity in Cordilleran orogenic systems. Nature Geoscience, 2(4), 251-257.

DeCelles, P. G., Graham, S. A., 2015. Cyclical processes in the North American Cordilleran orogenic system. Geology, 43(6), 499-502.

Dickinson, W. R., 2004. Evolution of the North American cordillera. Annual Review of Earth and Planetary Sciences, 32, 13-45.

Dickinson, W. R., Lawton, T. F., 2003. Sequential intercontinental suturing as the ultimate control for Pennsylvanian Ancestral Rocky Mountains deformation. Geology, 31(7), 609-612.

Dixon, J. E., Leist, L., Langmuir, C., Schilling, J. G., 2002. Recycled dehydrated lithosphere observed in plume-influenced mid-ocean-ridge basalt. Nature, 420(6914), 385-389.

Doblas, M., 1998. Slickenside kinematic indicators. Tectonophysics, 295(1), 187-197.

Dohmen, T. E., 2002. Age dating of expected MCSB seismic event suggests that it is the K/T boundary. Gulf Coast Association of Geological Societies Transactions, 52, 177-180.

Drenth, B. J., Grauch, V. J. S., Rodriguez, B. D., 2013. Geophysical constraints on Rio Grande rift structure in the central San Luis Basin, Colorado and New Mexico. Geological Society of America Special Papers, 494, 75-99.

du Bray, E. A., Harlan, S. S., 1996. The Eocene Big Timber stock, south-central Montana: Development of extensive compositional variation in an arc-related intrusion by side-wall crystallization and cumulate glomerocryst remixing. Geological Society of America Bulletin, 108(11), 1404-1424.

Dudás, F. Ö., 1991. Geochemistry of igneous rocks from the Crazy Mountains, Montana, and tectonic models for the Montana alkalic province. Journal of Geophysical Research: Solid Earth, 96(B8), 13261-13277.

Duke, G. I., 2009. Black Hills-Alberta carbonatite-kimberlite linear trend: Slab edge at depth?. Tectonophysics, 464(1), 186-194.

Duke, G. I., Carlson, R. W., Frost, C. D., Hearn, B. C., Eby, G. N., 2014. Continent-scale linearity of kimberlite-carbonatite magmatism, mid-continent North America. Earth and Planetary Science Letters, 403, 1-14.

Duncan, R. A., 1984. Age progressive volcanism in the New England Seamounts and the opening of the central Atlantic Ocean. Journal of Geophysical Research: Solid Earth, 89(B12), 9980-9990.

Dunn, D. P., 2002. Xenolith mineralogy and geology of the Prairie Creek lamproite province, Arkansas. Ph.D. Dissertation, University of Texas at Austin, Texas, USA, 147 p.

Ebinger, C. J., 1989. Tectonic development of the western branch of the East African rift system. Geological Society of America Bulletin, 101(7), 885-903.

Ebinger, C. J., Sleep, N. H., 1998. Cenozoic magmatism throughout east Africa resulting from impact of a single plume. Nature, 395(6704), 788-791.

Ebinger, C. J., van Wijk, J., Keir, D., 2013. The time scales of continental rifting: Implications for global processes. Geological Society of America Special Papers, 500, 371-396.

Eby, G. N. and Vasconcelos, P., 2009. Geochronology of the Arkansas Alkaline Province, Southeastern United States. The Journal of Geology, 117, 615-626. DOI: 10.1086/605779

Eby, G. N., Krueger, H. W., Creasy, J. W., 1992. Geology, geochronology, and geochemistry of the White Mountain batholith, New Hampshire. Geological Society of America Special Papers, 268, 379-398.

Eccles, D. R., Creaser, R. A., Heaman, L. M., Ward, J., 2008. Rb-Sr and U-Pb geochronology and setting of the Buffalo Head Hills kimberlite field, northern Alberta. Canadian Journal of Earth Sciences, 45(5), 513-529.

Eccles, D. R., Heaman, L. M., Luth, R. W., Creaser, R. A., 2004. Petrogenesis of the Late Cretaceous northern Alberta kimberlite province. Lithos, 76(1), 435-459.

Eddy, D. R., Van Avendonk, H. J., Christeson, G. L., Norton, I. O., Karner, G. D., Johnson, C. A., Snedden, J. W., 2014. Deep crustal structure of the northeastern Gulf of Mexico: Implications for rift evolution and seafloor spreading. Journal of Geophysical Research: Solid Earth, 119(9), 6802-6822.

Engebretsen, D.C., Cox, A., Gordon, R.G., 1985. Relative motions between oceanic and continental plates in the Pacific Basin. Geological Society of America Special Papers. 206, 560-569.

Erslev, E. A., 2001. Multistage, multidirectional Tertiary shortening and compression in north-central New Mexico. Geological Society of America Bulletin, 113(1), 63-74.

Ewing, T. E., 2009. The Ups and Downs of the Sabine Uplift and the Northern Gulf of Mexico Basin: Jurassic Basement Blocks, Cretaceous Thermal Uplifts, and Cenozoic Flexure. Gulf Coast Association of Geological Societies Transactions, 59, 253-269.

Faccenna, C., Becker, T. W., Lallemand, S., Lagabrielle, Y., Funiciello, F., Piromallo, C., 2010. Subduction-triggered magmatic pulses: A new class of plumes?. Earth and Planetary Science Letters, 299(1), 54-68.

Faulds, J. E., & Varga, R. J., 1998. The role of accommodation zones and transfer zones in the regional segmentation of extended terranes. Geological Society of America Special Papers, 323, 1-46.

Faulkner, D. R., Mitchell, T. M., Healy, D., Heap, M. J., 2006. Slip on'weak'faults by the rotation of regional stress in the fracture damage zone. Nature, 444(7121), 922-925.

Faure, S., Godey, S., Fallara, F., Trépanier, S., 2011. Seismic architecture of the Archean North American mantle and its relationship to diamondiferous kimberlite fields. Economic Geology, 106(2), 223-240.

Flament, N., Gurnis, M., Williams, S., Seton, M., Skogseid, J., Heine, C., Müller, R. D., 2014. Topographic asymmetry of the South Atlantic from global models of mantle flow and lithospheric stretching. Earth and Planetary Science Letters, 387, 107-119.

Flohr, M. J., Ross, M., 1990. Alkaline igneous rocks of Magnet Cove, Arkansas: mineralogy and geochemistry of syenites. Lithos, 26(1), 67-98.

Foley, S., Venturelli, G., Green, D. H., Toscani, L., 1987. The ultrapotassic rocks: characteristics, classification, and constraints for petrogenetic models. Earth-Science Reviews, 24(2), 81-134.

Forte, A. M., Mitrovica, J. X., Moucha, R., Simmons, N. A., Grand, S. P., 2007. Descent of the ancient Farallon slab drives localized mantle flow below the New Madrid seismic zone. Geophysical Research Letters, 34(4), L04308, doi:10.1029/2006GL027895.

Fossen, H., 2010. Structural geology. Cambridge University Press, 463 p.

Fraser, K. J., Hawkesworth, C. J., Erlank, A. J., Mitchell, R. H., Scott-Smith, B. H., 1985. Sr, Nd and Pb isotope and minor element geochemistry of lamproites and kimberlites. Earth and Planetary Science Letters, 76(1), 57-70.

Fukao, Y., Obayashi, M., 2013. Subducted slabs stagnant above, penetrating through, and trapped below the 660 km discontinuity. Journal of Geophysical Research: Solid Earth, 118(11), 5920-5938.

Fukao, Y., Obayashi, M., Inoue, H., Nenbai, M., 1992. Subducting slabs stagnant in the mantle transition zone. Journal of Geophysical Research: Solid Earth, 97(B4), 4809-4822.

Fukao, Y., Widiyantoro, S., Obayashi, M., 2001. Stagnant slabs in the upper and lower mantle transition region: Reviews of Geophysics, 39, 291-323, doi:10.1029/1999RG000068.

Gaffney, A. M., Blichert-Toft, J., Nelson, B. K., Bizzarro, M., Rosing, M., Albarede, F., 2007. Constraints on source-forming processes of West Greenland kimberlites inferred from Hf-Nd isotope systematics. Geochimica et Cosmochimica Acta, 71(11), 2820-2836.

Gaillard, F., Malki, M., Iacono-Marziano, G., Pichavant, M., Scaillet, B., 2008. Carbonatite melts and electrical conductivity in the asthenosphere. Science, 322(5906), 1363-1365.

Galloway, W. E., 2008. Depositional evolution of the Gulf of Mexico sedimentary basin. Sedimentary Basins of the World, 5, 505-549.

Gerya, T. V., Yuen, D. A., 2003. Rayleigh-Taylor instabilities from hydration and melting propel 'cold plumes' at subduction zones. Earth and Planetary Science Letters, 212(1), 47-62.

Goes, S., Capitanio, F. A., Morra, G., 2008. Evidence of lower-mantle slab penetration phases in plate motions. Nature, 451(7181), 981-984.

Gogineni, S. V., Melton, C. E., Giardini, A. A., 1978. Some petrological aspects of the Prairie Creek diamond-bearing kimberlite diatreme, Arkansas. Contributions to Mineralogy and Petrology, 66(3), 251-261.

Grand, S. P., 2002. Mantle shear-wave tomography and the fate of subducted slabs. Philosophical Transactions of the Royal Society of London A: Mathematical, Physical and Engineering Sciences, 360(1800), 2475-2491.

Grassi, D., Schmidt, M. W., 2011. The melting of carbonated pelites from 70 to 700 km depth. Journal of Petrology, egr002.

Griffin, W. L., Begg, G. C., Dunn, D., O'Reilly, S. Y., Natapov, L. M., Karlstrom, K., 2011. Archean lithospheric mantle beneath Arkansas: Continental growth by microcontinent accretion. Geological Society of America Bulletin, 123(9-10), 1763-1775.

Griffin, W. R., 2008. Geochemistry and geochronology of the Balcones Igneous Province, Texas. Ph.D. Dissertation, The University of Texas at Dallas, 241 p.

Griffin, W. R., Foland, K. A., Stern, R. J., Leybourne, M. I., 2010. Geochronology of bimodal alkaline volcanism in the Balcones Igneous Province, Texas: Implications for Cretaceous intraplate magmatism in the northern Gulf of Mexico magmatic zone. The Journal of Geology, 118(1), 1-21.

Gudfinnsson, G. H., Presnall, D. C., 2005. Continuous gradations among primary carbonatitic, kimberlitic, melilititic, basaltic, picritic, and komatiitic melts in equilibrium with garnet lherzolite at 3-8 GPa. Journal of Petrology, 46(8), 1645-1659.

Hamilton, J. S., 2009. A new multistage model for the Late Cenozoic to present tectonic evolution of north-central New Mexico. Master of Science thesis, University of Houston, 76p.

Hammouda, T., 2003. High-pressure melting of carbonated eclogite and experimental constraints on carbon recycling and storage in the mantle. Earth and Planetary Science Letters, 214(1), 357-368.

Hammouda, T., Keshav, S., 2015. Melting in the mantle in the presence of carbon: Review of experiments and discussion on the origin of carbonatites. Chemical Geology, 418, 171-188.

Hansen, D. M., Redfern, J., Federici, F., Di Biase, D., Bertozzi, G., 2008. Miocene igneous activity in the Northern Subbasin, offshore Senegal, NW Africa. Marine and Petroleum Geology, 25(1), 1-15.

Hart, S. R., Blijsztajn, J., Craddock, C., 1995. Cenozoic volcanism in Antarctica: Jones Mountains and Peter I Island. Geochimica et Cosmochimica Acta, 59(16), 3379-3388.

Hart, S. R., Blusztajn, J., 2006. Age and geochemistry of the mafic sills, ODP site 1276, Newfoundland margin. Chemical Geology, 235(3), 222-237.

Hawkesworth, C. J., Kemp, A. I. S., 2006. Evolution of the continental crust. Nature, 443(7113), 811-817.

Healy, D., 2008. Damage patterns, stress rotations and pore fluid pressures in strike-slip fault zones. Journal of Geophysical Research: Solid Earth, 113, B12407, doi:10.1029/2008JB005655.

Heaman, L. M., Kjarsgaard, B. A., 2000. Timing of eastern North American kimberlite magmatism: continental extension of the Great Meteor hotspot track?. Earth and Planetary Science Letters, 178(3), 253-268.

Heaman, L. M., Kjarsgaard, B. A., Creaser, R. A., 2004. The temporal evolution of North American kimberlites. Lithos, 76(1), 377-397.

Heaman, L. M., Pell, J., Grütter, H. S., Creaser, R. A., 2015. U-Pb geochronology and Sr/Nd isotope compositions of groundmass perovskite from the newly discovered Jurassic Chidliak kimberlite field, Baffin Island, Canada. Earth and Planetary Science Letters, 415, 183-199.

Heatherington, A. L., Mueller, P. A., 2003. Mesozoic igneous activity in the Suwannee terrane, southeastern USA: petrogenesis and Gondwanan affinities. Gondwana Research, 6(2), 296-311.

Hegner, E., Roddick, J. C., Fortier, S. M., Hulbert, L., 1995. Nd, Sr, Pb, Ar, and O isotopic systematics of Sturgeon Lake kimberlite, Saskatchewan, Canada: constraints on emplacement age, alteration, and source composition. Contributions to Mineralogy and Petrology, 120(2), 212-222.

Heydari, E., Byerly, G. R., Henry, D. J., 1997. Contact metamorphism and over maturation of organic matter associated with an igneous intrusion in the Smackover Formation, Northeastern Louisiana. Gulf Coast Association of Geological Societies Transactions, 47, 201-213.

Hildebrand, R. S., 2009. Did westward subduction cause Cretaceous-Tertiary orogeny in the North American Cordillera?. Geological Society of America Special Papers, 457, 1-71.

Hirose, K., 1997. Partial melt compositions of carbonated peridotite at 3 GPa and role of CO2 in alkali-basalt magma generation. Geophysical Research Letters, 24, 2837-2840.

Hirose, K., Fei, Y., Ma, Y., Mao, H. K., 1999. The fate of subducted basaltic crust in the Earth's lower mantle. Nature, 397(6714), 53-56.

Hirschmann, M. M., 2006. Water, melting, and the deep Earth H2O cycle. Annual Review of Earth and Planetary Sciences, 34, 629-653.

Hoernle, K., Tilton, G., Le Bas, M. J., Duggen, S., Garbe-Schönberg, D., 2002. Geochemistry of oceanic carbonatites compared with continental carbonatites: mantle recycling of oceanic crustal carbonate. Contributions to Mineralogy and Petrology, 142(5), 520-542.

Hofmann, A. W., Jochum, K. P., Seufert, M., & White, W. M., 1986. Nb and Pb in oceanic basalts: new constraints on mantle evolution. Earth and Planetary Science Letters, 79(1-2), 33-45.

Hofmann, C., Courtillot, V., Feraud, G., Rochette, P., Yirgu, G., Ketefo, E., Pik, R., 1997. Timing of the Ethiopian flood basalt event and implications for plume birth and global change. Nature, 389(6653), 838-841.

Hole, M. J., Millett, J. M., 2016. Controls of Mantle Potential Temperature and Lithospheric Thickness on Magmatism in the North Atlantic Igneous Province. Journal of Petrology, 57(2), 417-436.

Hooper, P. R., 1990. The timing of crustal extension and the eruption of continental flood basalts. Nature, 345(6272), 246-249.

Hopper, J. R., Mutter, J. C., Larson, R. L., Mutter, C. Z., 1992. Magmatism and rift margin evolution: Evidence from northwest Australia. Geology, 20(9), 853-857.

Huang, X., Xu, Y., Karato, S. I., 2005. Water content in the transition zone from electrical conductivity of wadsleyite and ringwoodite. Nature, 434(7034), 746-749.

Hudec, M. R., Jackson, M. P., Peel, F. J., 2013. Influence of deep Louann structure on the evolution of the northern Gulf of Mexico. AAPG Bulletin, 97(10), 1711-1735.

Humphreys, E. R., Niu, Y., 2009. On the composition of ocean island basalts (OIB): The effects of lithospheric thickness variation and mantle metasomatism. Lithos, 112(1), 118-136.

Humphreys, E., 2009. Relation of flat subduction to magmatism and deformation in the western United States. Geological Society of America Memoirs, 204, 85-98.

Ingersoll, R. V., 2001. Structural and stratigraphic evolution of the Rio Grande Rift, northern New Mexico and southern Colorado. International Geology Review, 43(10), 867-891.

Ingersoll, R. V., Cavazza, W., Baldridge, W. S., Shafiqullah, M., 1990. Cenozoic sedimentation and paleotectonics of north-central New Mexico: Implications for initiation and evolution of the Rio Grande rift. Geological Society of America Bulletin, 102(9), 1280-1296.

Jing, Z., Karato, S. I., 2009. The density of volatile bearing melts in the Earth's deep mantle: The role of chemical composition. Chemical Geology, 262(1), 100-107.

Kalt, A., Hegner, E., Satir, M., 1997. Nd, Sr, and Pb isotopic evidence for diverse lithospheric mantle sources of East African Rift carbonatites. Tectonophysics, 278(1), 31-45.

Karato, S. I., 2011. Water distribution across the mantle transition zone and its implications for global material circulation. Earth and Planetary Science Letters, 301(3), 413-423.

Karato, S. I., Bercovici, D., Leahy, G., Richard, G., Jing, Z., 2006. The Transition-Zone Water Filter Model for Global Material Circulation: Where Do We stand?. Earth's Deep Water Cycle, 289-313.

Karato, S. I., Wu, P., 1993. Rheology of the upper mantle- A synthesis. Science, 260(5109), 771-778.

Karlstrom, K. E., Cather, S. M., Kelley, S. A., Heizler, M. T., Pazzaglia, F. J., Roy, M., 1999. Sandia Mountains and Rio Grande rift: Ancestry of structures and history of deformation. In Albuquerque Geology, New Mexico Geological Society 50th Annual Field Conference Guidebook, 155-165.

Karlstrom, K. E., Dallmeyer, R. D., Grambling, J. A., 1997. 40Ar/39Ar evidence for 1.4 Ga regional metamorphism in New Mexico: Implications for thermal evolution of lithosphere in the southwestern USA. The Journal of Geology, 105(2), 205-224.

Karner, G. D., Shillington, D. J., 2005. Basalt sills of the U reflector, Newfoundland Basin: A serendipitous dating technique. Geology, 33(12), 985-988.

Kelbert, A., Schultz, A., Egbert, G., 2009. Global electromagnetic induction constraints on transition-zone water content variations. Nature, 460(7258), 1003-1006.

Kelley, S. A., & Chapin, C. E., 1995. Apatite fission-track thermochronology of southern Rocky Mountain-Rio Grande rift-western High Plains provinces. Geology of the Santa Fe region: New Mexico Geological Society Field Guidebook, 46, 87-96.

Kelley, S. A., Duncan, I. J., 1986. Late Cretaceous to middle Tertiary tectonic history of the northern Rio Grande rift, New Mexico. Journal of Geophysical Research: Solid Earth, 91(B6), 6246-6262.

Kelley, S. A., Osburn, G. R., Ferguson, C. F., Moore, J., Kempter, K., 2005. Geologic map of the Cañones quadrangle, Rio Arriba County, New Mexico. New Mexico Bureau of Geology and Mineral Resources Open-file Geologic Map 107, scale 1:22,732.

Kelley, S.A., Kempter, K.A., McIntosh, W.C., Maldonado, F., Smith, G.A., Connell, S.D., Koning, D.J. and Whiteis, J., 2013.Syndepositional deformation and provenance of Oligocene to Lower Miocene sedimentary rocks along the western margin of the Rio Grande rift, Jemez Mountains, New Mexico. Geological Society of America Special Papers, 494, 101-123.

Kelley, V. C., 1979. Tectonics, Middle Rio Grande Rift, New Mexico, in Rio Grande Rift: Tectonics and Magmatism (ed R. E. Riecker), American Geophysical Union, Washington, D. C., 57-70. doi: 10.1029/SP014p0057

Kelley, V. C., 1982. The right-relayed Rio Grande rift, Taos to Hatch, New Mexico. Albuquerque Country II: New Mexico Geological Society Guidebook, 33, 147-151.

Kelson, K. I., Bauer, P. W., Unruh, J. R., Bott, J. D. J., 2004. Late Quaternary characteristics of the northern Embudo fault, Taos County, New Mexico. Geology of the Taos Region: New Mexico Geological Society Guidebook, 55, 147-157.

Kempter, K., Kelley, S., Koning, D., Ferguson, C., Osburn, B., Fluk, L., 2005. Preliminary geologic map of the Vallecitos quadrangle, Rio Arriba County, New Mexico. New Mexico Bureau of Geology and Mineral Resources Open-file Geologic Map 108, scale 1:24,000.

Kempter, K., Koning, D. J., Karlstrom, K. E., 2008. Geologic map of the Valle Grande Peak quadrangle, Rio Arriba County, New Mexico. New Mexico Bureau of Geology and Mineral Resources Open-file Geologic Map 180, scale 1:24,000.

Kempter, K., Zeigler, K., Koning, D., Lucas, S., 2007. Preliminary geologic map of the Canjilon SE quadrangle, Rio Arriba County, New Mexico. New Mexico Bureau of Geology and Mineral Resources Open-file Digital Geologic Map OF-GM 150, scale 1:24,000.

Kim, Y. S., Sanderson, D. J., 2005. The relationship between displacement and length of faults: a review. Earth-Science Reviews, 68(3), 317-334.

King, S. D., 2007. Hotspots and edge-driven convection. Geology, 35(3), 223-226.

King, S. D., Anderson, D. L., 1998. Edge-driven convection. Earth and Planetary Science Letters, 160(3), 289-296.

King, S. D., Frost, D. J., Rubie, D. C., 2015. Why cold slabs stagnate in the transition zone. Geology, 43(3), 231-234.

King, S. D., Ritsema, J., 2000. African hot spot volcanism: small-scale convection in the upper mantle beneath cratons. Science, 290(5494), 1137-1140.

Kirkpatrick, J. D., Brodsky, E. E., 2014. Slickenline orientations as a record of fault rock rheology. Earth and Planetary Science Letters, 408, 24-34.

Kiseeva, E. S., Litasov, K. D., Yaxley, G. M., Ohtani, E., Kamenetsky, V. S., 2013. Melting and phase relations of carbonated eclogite at 9-21 GPa and the petrogenesis of alkali-rich melts in the deep mantle. Journal of Petrology, 54(8), 1555-1583.

Kjarsgaard, B. A., Harvey, S., McClintock, M., Zonneveld, J. P., Du Plessis, P., McNeil, D., Heaman, L., 2009. Geology of the Orion South kimberlite, Fort à la Corne, Canada. Lithos, 112, 600-617.

Kluth, C. F., 1986. Plate tectonics of the Ancestral Rocky Mountains: Part III. Middle Rocky Mountains. AAPG Memoir 41: Paleotectonics and Sedimentation in the Rocky Mountain Region, United States, 353-369.

Koning, D. J., 2004a. Preliminary geologic map of the Lyden quadrangle, Rio Arriba County, New Mexico. New Mexico Bureau of Geology and Mineral Resources Open-file Geologic Map 083, scale 1:24,000.

Koning, D. J., Ferguson, J. F., Paul, P. J., Baldridge, W. S., 2004b. Geologic structure of the Velarde graben and the southern Embudo fault system, north-central New Mexico. Geology of the Taos Region: New Mexico Geological Society Guidebook, 55, 158-171.

Koning, D. J., Karlstrom, K., May, J., Skotnicki, S., Horning, R., Newell D., Muehlberger, W. R., 2005a. Preliminary geologic map of the Ojo Caliente quadrangle, Rio Arriba and Taos Counties, New Mexico. New Mexico Bureau of Geology and Mineral Resources Open-file Geologic Map 101, scale 1:24,000.

Koning, D. J., Karlstrom, K., Salem, A., Lombardi, C., 2007. Preliminary geologic map of the La Madera quadrangle, Rio Arriba County, New Mexico. New Mexico Bureau of Geology and Mineral Resources Open-file Geologic Map 141, scale 1:24,000.

Koning, D. J., Kelley, S., Zeigler, K. E., Lucas, S. G., 2006. Geologic map of the Ghost Ranch quadrangle, Rio Arriba County, New Mexico. New Mexico Bureau of Geology and Mineral Resources Open-file Geologic Map 127, scale 1:23,386.

Koning, D. J., May, J., Aby, S., Horning, R., 2004. Geologic map of the Medanales quadrangle, Rio Arriba County, New Mexico. New Mexico Bureau of Geology and Mineral Resources Open-file Geologic Map 089, scale 1:24,000.

Koning, D. J., Smith, G. A., Aby, S., 2008. Geologic map of the El Rito quadrangle, Rio Arriba County, New Mexico. Mexico. New Mexico Bureau of Geology and Mineral Resources Open-file Geologic Map 166, scale 1:24,000.

Koning, D., Skotnicki, S., Kelley, S., Moore, J., 2005b. Geologic Map of the Chili quadrangle, Rio Arriba County, New Mexico. New Mexico Bureau of Geology and Mineral Resources Open-file Geologic Map 103, scale 1:24,000.

Koning, D.J., Grauch, V.J.S., Connell, S.D., Ferguson, J., McIntosh, W., Slate, J.L., Wan, E., Baldridge, W. S., 2013. Structure and tectonic evolution of the eastern Espanola Basin, Rio Grande rift, north-central New Mexico. Geological Society of America Special Papers, 494, 185-219.

Koptev, A., Calais, E., Burov, E., Leroy, S., Gerya, T., 2015. Dual continental rift systems generated by plume-lithosphere interaction. Nature Geoscience, 8(5), 388-392.

Kreemer, C., Blewitt, G., Bennett, R. A., 2010. Present-day motion and deformation of the Colorado Plateau. Geophysical Research Letters, 37(10), L10311, doi:10.1029/2010GL043374.

Lambert, D. D., Shirey, S. B., Bergman, S. C., 1995. Proterozoic lithospheric mantle source for the Prairie Creek lamproites: Re-Os and Sm-Nd isotopic evidence. Geology, 23(3), 273-276.

Landman, R. L., Flowers, R. M., 2013. (U-Th)/He thermochronologic constraints on the evolution of the northern Rio Grande Rift, Gore Range, Colorado, and implications for rift propagation models. Geosphere, 9(1), 170-187.

Le Bas, M. J., Le Maitre, R. W., Streckeisen, A., Zanettin, B., 1986. A chemical classification of volcanic rocks based on the total alkali-silica diagram. Journal of petrology, 27(3), 745-750.

Leckie, D. A., Kjarsgaard, B. A., Bloch, J., McIntyre, D., McNeil, D., Stasiuk, L., Heaman, L., 1997. Emplacement and reworking of Cretaceous, diamond-bearing, crater facies kimberlite of central Saskatchewan, Canada. Geological Society of America Bulletin, 109(8), 1000-1020.

Ledger, E. B., Rowe, M. W., Howard, J. M., 1988. Uranium contents of carbonatite minerals, Magnet Cove, Arkansas, USA. Chemical geology, 69(1), 165-169.

Li, C., van der Hilst, R. D., Engdahl, E. R., Burdick, S., 2008. A new global model for P wave speed variations in Earth's mantle. Geochemistry, Geophysics, Geosystems, 9(5).

Li, Z., Li, J., Lange, R., Liu, J., Militzer, B., 2016. Determination of calcium carbonate and sodium carbonate melting curves up to Earth's transition zone pressures with implications for the deep carbon cycle. Earth and Planetary Science Letters, in press.

Litasov, K. D., Ohtani, E., 2005. Phase relations in hydrous MORB at 18-28GPa: implications for heterogeneity of the lower mantle. Physics of the Earth and Planetary Interiors, 150(4), 239-263.

Liu, L., 2014. Rejuvenation of Appalachian topography caused by subsidence-induced differential erosion. Nature Geoscience, 7(7), 518-523.

Liu, L., Gurnis, M., Seton, M., Saleeby, J., Müller, R. D., Jackson, J. M., 2010. The role of oceanic plateau subduction in the Laramide orogeny. Nature Geoscience, 3(5), 353-357.

Liu, L., Stegman, D. R., 2011. Segmentation of the Farallon slab. Earth and Planetary Science Letters, 311(1), 1-10.

Liu, S., Nummedal, D., Liu, L., 2011. Migration of dynamic subsidence across the Late Cretaceous United States Western Interior Basin in response to Farallon plate subduction. Geology, 39(6), 555-558.

Liu, Y., Murphy, M., 2013. Oblique Extension and Basinward Tilting along the Cañones Fault Zone, West Margin of the Rio Grande Rift. Geological Society of America Annual Meeting in Denver, Abstracts with Programs 45 (7), 443.

Lucazeau, F., Leroy, S., Bonneville, A., Goutorbe, B., Rolandone, F., d'Acremont, E., Watremez, L., Düsünur, D., Tuchais, P., Huchon, P., Bellahsen, N., Al-Toubi, K., 2008. Persistent thermal activity at the Eastern Gulf of Aden after continental break-up. Nature Geoscience, 1(12), 854-858.

Mack, G. H., Seager, W. R., Kieling, J., 1994. Late Oligocene and Miocene faulting and sedimentation, and evolution of the southern Rio Grande rift, New Mexico, USA. Sedimentary Geology, 92(1-2), 79-96.

Maldonado, F., 2008. Geologic map of the Abiquiu quadrangle, Rio Arriba County, New Mexico. U.S. Geological Survey Scientific Investigations Map 2998, scale 1:24,000.

Maldonado, F., Miggins, D. P., Budahn, J. R., Spell, T., 2013. Deformational and erosional history for the Abiquiu and contiguous area, north-central New Mexico: Implications for formation of the Abiquiu embayment and a discussion of new geochronological and geochemical analysis. Geological Society of America Special Papers, 494, 125-155.

Manley, K., 1982. Geologic map of the Broke Off Mountain quadrangle, Rio Arriba County, New Mexico. U.S. Geological Survey Miscellaneous Field Studies Map 1450, scale 1:24,000.

Manley, K., Wobus, R. A., 1982. Reconnaissance geologic map of the Mule Canyon quadrangle, Rio Arriba County, New Mexico. U.S. Geological Survey Miscellaneous Field Studies Map 1407, scale 1:24,000.

Marshak, S., Karlstrom, K., Timmons, J. M., 2000. Inversion of Proterozoic extensional faults: An explanation for the pattern of Laramide and Ancestral Rockies intracratonic deformation, United States. Geology, 28(8), 735-738.

Marton, G., Buffler, R. T., 1994. Jurassic reconstruction of the Gulf of Mexico Basin. International Geology Review, 36(6), 545-586.

Marzoli, A., Renne, P. R., Piccirillo, E. M., Ernesto, M., Bellieni, G., De Min, A., 1999. Extensive 200-million-year-old continental flood basalts of the Central Atlantic Magmatic Province. Science, 284(5414), 616-618.

Matsukage, K. N., Jing, Z., Karato, S. I., 2005. Density of hydrous silicate melt at the conditions of Earth's deep upper mantle. Nature, 438(7067), 488-491.

Matton, G., Jébrak, M., 2009. The Cretaceous Peri-Atlantic Alkaline Pulse (PAAP): Deep mantle plume origin or shallow lithospheric break-up?. Tectonophysics, 469(1), 1-12.

Mazza, S. E., Gazel, E., Johnson, E. A., Kunk, M. J., McAleer, R., Spotila, J. A., Bizimis, M., Coleman, D. S., 2014. Volcanoes of the passive margin: The youngest magmatic event in eastern North America. Geology, 42(6), 483-486.

McCandless, T.E., 1999. Kimberlites: mantle expressions of deep-seated subduction. In: Gurney, J.J., Gurney, J.L., Pacsoe, M.D., Richardson, S.H., Eds., Proceedings of the Seventh International Kimberlite Conference, 2, 545- 549.

McCulloch, M. T., Jaques, A. L., Nelson, D. R., Lewis, J. D., 1983. Nd and Sr isotopes in kimberlites and lamproites from Western Australia: an enriched mantle origin. Nature, 302(5907), 400-403.

McDonough, W. F., Sun, S. S., 1995. The composition of the Earth. Chemical geology, 120(3), 223-253.

McKenzie, D., 1978. Some remarks on the development of sedimentary basins. Earth and Planetary science letters, 40(1), 25-32.

McQuarrie, N., & Oskin, M., 2010. Palinspastic restoration of NAVDat and implications for the origin of magmatism in southwestern North America. Journal of Geophysical Research: Solid Earth, 115(B10).

McQuarrie, N., & Wernicke, B. P., 2005. An animated tectonic reconstruction of southwestern North America since 36 Ma. Geosphere, 1(3), 147-172.

Menzies, M., Gallagher, K., Yelland, A., Hurford, A. J., 1997. Volcanic and nonvolcanic rifted margins of the Red Sea and Gulf of Aden: crustal cooling and margin evolution in Yemen. Geochimica et Cosmochimica Acta, 61(12), 2511-2527.

Meyer, R., Van Wijk, J., Gernigon, L., 2007. The North Atlantic Igneous Province: A review of models for its formation. Geological Society of America Special Papers, 430, 525-552.

Miggins, D. P., Blome, C. D., Smith, D. V., 2004. Preliminary 40Ar/39Ar geochronology of igneous intrusions from Uvalde County, Texas defining a more precise eruption history for the southern Balcones Volcanic Province. U.S. Geological Survey Open-File Report 2004-1031, 31 p.

Millonig, L. J., Gerdes, A., Groat, L. A., 2012. U-Th-Pb geochronology of meta-carbonatites and meta-alkaline rocks in the southern Canadian Cordillera: a geodynamic perspective. Lithos, 152, 202-217.

Minor, S. A., Hudson, M. R., Caine, J. S., Thompson, R. A., 2013. Oblique transfer of extensional strain between basins of the middle Rio Grande rift, New Mexico: Fault kinematic and paleostress constraints. Geological Society of America Special Papers, 494, 345-382.

Mirnejad, H., Bell, K., 2006. Origin and source evolution of the Leucite Hills lamproites: evidence from Sr-Nd-Pb-O isotopic compositions. Journal of Petrology, 47(12), 2463-2489.

Mitrovica, J. X., Beaumont, C., Jarvis, G. T., 1989. Tilting of continental interiors by the dynamical effects of subduction. Tectonics, 8(5), 1079-1094.

Morgan, P., Seager, W. R., Golombek, M. P., 1986. Cenozoic thermal, mechanical and tectonic evolution of the Rio Grande rift. Journal of Geophysical Research: Solid Earth, 91(B6), 6263-6276.

Morgan, W. J., 1983. Hotspot tracks and the early rifting of the Atlantic. Tectonophysics, 94(1-4), 123-139.

Morley, C. K., 2010. Stress re-orientation along zones of weak fabrics in rifts: An explanation for pure extension in 'oblique'rift segments?. Earth and Planetary Science Letters, 297(3), 667-673.

Motoki, M. H., Ballmer, M. D., 2015. Intraplate volcanism due to convective instability of stagnant slabs in the Mantle Transition Zone. Geochemistry, Geophysics, Geosystems, 16(2), 538-551.

Muehlberger, W. R., 1979. The Embudo fault between Pilar and Arroyo Hondo, New Mexico: an active intracontinental transform fault. In Field Conference Guidebook. NM Geologic Society, 30, 77-82.

Müller, R.D., Seton, M., Zahirovic, S., Williams, S.E., Matthews, K.J., Wright, N.M., Shephard, G.E., Maloney, K., Barnett-Moore, N., Hosseinpour, M., Bower, D. J., 2016. Ocean basin evolution and global-scale plate reorganization events since Pangea breakup. Annual Review of Earth and Planetary Sciences, 44(1), 107-138.

Murphy, D. T., Collerson, K. D., Kamber, B. S., 2002. Lamproites from Gaussberg, Antarctica: possible transition zone melts of Archaean subducted sediments. Journal of Petrology, 43(6), 981-1001.

Murphy, D. T., Kamber, B. S., Collerson, K. D., 2003. A refined solution to the first terrestrial Pb-isotope paradox. Journal of Petrology, 44(1), 39-53.

Nelson, D. R., Chivas, A. R., Chappell, B. W., McCulloch, M. T., 1988. Geochemical and isotopic systematics in carbonatites and implications for the evolution of ocean-island sources. Geochimica et Cosmochimica Acta, 52(1), 1-17.

Nowicki, T., Crawford, B., Dyck, D., Carlson, J., McElroy, R., Oshust, P., Helmstaedt, H., 2004. The geology of kimberlite pipes of the Ekati property, Northwest Territories, Canada. Lithos, 76(1), 1-27.

Nowicki, T., Porritt, L., Crawford, B., Kjarsgaard, B., 2008. Geochemical trends in kimberlites of the Ekati property, Northwest Territories, Canada: insights on volcanic and resedimentation processes. Journal of Volcanology and Geothermal Research, 174(1), 117-127.

Obayashi, M., Yoshimitsu, J., Fukao, Y., 2009. Tearing of stagnant slab. Science, 324(5931), 1173-1175.

O'Brien, H. E., Irving, A. J., McCallum, I. S., 1991. Eocene potassic magmatism in the Highwood Mountains, Montana: petrology, geochemistry, and tectonics implications. Journal of Geophysical Research: Solid Earth, 96(B8), 13,237-13,260.

O'Brien, H. E., Irving, A. J., McCallum, I. S., Thirlwall, M. F., 1995. Strontium, neodymium, and lead isotopic evidence for the interaction of post-suhduction asthenospheric potassic mafic magmas of the Highwood Mountains, Montana, USA, with ancient Wyoming craton lithospheric mantle. Geochimica et Cosmochimica Acta, 59(21), 4539-4556.

Ortega-Guti érrez, F., El ás-Herrera, M., Mor án-Zenteno, D. J., Solari, L., Luna-Gonzalez, L., Schaaf, P., 2014. A review of batholiths and other plutonic intrusions of Mexico. Gondwana Research, 26(3), 834-868.

Pandit, M. K., Kumar, M., Sial, A. N., Sukumaran, G. B., Piementle, M., Ferreira, V. P., 2016. Geochemistry and C-O and Nd-Sr isotope characteristics of the 2.4 Ga Hogenakkal carbonatites from the South Indian Granulite Terrane: evidence for an end-Archaean depleted component and mantle heterogeneity. International Geology Review, 1-20.

Panero, W. R., Pigott, J. S., Reaman, D. M., Kabbes, J. E., Liu, Z., 2015. Dry (Mg, Fe) SiO3 perovskite in the Earth's lower mantle. Journal of Geophysical Research: Solid Earth, 120(2), 894-908.

Pantaleo, N. S., Newton, M. G., Gogineni, S. V., Melton, C. E., Giardini, A. A., 1979. Mineral inclusions in four Arkansas diamonds: their nature and significance. American Mineralogist, 64, 1059-1062.

Paterson, S. R., Ducea, M. N., 2015. Arc magmatic tempos: gathering the evidence. Elements, 11(2), 91-98.

Pavlis, G. L., Sigloch, K., Burdick, S., Fouch, M. J., Vernon, F. L., 2012. Unraveling the geometry of the Farallon plate: Synthesis of three-dimensional imaging results from USArray. Tectonophysics, 532, 82-102.

Perry, F. V., Baldridge, W. S., DePaolo, D. J., 1988. Chemical and isotopic evidence for lithospheric thinning beneath the Rio Grande rift. Nature, 332, 432-434.

Petit, J. P., 1987. Criteria for the sense of movement on fault surfaces in brittle rocks. Journal of Structural Geology, 9(5), 597-608.

Philippon, M., & Corti, G., 2016. Obliquity along plate boundaries. Tectonophysics, in press.

Philippon, M., Willingshofer, E., Sokoutis, D., Corti, G., Sani, F., Bonini, M., Cloetingh, S., 2015. Slip re-orientation in oblique rifts. Geology, 43(2), 147-150.

Phipps, S.P., 1988. Deep rifts as sources for alkaline intraplate magmatism in eastern North America. Nature, 334, 27-31.

Pindell, J. L., Kennan, L., 2009. Tectonic evolution of the Gulf of Mexico, Caribbean and northern South America in the mantle reference frame: an update. Geological Society, London, Special Publications, 328(1), 1-55.

Poli, S., 2015. Carbon mobilized at shallow depths in subduction zones by carbonatitic liquids. Nature Geoscience, 8(8), 633-636.

Prelević, D., Foley, S. F., Romer, R., Conticelli, S., 2008. Mediterranean Tertiary lamproites derived from multiple source components in postcollisional geodynamics. Geochimica et Cosmochimica Acta, 72(8), 2125-2156.

Raddick, M. J., Parmentier, E. M., Scheirer, D. S., 2002. Buoyant decompression melting: A possible mechanism for intraplate volcanism. Journal of Geophysical Research: Solid Earth, 107(B10).

Rapp, R. P., Irifune, T., Shimizu, N., Nishiyama, N., Norman, M. D., Inoue, T., 2008. Subduction recycling of continental sediments and the origin of geochemically enriched reservoirs in the deep mantle. Earth and Planetary Science Letters, 271(1), 14-23.

Ray, J. S., 2009. Radiogenic isotopic ratio variations in carbonatites and associated alkaline silicate rocks: role of crustal assimilation. Journal of Petrology, 50(10), 1955-1971.

Rezak, R., Tieh, T. T., 1984. Basalt from Louisiana continental shelf. Geo-Marine Letters, 4, 69-76.

Richard, G. C., Bercovici, D., 2009. Water-induced convection in the Earth's mantle transition zone. Journal of Geophysical Research: Solid Earth, 114, B01205, doi:10.1029/2008JB005734.

Richard, G., Bercovici, D., Karato, S. I., 2006. Slab dehydration in the Earth's mantle transition zone. Earth and Planetary Science Letters, 251(1), 156-167.

Ricketts, J. W., Kelley, S. A., Karlstrom, K. E., Schmandt, B., Donahue, M. S., van Wijk, J., 2016. Synchronous opening of the Rio Grande rift along its entire length at 25-10 Ma supported by apatite (U-Th)/He and fission-track thermochronology, and evaluation of possible driving mechanisms. Geological Society of America Bulletin, 128(3-4), 397-424.

Ringwood, A. E., Kesson, S. E., Hibberson, W., Ware, N., 1992. Origin of kimberlites and related magmas. Earth and Planetary Science Letters, 113(4), 521-538.

Ritsema, J., Deuss, A., Van Heijst, H. J., Woodhouse, J. H., 2011. S40RTS: a degree-40 shear-velocity model for the mantle from new Rayleigh wave dispersion, teleseismic traveltime and normal-mode splitting function measurements. Geophysical Journal International, 184(3), 1223-1236.

Rohrbach, A., Schmidt, M. W., 2011. Redox freezing and melting in the Earth/'s deep mantle resulting from carbon-iron redox coupling. Nature, 472(7342), 209-212.

Rukhlov, A. S., Blinova, A. I., Pawlowicz, J. G., 2013. Geochemistry, mineralogy and petrology of the Eocene potassic magmatism from the Milk River area, southern Alberta, and Sweet Grass Hills, northern Montana. Chemical Geology, 353, 280-302.

Russell, J. K., Porritt, L. A., Lavallée, Y., Dingwell, D. B., 2012. Kimberlite ascent by assimilation-fuelled buoyancy. Nature, 481(7381), 352-356.

Saleeby, J., 2003. Segmentation of the Laramide slab—Evidence from the southern Sierra Nevada region. Geological Society of America Bulletin, 115(6), 655-668.

Salpas, P. A., Taylor, L. A., Shervais, J. W., 1986. The Blue Ball, Arkansas kimberlite: mineralogy, petrology, and geochemistry. The Journal of Geology, 891-901.

Salvador, A., 1991. Origin and development of the Gulf of Mexico basin. The Gulf of Mexico basin, 389-444.

Sandwell, D. T., Müller, R. D., Smith, W. H., Garcia, E., Francis, R., 2014. New global marine gravity model from CryoSat-2 and Jason-1 reveals buried tectonic structure. Science, 346(6205), 65-67.

Saunders, J. A., Harrelson, D. W., 1992. Age and petrology of the Jackson Dome igneous-volcanic complex, Mississippi: Implications for the tectonic history of the Mississippi Salt Dome Basin. Gulf Coast Association of Geological Societies Transactions, 42, 659-667.

Schaeffer, A. J., Lebedev, S., 2014. Imaging the North American continent using waveform inversion of global and USArray data. Earth and Planetary Science Letters, 402, 26-41.

Schlische, R. W., Young, S. S., Ackermann, R. V., Gupta, A., 1996. Geometry and scaling relations of a population of very small rift-related normal faults. Geology, 24(8), 683-686.

Schmandt, B., Dueker, K. G., Hansen, S. M., Jasbinsek, J. J., Zhang, Z., 2011. A sporadic low-velocity layer atop the western US mantle transition zone and short-wavelength variations in transition zone discontinuities. Geochemistry, Geophysics, Geosystems, 12(8), Q08014, doi:10.1029/2011GC003668.

Schmandt, B., Jacobsen, S. D., Becker, T. W., Liu, Z., Dueker, K. G., 2014. Dehydration melting at the top of the lower mantle. Science, 344(6189), 1265-1268.

Schmandt, B., Lin, F. C., 2014. P and S wave tomography of the mantle beneath the United States. Geophysical Research Letters, 41(18), 6342-6349.

Schmidt, M. W., Poli, S., 2014. Devolatilization during subduction. The Crust, Treatise on Geochemistry (eds. HD Holland and KK Turekian, Second Edition), Elsevier-Pergamon, Oxford, 669-701.

Scholle, P. A., 2003. Geologic map of New Mexico. New Mexico Bureau of Geology and Mineral Resources, scale 1:500,000.

Seton, M., Müller, R. D., Zahirovic, S., Gaina, C., Torsvik, T., Shephard, G., Talsma, A., Gurnis, M., Turner, M., Maus, S., Chandler, M., 2012. Global continental and ocean basin reconstructions since 200Ma. Earth-Science Reviews, 113(3), 212-270.

Sharp, W. E., 1974. A plate tectonic origin for diamond-bearing kimberlites. Earth and Planetary Science Letters, 21(4), 351-354.

Shephard, G. E., Flament, N., Williams, S., Seton, M., Gurnis, M., Müller, R. D., 2014. Circum-Arctic mantle structure and long-wavelength topography since the Jurassic. Journal of Geophysical Research: Solid Earth, 119(10), 7889-7908.

Shephard, G. E., Müller, R. D., Seton, M., 2013. The tectonic evolution of the Arctic since Pangea breakup: Integrating constraints from surface geology and geophysics with mantle structure. Earth-Science Reviews, 124, 148-183.

Shilobreeva, S., Martinez, I., Busigny, V., Agrinier, P., Laverne, C., 2011. Insights into C and H storage in the altered oceanic crust: Results from ODP/IODP Hole 1256D. Geochimica et Cosmochimica Acta, 75(9), 2237-2255.

Sigloch, K., 2011. Mantle provinces under North America from multifrequency P wave tomography. Geochemistry, Geophysics, Geosystems, 12(2).

Sigloch, K., Mihalynuk, M. G., 2013. Intra-oceanic subduction shaped the assembly of Cordilleran North America. Nature, 496(7443), 50-56.

Simmons, N. A., Forte, A. M., Boschi, L., Grand, S. P., 2010. GyPSuM: A joint tomographic model of mantle density and seismic wave speeds. Journal of Geophysical Research: Solid Earth (1978-2012), 115(B12).

Simonetti, A., Bell, K., 1994. Isotopic and geochemical investigation of the Chilwa Island carbonatite complex, Malawi: evidence for a depleted mantle source region, liquid immiscibility, and open-system behaviour. Journal of Petrology, 35(6), 1597-1621.

Sleep, N. H., 2008. Channeling at the base of the lithosphere during the lateral flow of plume material beneath flow line hot spots. Geochemistry, Geophysics, Geosystems, 9(8).

Smith, C. B., 1983. Pb, Sr and Nd isotopic evidence for sources of southern African Cretaceous kimberlites. Nature, 304, 51-54.

Snedden, J. W., Virdell, J., Whiteaker, T. L., Ganey-Curry, P., 2015. A basin-scale perspective on Cenomanian-Turonian (Cretaceous) depositional systems, greater Gulf of Mexico (USA. Interpretation, 4(1), SC1-SC22.

Snow, J. K., Wernicke, B. P., 2000. Cenozoic tectonism, in the central Basin and Range: Magnitude, rate, and distribution of upper crustal strain. American Journal of Science, 300(9), 659-719.

Sparks, R. S. J., Baker, L., Brown, R. J., Field, M., Schumacher, J., Stripp, G., Walters, A., 2006. Dynamical constraints on kimberlite volcanism. Journal of Volcanology and Geothermal Research, 155(1), 18-48.

Spencer, A. B., 1969. Alkalic igneous rocks of the Balcones province, Texas. Journal of Petrology, 10(2), 272-306.

Stern, R. J., Leybourne, M. I., Tsujimori, T., 2016. Kimberlites and the start of plate tectonics. Geology, 44(10), 799-802.

Stern, R.J., Anthony, E.Y., Ren, M., Lock, B.E., Norton, I., Kimura, J.I., Miyazaki, T., Hanyu, T., Chang, Q. and Hirahara, Y., 2011. Southern Louisiana salt dome xenoliths: First glimpse of Jurassic (ca. 160 Ma) Gulf of Mexico crust. Geology, 39(4), 315-318.

Storey, M., Mahoney, J. J., Saunders, A. D., Duncan, R. A., 1995. Timing of hot spot-related volcanism and the breakup of Madagascar and India. Science, 267(5199), 852.

Stracke, A., 2012. Earth's heterogeneous mantle: A product of convection-driven interaction between crust and mantle. Chemical Geology, 330, 274-299.

Stracke, A., Hofmann, A. W., Hart, S. R., 2005. FOZO, HIMU, and the rest of the mantle zoo. Geochemistry, Geophysics, Geosystems, 6(5).

Sun, S. S., McDonough, W. F., 1989. Chemical and isotopic systematics of oceanic basalts: implications for mantle composition and processes. Geological Society, London, Special Publications, 42(1), 313-345.

Sykes, L. R., 1978. Intraplate seismicity, reactivation of preexisting zones of weakness, alkaline magmatism, and other tectonism postdating continental fragmentation. Reviews of Geophysics, 16(4), 621-688.

Syracuse, E. M., van Keken, P. E., Abers, G. A., 2010. The global range of subduction zone thermal models. Physics of the Earth and Planetary Interiors, 183(1), 73-90.

Tackley, P. J., Stevenson, D. J., Glatzmaier, G. A., Schubert, G., 1993. Effects of an endothermic phase transition at 670 km depth in a spherical model of convection in the Earth's mantle. Nature, 361(6414), 699-704.

Tappe, S., Foley, S. F., Stracke, A., Romer, R. L., Kjarsgaard, B. A., Heaman, L. M., Joyce, N., 2007. Craton reactivation on the Labrador Sea margins: 40 Ar/39 Ar age and Sr-Nd-Hf-Pb isotope constraints from alkaline and carbonatite intrusives. Earth and Planetary Science Letters, 256(3), 433-454.

Tappe, S., Pearson, D. G., Kjarsgaard, B. A., Nowell, G., Dowall, D., 2013. Mantle transition zone input to kimberlite magmatism near a subduction zone: origin of anomalous Nd-Hf isotope systematics at Lac de Gras, Canada. Earth and Planetary Science Letters, 371, 235-251.

Tappe, S., Steenfelt, A., Heaman, L. M., Simonetti, A., 2009. The newly discovered Jurassic Tikiusaaq carbonatite-aillikite occurrence, West Greenland, and some remarks on carbonatite-kimberlite relationships. Lithos, 112, 385-399.

Tappert, R., Foden, J., Stachel, T., Muehlenbachs, K., Tappert, M., Wills, K., 2009. Deep mantle diamonds from South Australia: A record of Pacific subduction at the Gondwanan margin. Geology, 37(1), 43-46.

Tate, M. P., Dobson, M. R., 1988. Syn-and post-rift igneous activity in the Porcupine Seabight Basin and adjacent continental margin W of Ireland. Geological Society, London, Special Publications, 39(1), 309-334.

Thomas, W. A., 2006. Tectonic inheritance at a continental margin. GSA Today, 16(2), 4-11.

Thomson, A. R., Walter, M. J., Kohn, S. C., Brooker, R. A., 2016. Slab melting as a barrier to deep carbon subduction. Nature, 529(7584), 76-79.

Tilton, G. R., Kwon, S. T., Frost, D. M., 1987. Isotopic relationships in Arkansas Cretaceous alkalic complexes. Geological Society of America Special Papers, 215, 241-248.

Torsvik, T. H., Burke, K., Steinberger, B., Webb, S. J., Ashwal, L. D., 2010. Diamonds sampled by plumes from the core-mantle boundary. Nature, 466(7304), 352-355.

Torsvik, T.H., van der Voo, R., Doubrovine, P.V., Burke, K., Steinberger, B., Ashwal, L.D., Trønnes, R.G., Webb, S.J., Bull, A. L., 2014. Deep mantle structure as a reference frame for movements in and on the Earth. Proceedings of the National Academy of Sciences, 111(24), 8735-8740.

Turner, S. P., Platt, J. P., George, R. M. M., Kelley, S. P., Pearson, D. G., Nowell, G. M., 1999. Magmatism associated with orogenic collapse of the Betic-Alboran domain, SE Spain. Journal of Petrology, 40(6), 1011-1036.

Turner, S., Regelous, M., Kelley, S., Hawkesworth, C., Mantovani, M., 1994. Magmatism and continental break-up in the South Atlantic: high precision 40 Ar-39 Ar geochronology. Earth and Planetary Science Letters, 121(3), 333-348.

Ukstins, I. A., Renne, P. R., Wolfenden, E., Baker, J., Ayalew, D., Menzies, M., 2002. Matching conjugate volcanic rifted margins: 40 Ar/39 Ar chrono-stratigraphy of pre-and syn-rift bimodal flood volcanism in Ethiopia and Yemen. Earth and Planetary Science Letters, 198(3), 289-306.

Van Achterbergh, E., Griffin, W. L., Ryan, C. G., O'Reilly, S. Y., Pearson, N. J., Kivi, K., Doyle, B. J., 2002. Subduction signature for quenched carbonatites from the deep lithosphere. Geology, 30(8), 743-746.

Van der Hilst, R. D., Widiyantoro, S., Engdahl, E. R., 1997. Evidence for deep mantle circulation from global tomography. Nature, 386, 578-584.

Van Der Meer, D. G., Spakman, W., Van Hinsbergen, D. J., Amaru, M. L., Torsvik, T. H., 2010. Towards absolute plate motions constrained by lower-mantle slab remnants. Nature Geoscience, 3(1), 36-40.

van Keken, P. E., Hacker, B. R., Syracuse, E. M., Abers, G. A., 2011. Subduction factory: 4. Depth-dependent flux of H2O from subducting slabs worldwide. Journal of Geophysical Research: Solid Earth, 116(B1).

Van Mierlo, W. L., Langenhorst, F., Frost, D. J., Rubie, D. C., 2013. Stagnation of subducting slabs in the transition zone due to slow diffusion in majoritic garnet. Nature Geoscience, 6(5), 400-403.

Van Wijk, J. W., 2005. Role of weak zone orientation in continental lithosphere extension. Geophysical Research Letters, 32(2).

Van Wijk, J. W., Huismans, R. S., Ter Voorde, M., Cloetingh, S. A. P. L., 2001. Melt generation at volcanic continental margins: no need for a mantle plume. Geophysical Research Letters, 28(20), 3995-3998.

Versfelt, J., Rosendahl, B. R., 1989. Relationships between pre-rift structure and rift architecture in Lakes Tanganyika and Malawi, East Africa. Nature, 337, 354-357.

Waldman, M. A., McCandless, T. E., Dummett, H. T., 1987. Geology and petrography of the Twin Knobs# 1 lamproite, Pike County, Arkansas. Geological Society of America Special Papers, 215, 205-216.

Walter, M.J., Kohn, S.C., Araujo, D., Bulanova, G.P., Smith, C.B., Gaillou, E., Wang, J., Steele, A., Shirey, S. B., 2011. Deep mantle cycling of oceanic crust: evidence from diamonds and their mineral inclusions. Science, 334(6052), 54-57.

Wang, X. C., Wilde, S. A., Li, Q. L., Yang, Y. N., 2015. Continental flood basalts derived from the hydrous mantle transition zone. Nature communications, 6.

Wawrzyniec, T. F., Geissman, J. W., Melker, M. D., Hubbard, M., 2002. Dextral shear along the eastern margin of the Colorado Plateau: A kinematic link between Laramide contraction and Rio Grande rifting (ca. 75-13 Ma. The Journal of Geology, 110(3), 305-324.

Wei, S. S., Chen, Y. J., 2016. Seismic evidence of the Hainan mantle plume by receiver function analysis in southern China. Geophysical Research Letters, 43(17), 8978-8985.

Wernicke, B., Snow, J. K., 1998. Cenozoic tectonism in the central Basin and Range: Motion of the Sierran-Great Valley block. International Geology Review, 40(5), 403-410.

White, R. S., Spence, G. D., Fowler, S. R., McKenzie, D. P., Westbrook, G. K., 1987. Magmatism at rifted continental margins. Nature, 330, 439-444.

White, R., McKenzie, D., 1989. Magmatism at rift zones: the generation of volcanic continental margins and flood basalts. Journal of Geophysical Research: Solid Earth, 94(B6), 7685-7729.

White, R.S., Smith, L.K., Roberts, A.W., Christie, P.A.F., Kusznir, N.J., Roberts, A.M., Healy, D., Spitzer, R., Chappell, A., Eccles, J.D. and Fletcher, R., 2008. Lower-crustal intrusion on the North Atlantic continental margin. Nature, 452(7186), 460-464.

Whitmeyer, S. J., Karlstrom, K. E., 2007. Tectonic model for the Proterozoic growth of North America. Geosphere, 3(4), 220-259.

Williams, M. L., 1991. Heterogeneous deformation in a ductile fold-thrust belt: The Proterozoic structural history of the Tusas Mountains, New Mexico. Geological Society of America Bulletin, 103(2), 171-188.

Williams, M.L., Karlstrom, K.E., Lanzirotti, A., Read, A.S., Bishop, J.L., Lombardi, C.E., Pedrick, J.N., Wingsted, M. B., 1999. New Mexico middle-crustal cross sections. Rocky Mountain Geology, 34(1), 53-66.

Williams, R. T., Goodwin, L. B., Mozley, P. S., Beard, B. L., Johnson, C. M., 2015. Tectonic controls on fault zone flow pathways in the Rio Grande rift, New Mexico, USA. Geology, 43(8), 723-726.

Wilson, D., Aster, R., West, M., Ni, J., Grand, S., Gao, W., Baldridge, W.S., Semken, S., Patel, P., 2005. Lithospheric structure of the Rio Grande rift. Nature, 433(7028), 851-855.

Wilson, L., Head Iii, J. W., 2007. An integrated model of kimberlite ascent and eruption. Nature, 447(7140), 53-57.

Winker, C. D., Buffler, R. T., 1988. Paleogeographic evolution of early deep-water Gulf of Mexico and margins, Jurassic to Middle Cretaceous (Comanchean. AAPG Bulletin, 72(3), 318-346.

Wittke, J. H., Mack, L. E., 1993. OIB-like mantle source for continental alkaline rocks of the Balcones Province, Texas: trace-element and isotopic evidence. The Journal of Geology, 333-344.

Wobus, R. A., Manley, K., 1982) Reconnaissance geologic map of the Burned Mountain quadrangle, Rio Arriba County, New Mexico. U.S. Geological Survey Miscellaneous Field Studies Map 1409, scale 1:24,000.

Wortel, M. J. R., Spakman, W., 2000. Subduction and slab detachment in the Mediterranean-Carpathian region. Science, 290(5498), 1910-1917.

Wu, F. Y., Yang, Y. H., Mitchell, R. H., Li, Q. L., Yang, J. H., Zhang, Y. B., 2010. In situ U-Pb age determination and Nd isotopic analysis of perovskites from kimberlites in southern Africa and Somerset Island, Canada. Lithos, 115(1), 205-222.

Wu, J., Suppe, J., Lu, R., Kanda, R., 2016. Philippine Sea and East Asian plate tectonics since 52 Ma constrained by new subducted slab reconstruction methods. Journal of Geophysical Research: Solid Earth, 121, 4670-4741, doi:10.1002/2016JB012923.

Yang, Z., & Chen, W. P., 2010. Earthquakes along the East African Rift System: A multiscale, system-wide perspective. Journal of Geophysical Research: Solid Earth, 115(B12).

Ye, H., Royden, L., Burchfiel, C., Schuepbach, M., 1996. Late Paleozoic deformation of interior North America: the greater Ancestral Rocky Mountains. American Association of Petroleum Geologists Bulletin, 80(9), 1397-1432.

Yin, A., Ingersoll, R. V., 1997. A model for evolution of Laramide axial basins in the Southern Rocky Mountains, USA. International Geology Review, 39(12), 1113-1123.

Yonkee, W. A., Weil, A. B., 2015. Tectonic evolution of the Sevier and Laramide belts within the North American Cordillera orogenic system. Earth-Science Reviews, 150, 531-593.

Young, H. P., Lee, C. T., 2009. Fluid-metasomatized mantle beneath the Ouachita belt of southern Laurentia: Fate of lithospheric mantle in a continental orogenic belt. Lithosphere, 1(6), 370-383.

Yuan, H., Romanowicz, B., 2010. Lithospheric layering in the North American craton. Nature, 466(7310), 1063-1068.

Zartman, R. E., 1977. Geochronology of some alkalic rock provinces in eastern and central United States. Annual Review of Earth and Planetary Sciences, 5, 257-286.

Zartman, R. E., Brock, M. R., Heyl, A. V., Thomas, H. H., 1967. K-Ar and Rb-Sr ages of some alkalic intrusive rocks from central and eastern United States. American Journal of Science, 265(10), 848-870.

Zhao, D., Tian, Y., Lei, J., Liu, L., Zheng, S., 2009. Seismic image and origin of the Changbai intraplate volcano in East Asia: role of big mantle wedge above the stagnant Pacific slab. Physics of the Earth and Planetary Interiors, 173(3), 197-206.

Zhao, F., Alves, T.M., Wu, S., Li, W., Huuse, M., Mi, L., Sun, Q. and Ma, B., 2016. Prolonged post-rift magmatism on highly extended crust of divergent continental margins (Baiyun Sag, South China Sea. Earth and Planetary Science Letters, 445, 79-91.

Zoback, M. L., 1992. First- and second-order patterns of stress in the lithosphere: The World Stress Map Project. Journal of Geophysical Research: Solid Earth, 97(B8), 11703-11728.

Zoback, M. L., Anderson, R. E., & Thompson, G. A., 1981. Cainozoic evolution of the state of stress and style of tectonism of the Basin and Range province of the western United States. Philosophical Transactions of the Royal Society of London A: Mathematical, Physical and Engineering Sciences, 300(1454), 407-434.

Zonneveld, J. P., Kjarsgaard, B. A., Harvey, S. E., Heaman, L. M., McNeil, D. H., Marcia, K. Y., 2004. Sedimentologic and stratigraphic constraints on emplacement of the Star Kimberlite, east-central Saskatchewan. Lithos, 76(1), 115-138.